# Lawrence Berkeley Laboratory
UNIVERSITY OF CALIFORNIA

## CHEMICAL BIODYNAMICS DIVISION

BACTERIOCHLOROPHYLL PROTEIN STRUCTURE--STUDIES WITH POLARIZED LIGHT AND TRIPLET STATE ELECTRON PARAMAGNETIC RESONANCE

John Davis Bolt
(Ph.D. thesis)



February 1980



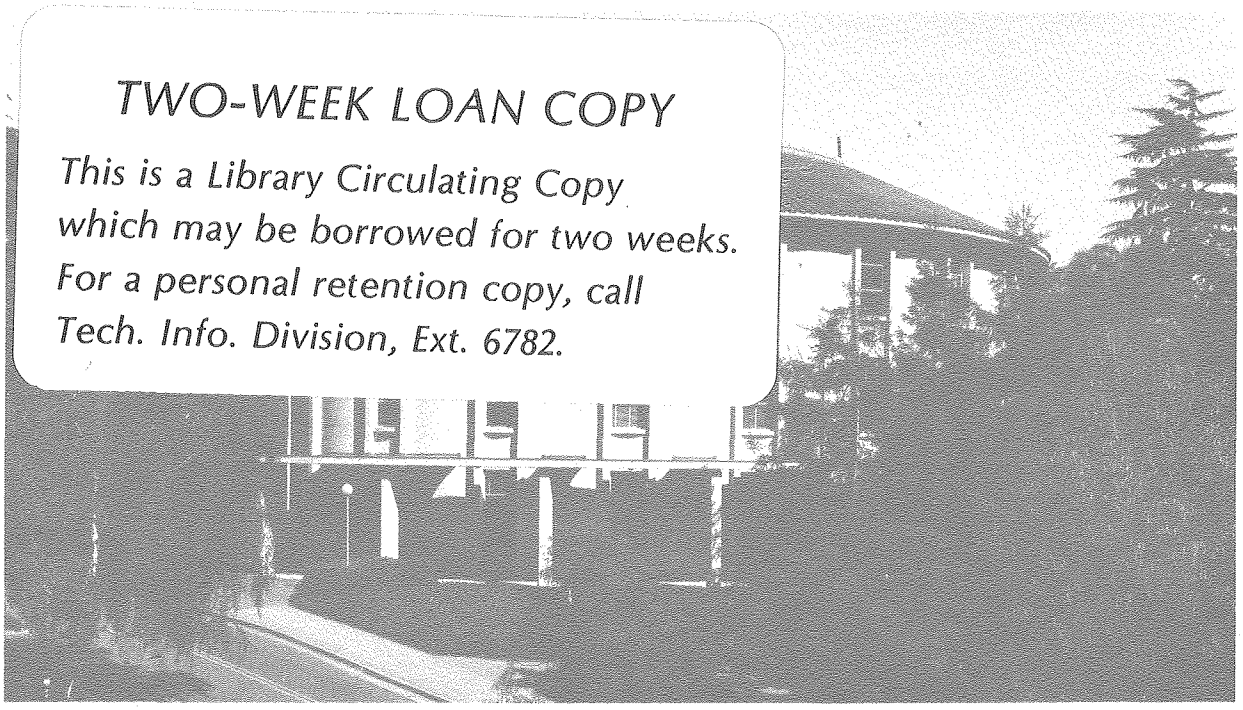

Prepared for the U.S. Department of Energy under Contract W-7405-ENG-48

## DISCLAIMER

# BACTERIOCHLOROPHYLL PROTEIN STRUCTURE---- STUDIES WITH POLARIZED LIGHT AND TRIPLET STATE ELECTRON PARAMAGNETIC RESONANCE

by

John Davis Bolt

February 1980

## ABSTRACT

Light harvesting bacteriochlorophyll-protein complexes from Rhodopseudomonas sphaeroides 2.4.1 (B800+850) and R-26 (LH-R26) mutant are solubilized in SDS and imbedded in polyvinyl alcohol. Stretching induces orientation, and the linear dichroism of visible and near infrared absorption is analyzed. Based on a simple model, angles between the particle axis system and the transition dipole moments are found. In the near infrared absorption band of the LH-R26 protein the dichroic ratio varies from 1.30 to 1.57. Using the absorption and linear dichroism curves, the band is resolved into two exciton components. Simultaneous gaussian band resolution of the absorption and circular dichroism spectra confirms the assignment of exciton components. In the visible ($Q_x$) absorption band the dichroic ratio has a constant value of 0.43 for the R-26 protein but varies with wavelength for the wild type light harvesting protein. This variation is

attributed to an additional bacteriochlorophyll not present in the R-26 protein.

Fluorescence and fluorescence polarization studies of the LH-R26 protein show transitions that are nearly planar degenerate. They can be interpreted as arising from monomeric bacteriochlorophyll excited states. The fluorescence polarization of the $Q_x$ absorption band is nearly perpendicular to the fluorescence transitions. These results are used to formulate a model for the mutual orientation of the x and y axes of the two bacteriochlorophylls which comprise the complex.

Reaction centers of the photosynthetic bacterium Rhodopseudomonas sphaeroides R-26, give rise to large triplet state EPR signals upon illumination at low temperature (11 K). Utilizing monochromatic polarized light to generate the EPR spectra (magnetophotoselection), it is shown that the intensities of the observed triplet signals are strongly dependent upon the wavelength and polarization direction of the excitation. These data can be used to calculate the orientations of the excited transition moments with respect to each other and with respect to the triplet state principal magnetic axes system. The transition moment at 870 nm which is associated with the bacteriochlorophyll "special pair" lies almost entirely along one of the principal magnetic axes of the triplet state. Also, the 870 nm transition moment makes an angle of $\sim 60^{\circ}$ with the 546 nm transition moment, which is associated with a bacteriopheophytin. This latter result is

in agreement with previous photoselection studies on the same bacterial species.

Triplet states of carotenoids have been detected by EPR and are reported here for the first time. The systems in which carotenoid triplets are observed include cells of photosynthetic bacteria, isolated bacteriochlorophyll-protein complexes, and detergent micelles which contain β-carotene. The carotenoid triplet state is detected in reaction centers of Rhodopseudomonas sphaeroides 2.4.1 (wild type), which contain the carotenoid spheroidene. The zero-field splitting parameters of the triplet spectrum are: $|D| = 0.0290 \pm 0.0005$ cm$^{-1}$ and $|E| = 0.0044 \pm 0.0006$ cm$^{-1}$, in contrast with the parameters of the reaction center bacteriochlorophyll dimer triplet which are $|D| = 0.0189 \pm 0.0004$ cm$^{-1}$ and $|E| = 0.0032 \pm 0.0004$ cm$^{-1}$. Bacteriochlorophyll in a light harvesting protein complex from Rps. sphaeroides, wild type, also sensitizes carotenoid triplet formation. In whole cells the EPR spectra vary with temperature between 100°K and 10°K. Carotenoid triplets also have been observed by EPR in whole cells of Rps. sphaeroides and cells of Rhodospirillum rubrum which contain the carotenoid spirilloxanthin. Attempts to observe the triplet state EPR spectrum of β-carotene in numerous organic solvents failed. However, in nonionic detergent micelles and in phospholipid bilayer vesicles β-carotene gives a triplet state spectrum with $|D| = 0.0333 \pm 0.0010$ cm$^{-1}$ and $|E| = 0.0037 \pm 0.0010$ cm$^{-1}$.

Kenneth Sauer

ACKNOWLEDGEMENTS

I feel that my stay in Berkeley has broadened and strengthened me enormously, both professionally and personally. A Ph.D. thesis is not possible without the help of many people. In particular I am indebted,

To Kenneth Sauer, my research director, for his unerring scientific guidance and for always having time to listen to his students.

To Harry Frank for his enthusiasm and for introducing me to EPR and the triplet state.

To all of the members and visitors to Ken's research group, especially to Jacques Breton, Mary McLean, John Nairn, Richard Friesner and Harry for their friendship and scientific insights.

To the staff of LCB, especially to Dick O'Brien, Bill McCallister, Gary Smith and Beth Klingel for their cheerfulness and skills.

To Susan Lund for patiently typing this thesis.

To my parents for their encouragement throughout my education.

For their friendship and love during my years in Berkeley and I hope forever, I thank John Robbins and Marilee Hartley.

This work was supported in part by the U.S. Department of Energy uncer Contract W-7405-ENG-48.

## ABBREVIATIONS

| | |
|---|---|
| A | absorbance |
| BChl | bacteriochlorophyll |
| BPheo | bacteriopheophytin |
| B800+850, B890 | classes of light harvesting BChl proteins with $\lambda$ max indicated |
| Car | carotenoid, usually within an RC |
| CD | circular dichroism |
| D | dipole strength |
| DDAO | dodecyldimethylamine oxide |
| $D_r$ | dichroic ratio ($A_{\parallel}/A_{\perp}$) |
| $\|D\|$ $\|E\|$ | zero field splitting parameters |
| $\underset{\sim}{E}$ | electric vector |
| EPR | electron paramagnetic resonance |
| f | fraction of sample with "perfect ordering" |
| H, $\underset{\sim}{H}$ | magnetic field |
| h.w.p. | half wave plate |
| $k_{x,y,z}$ | relative rates for intersystem crossing to ground state from the zero field triplet spin sublevels |
| LD | linear dichroism |
| LDAO | DDAO (lauryl) |
| LH-R26 | light harvesting BChl protein complex from Rps. sphaeroides carotenoidless mutant R-26 |
| p | polarization of fluorescence |
| $P_{x,y,z,}$ | projections of a vector onto the principal magnetic axes of a triplet state |
| PVA | polyvinyl alcohol |

| | |
|---|---|
| $Q_y$ | absorption band of chlorophyll in the near infrared, 800-900 nm usually |
| $Q_x$ | absorption band of chlorophyll in the visible, near 600 nm |
| $Q_{A,B}$ | quinones of the RC |
| R | rotational strength (of CD band) |
| RC | reaction center |
| Rps. | Rhodospirrillum |
| Rps. | Rhodopseudomonas |
| $R_s$ | stretch ratio |
| SDS | sodium dodecyl sulfate |
| $T_{+1,0,-1}$ | high field triplet spin sublevels |
| $V_{12}$ | exciton splitting |
| a,e | indicate triplet EPR signals in absorption and emission |
| $\|\|$ | parallel |
| $\perp$ | perpendicular |
| $\underset{\sim}{\mu}$ | absorption transition dipole moment |
| $\bar{\nu}$ | frequency (in $cm^{-1}$) |
| $\lambda$ max | wavelength of maximum abosrbance |

TABLE OF CONTENTS

# CHAPTER I

## INTRODUCTION

Photosynthesis is the conversion of light energy into chemical energy by living organisms. This broad definition includes many processes. Photons are initially absorbed by light harvesting (antenna) pigments, including carotenoids, chlorophylls and other tetrapyrrole pigments. The excitation energy is then transferred to specialized chlorophyll complexes, the reaction centers, where photochemistry occurs. These reaction center chlorophylls lose one electron from their first excited singlet state, reducing an initial acceptor. The electron is then passed along a series of acceptors. In green plants the terminal acceptor is nicotinamide adenine dinucleotide phosphate. Its reducing power is used in the formation of carbohydrates from carbon dioxide. In green plants water is the terminal electron donor for the reduction of oxidized chlorophyll, which results in oxygen evolution. In photosynthetic bacteria the electron transport chain is cyclic, returning electrons to the oxidized bacteriochlorophyll (BChl). In both plants and bateria photosynthetic electron transport leads to energy storage in the form of a chemical and electrical potential of a proton gradient across a membrane. This stored energy is used to generate adenosine triphosphate. References (1)-(3) are recent general reviews of photosynthesis. References to reviews of the specific topics discussed in this thesis will follow.

Most of the work described here involves studies of bacteriochlorophyll protein complexes. Early workers determined that chlorophyll (Chl) was associated with proteins (4). Through the work of Clayton (5) and Thornber (6,7) the idea of isolable, stoichiometric complexes developed. The isolation of Chl proteins requires the use of detergents to solubilize the photosynthetic membranes, where the complexes reside. All complexes which have been found are non-covalent. This contrasts with the phycobiliproteins which contain linear tetrapyrroles covalently attached to proteins, typically through thioether linkages (8).

There are two functionally different BChl proteins; light harvesting complexes contain the bulk of the pigments, and reaction centers (RCs) contain only a small fraction of the BChl. RCs receive excitation energy, usually by transfer from the light harvesting pigments, and undergo photochemical electron transfer. The first isolation and purification of RCs by Clayton and co-workers led to a proliferation of studies on their photophysical properties (9,10,11). At first the light harvesting proteins were given little attention. This was a natural tendency because the light-harvesting pigments are photochemically inactive. Nevertheless, they are interesting in terms of chromophore aggregate properties, chromophore protein interactions, energy transfer, and structure determination, all of which may be probed by optical spectroscopy.

Determining the structure of the BChl proteins is not

straightforward. Inability to crystalize the detergent solubilized proteins has blocked the path of direct structure determination. Therefore, spectroscopic methods must be used. In any structural approach the light harvesting proteins provide a distinct advantage because of their simplicity. Typical light harvesting proteins contain 3BChls, one carotenoid, two proteins of about 10,000 daltons, and accompanying lipids and detergents (see below). The reaction centers from bacteria contain at least 4 BChls, 2 bacteriopheophytins (BPh), one ferrous iron atom, one or two ubiquinones, lipids and detergents. Many reaction centers also contain two or more cytochromes. The minimum molecular weight of a RC is 85,000. Determining structural information from optical measurements is complicated by the aggregated nature of the chlorophylls. Proximity of two or more chromophores (especially identical chromophores) can result in interaction such that the excited states are properties of the aggregate. In many cases is is not possible to excite individual chlorophylls.

Sauer and Austin were able to isolate and characterize a simple light harvesting bacteriochlorophyll protein from Rhodopseudomonas sphaeroides R-26 (13). It contains two BChls per two polypeptides. In the presence of sodium dodecyclsulfate (SDS) the complex does not aggregate further. As such, it is the simplest native chlorophyll protein complex known. The assertion that the complex remains in a native conformation during isolation and purification is supported

by: (a) the retention of a large shift in the near infrared absorption band, and (b) the retention of circular dichroism in the near infrared and visible regions, including the sign, magnitude, and position of the observed bands (13). The dimer of BChls presents the smallest possible aggregate. Much of the attention of this thesis is directed toward this complex, designated here as LH-R26.

An overview of light harvesting BChl proteins is appropriate at this point. The subject has been recently reviewed by Thornber et. al. (7) and by Cogdell and Thornber (14). The near infrared absorption of BChl in vivo shows an assortment of wavelength maxima. All are shifted to lower energy than BChl in polar organic solvents. The in vivo spectral forms are designated by B800, B820, B850 and B890 (15), to indicate the approximate maxima. The exact values differ considerably. For example B890 can range from 870 nm (Rps. sphaeroides) to 890 nm (Rsp. rubrum). Different types of bacteria show various combinations of the spectral forms. Furthermore, differing growth conditions lead to variability in the relative amounts of each spectral form in a particular culture. The observation with Rps. sphaeroides of constant ratios of B800 to B850 and B890 to RCs by Aagaard and Sistrom (16) suggests that B800 and B850 are components of a single complex separate from B890. Rps. capsulata shows similar trends (17). Isolation of submembrane particles confirmed this hypothesis.

Thornber, working with Chr. vinosum, isolated frac-

tions containing B890 alone, B800 and B850 together, and B800 with B820 (18). Clayton and Clayton isolated a protein containing B800 and B850 from Rps. sphaeroides (5). These results confirmed the existence of the B800 and B850 in the same protein complex. Recently Broglie et. al. isolated both the B800+850 protein and the B890 protein from Rps. sphaeroides using lithium dodecylsulfate gel electrophoresis (19). The B800+820 complex of Chr. vinosum is probably an altered form of B800+850 (14).

Clayton reported the association of a single peptide of 9,000 daltons with the B800+850 protein. Other workers also reported a single polypeptide from the light harvesting components in Rps. sphaeroides (13,20). However this result appears to be in error. Conventional SDS gel systems resolve peptides of less than 12,000 daltons poorly. Moskalenko and Erokhin reported two low molecular weight peptides from the light harvesting components of Rps. sphaeroides and five other types of bacteria (21). The ability to resolve one or two peptides depended upon the gel system and electrode buffers used. Results of Cogdell (22) and from this laboratory (see Appendix I) confirm the existence of two or more peptides in the light harvesting complexes of Rps. sphaeroides. Feick and Drews report three peptides in the light harvesting components of Rps. capsulata, one associated with B890 and two with B800+850 (23).

The assignment of the LH-R26 protein to either the B800+850 class or the B890 class is difficult. It has a single

maximum at 860 nm in vivo. If it belongs to the B890 class it is then the shortest wavelength absorbing member. However, the constant ratio of RCs to LH-R26 in native membranes suggests this is the correct assignment (16,19). Austin and Sauer, who have characterized the protein (13), postulated that it was an altered form of the B800+850 protein, found in the wild type organism, based on the circular dichroism (CD) spectra. Linear dichroism spectra (See Chapter II) also suggests similarity between B800+850 and LH-R26. Until detailed biochemical characterization of the component peptides is obtained, a definite assignment is impossible.

Cogdell and co-workers have studied the pigment stoichiometry in B800+850 and B890 complexes from several bacteria (14,24). In the B800+850 complex a ratio of 3:1 BChl to carotenoid is found, regardless of the type of carotenoid. B890 complexes have a ratio of 2:1 BCHl:carotenoid. Austin found a ratio of 2:2 peptide:BChl in the LH-R26 protein (13). Broglie et. al. found BChl to peptide ratios of 3:2 for B800+850 and 2:2 for B890 (19). When considered together these results indicate specific stoichiometric complexes between Bchl, carotenoid and protein. Most certainly these are the building blocks of the light harvesting arrays in photosynthetic bacteria. Combined with RCS they account for all BChl in the membranes.

A detailed picture of the photosynthetic membrane can now be sought by a) determining the relative orientations of BChl and carotenoid within the isolated proteins and b) deter-

mining the mutual arrangements of these building blocks within the membranes. The major thrust of Chapters II and III is aimed toward the first of these goals. The chapters deal with the interaction of plane polarized light with BChl proteins. Figure 1 helps to illustrate the approach. BChl has two well separated absorption bands due to transitions polarized along nearly perpendicular axes within the porphyrin plane (25). These transition dipole moments are labeled $Q_x$ (at about 590 nm) and $Q_y$ (at 770 nm in organic solvents and at wavelengths greater than 800 nm in vivo). Linear dichroism measurements of the preferential absorption of plane polarized light in an oriented sample can determine the angles between the transition moments and the unique axis of the molecule or complex responsible for its orientation. Chapter II discusses in detail the linear dichroism of light harvesting BChl proteins oriented in stretched polyvinyl alcohol films.

Fluorescence polarization is the polarization of emitted light dependent upon the wavelength of excitation or emission. It leads to information on the relative orientations between absorbing and fluorescing transition moments. Chapter III describes the fluorescence polarization and other fluorescence properties of the BChl proteins. A model is proposed for the mutual orientations of the two BChls within the LH-R26 protein.

The structure of one BChl protein has been determined by X-ray crystallography (26). Unlike other BChl proteins, this protein is water soluble. Generalization about the structure

FIGURE I-1

Structure and absorption spectrum of bacteriochlorophyll a. $B_X$, $B_Y$, $Q_X$ and $Q_Y$ transition moments are polarized along the x and y axes of the porphyrin plane.

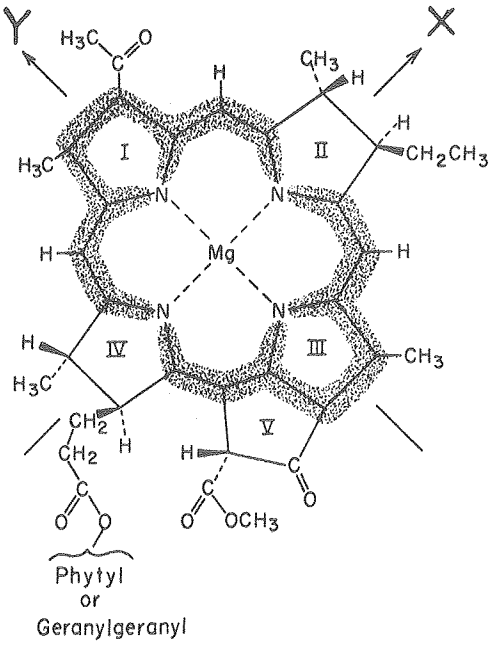


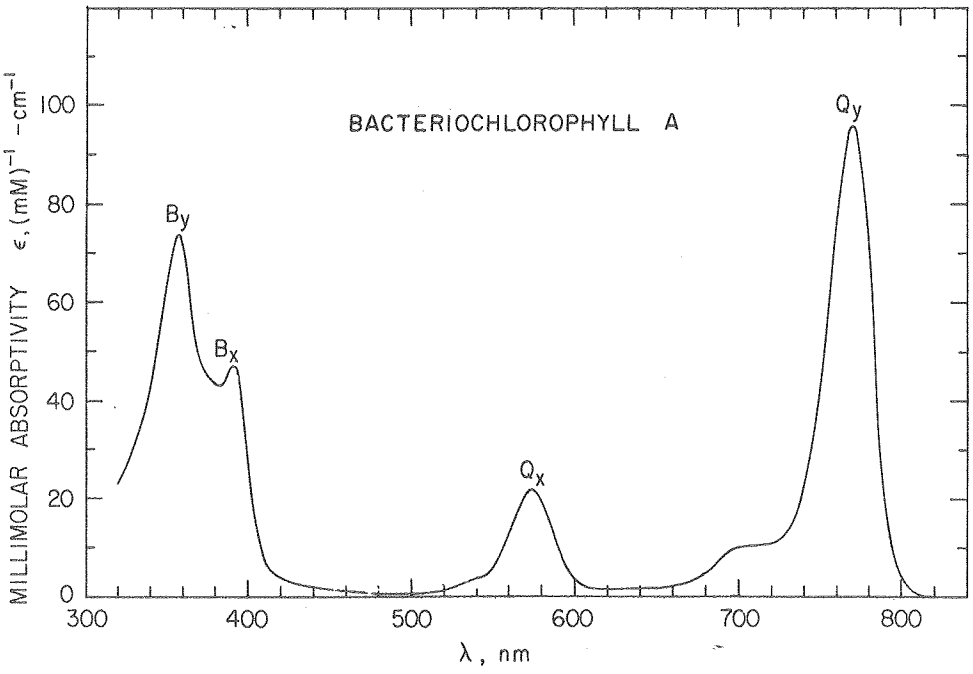


XBL 7912-13642

of other BChl proteins from its structure should be made cautiously. The protein exists as a trimer of 50,000 dalton polypeptides each of which encloses seven BChls. Each Mg is coordinated by a fifth ligand from an amino acid side chain. The protein has an unusual amount of beta-sheet structure. Analysis of the near ultraviolet CD of BChl proteins isolated from Rps. sphaeroides suggests there is about 40 percent alpha-helix and little beta-sheet structure (27). Other similarities and differences between this water soluble BChl protein and typical membrane bound BChl proteins are unclear; a comparison awaits better structural analysis of the membrane proteins.

As mentioned earlier, the BChls within these proteins interact, producing excited states which differ from monomeric exicted states. The theory of aggregate chromophore interaction and alteration of optical spectra, exciton theory, has direct bearing on the interpretation of the results in Chapters II and III. Because of its simplicity as a dimer of BChls, the LH-R26 protein is a useful system in which to apply exciton theory. The protein probably provides a rigid, well defined geometry. Its study may be advantageous compared to solution or loosely linked covalent dimers (28) which can present a statistical distribution of differing conformations. It is hoped that the results presented here will help to further exciton theory, if not by myself, then by more competent theoreticians.

The results presented in Chapter IV diverge from the

topics in Chapters II and III. During the investigation of triplet excited states of the BChl proteins new electron paramagnetic resonance (EPR) signals were found. These signals are assigned to carotenoid triplets sensitized by BCHl. No precedent for EPR detectable carotenoid triplets exists in the literature, despite the abundance of optically detectable carotenoid triplets. To confirm the assignment of the EPR triplets to carotenoids, in vitro systems were found in which carotenoid triplets could be observed at the low temperature necessary for the EPR measurements. Both in vivo and in vitro results are presented in Chapter IV.

## REFERENCES


(1) Bioenergetics of Photosynthesis (Govindjee, ed.) Academic Press, New York, N.Y. (1975) especially chapters by K. Sauer, R.S. Knox, M. Avron, P. Joliot and B. Kok.

(2) R.K. Clayton and W.R. Sistrom, editors, The Photosynthetic Bacteria, Plenum Press, New York, N.Y. (1978).

(3) K. Sauer, Ann. Rev. Phys. Chem. 30, 155 (1979) and Accts. Chem. Res. 11, 247 (1978).

(4) J.H.C. Smith and C.S. French, Ann. Rev. Plant Physiology 14, 181 (1963).

(5) R.K. Clayton and B.J. Clayton, Biochim. Biophys. Acta 283, 492 (1972).

(6) J.P. Thornber, Ann. Rev. Plant Physiology 26, 127 (1975).

(7) J.P. Thornber, T.L. Trosper, C.E. Strouse, in reference (2), p. 133.

(8) L. Bogorad, Ann. Rev. Plant Physiol. 26, 369 (1975).

(9) D.W. Reed and R.K. Clayton, Biochem. Biophys. Res. Comm. 30, 471 (1968).

(10) R.K. Clayton and R.T. Wang, Methods Enzymol. 23, 696 (1971).

(11) In reference (2), chapters by W.W. Parson, G. Feher and M.Y. Okamura, R.K. Clayton, J.S. Leigh, P.L. Dutton and R.C. Prince, and G. Gingras.

(12) G. Gingras, in reference (2), p. 119.

(13) L.A. Austin, Ph.D. Thesis, University of California, Berkeley, 1976. K. Sauer and L.A. Austin, Biochem. 17, 2011 (1978).

(14) R.J. Cogdell and J.P. Thornber, Ciba Foundation Symp. No. 61, London, England, Elsevier, Holland, p. 61 (1978).

(15) W.J. Vredenberg and J. Amesz in Brookhaven Symp. in Biology No. 19, p. 49 (1967).

(16) J. Aagaard and W.R. Sistrom, Photochem. Photobiol. 15, 209 (1972).

(17) A. Schumacher and G. Drews, Biochim. Biophys. Acta 501, 183 (1978).

(18) J.P. Thornber, Biochem. 9, 2688 (1970).

(19) R.M. Broglie, C.N. Hunter, P. Delepelaire, R.A. Neiderman, N.H. Chua, R.K. Clayton, in press Proc. Nat. Acad. Sci. USA for January 1980.

(20) J.W. Huang and S. Kaplan, Biochim. Biophys. Acta 307, 317 (1973).

(21) A.A. Moskalenko, Yu. E. Erokhin, FEBS Lett. 87, 254 (1978).

(22) R.J. Cogdell, personal communication.

(23) R. Feick and G. Drews, Biochim. Biophys. Acta 501, 499, (1978), and Z. Naturforsch 34, 196 (1979).

(24) R.J. Cogdell and A.R. Crofts, Biochim. Biophys. Acta 502, 409 (1978).

(25) K. Sauer in reference (1), p. 115.

(26) R.E. Fenna and B.W. Mathews in Brookhaven Symposia in Biology No. 28, p. 170 (1976).

(27) Unpublished results of this author.

(28) J.J. Katz, J.R. Norris, L.L. Shipman in Brookhaven Symposia in Biology No. 28, p. 16 (1976), and E.A. Dratz, A.J. Schultz, and K. Sauer, in Brookhaven Symposia in Biology No. 19, 303 (1967).

# CHAPTER II

# LINEAR DICHROISM OF BCHL PROTEINS

## Introduction

Linear dichroism is the selective absorption of plane polarized light by an oriented sample. For electric dipole transitions, if the electric vector, $\underset{\sim}{E}$, of light of appropriate energy makes an angle, $\alpha$, with the transition moment, $\underset{\sim}{\mu}$, then the probability of absorption is:

$$|\underset{\sim}{E}|^2 |\underset{\sim}{\mu}|^2 \cos^2\alpha \qquad [1]$$

The transition moments of monomeric BChl are polarized close to the bacteriochlorin symmetry axes, see Figure I-1. These assignments are supported by quantum mechanical calculations, fluorescence polarization measurements and magnetic circular dichroism (1-4). Knowledge of the transition moment directions and linear dichroism measurements can provide information on molecular orientation. The LD of biological chromophores has been recently reviewed by Hofrichter and Eaton (5).

LD measurements of photosynthetic systems have been used primarily to determine transition moment orientation with respect to membrane planes. In whole cells or chloroplasts, membranes often show internal organization. In such cases, orientation of the cells or organelles leads to orientation of the membranes. These large particles have been oriented most successfully by shear gradients (flow to spreading techniques) (6), and magnetic fields (7,8). [Note: Photosynthetic references are cited for work on bacterial systems. For references to

chloroplast linear dichroism, see reference (5).]

Even in the absence of membrane organization within cells, the membranes can be oriented. When dried onto a flat surface, membranes achieve a high degree of order, with membrane planes parallel to the surface (9). Chromatophores, the intracytoplasmic membranes of photosynthetic bacteria, can be oriented by drying. LD has been reported by several groups (7,9,10). Generally, the results indicate that the $Q_y$ transitions lie at an angle of 20 to 30 degrees to the plane (7,9). Carotenoid transitions are approximately 45 degrees to the plane. These numbers are based on the assumption of uniform distribution of transition moments. Since the bulk of the absorption of light is due to light harvesting pigments, these angles represent the orientation of light harvesting transitions. In membranes containing more than one light harvesting complex (e.g. Chr. vinosum or Rps. sphaeroides Y, wild type) different orientations for different complexes might be expected. Close examination of oriented membrane LD, figure 2, reference (9) and figure 2 reference (7), suggests this possibility.

The presence of reaction center absorption also leads to a more complicated interpretation of LD. Vermeglio and Clayton were able to selectively oxidize the light harvesting components in chromatophores (10). The residual absorption and LD of oriented membranes was due to the RC components. Alternatively, the absorption changes due to RC photochemistry (reversible oxidation of the BChl special pair) were studied (10).

[These studies were performed under saturating light conditions. They should not be confused with photoselection experiments, see Chapter III, where only a small fraction of RCs are bleached by polarized light.] Vermeglio and Clayton concluded that the transition moments of the RC special pair absorb at 870 nm (strong) and 810 nm (weak) and are the two exciton components of the dimer. (See Discussion for exciton theory.)

As discussed above, the multicomponent nature of whole membrane absorption complicates the interpretation of linear dichroism. LD measurements on purified membrane components will lead to more unambiguous interpretations. Several reports of LD of isolated BChl proteins have appeared in the literature (11-15). Rafferty and Clayton (11,12) oriented RCs in gelatin by drying to a thin film and by stretching the film. In our laboratory we were able to orient light-harvesting components in stretched polyvinal alcohol (PVA) films (13). Some of the results presented in this chapter were reported in reference (13). Stretched film orientation is a familiar technique for linear dichroism of small molecules (16-21). Its application to biological macromolecules, especially BChl proteins, has been useful.

The basic principles of stretched film LD are outlined in Figure II-1. A BChl protein is embedded in a polymer film and the film is stretched (a). The shear forces in the film cause the long axis, P, of the protein to align along the stretch direction, Z (b). Absorption parallel, $A_{||}$, and

FIGURE II-1

Stretched film linear dichroism. Protein-detergent particles (or whole membranes) are embedded in polyvinyl alcohol film. The film is stretched along the z direction. Proteins tend to align with their long axis, P, aligned along z. Absorption is measured with the light polarized parallel and perpendicular to z.

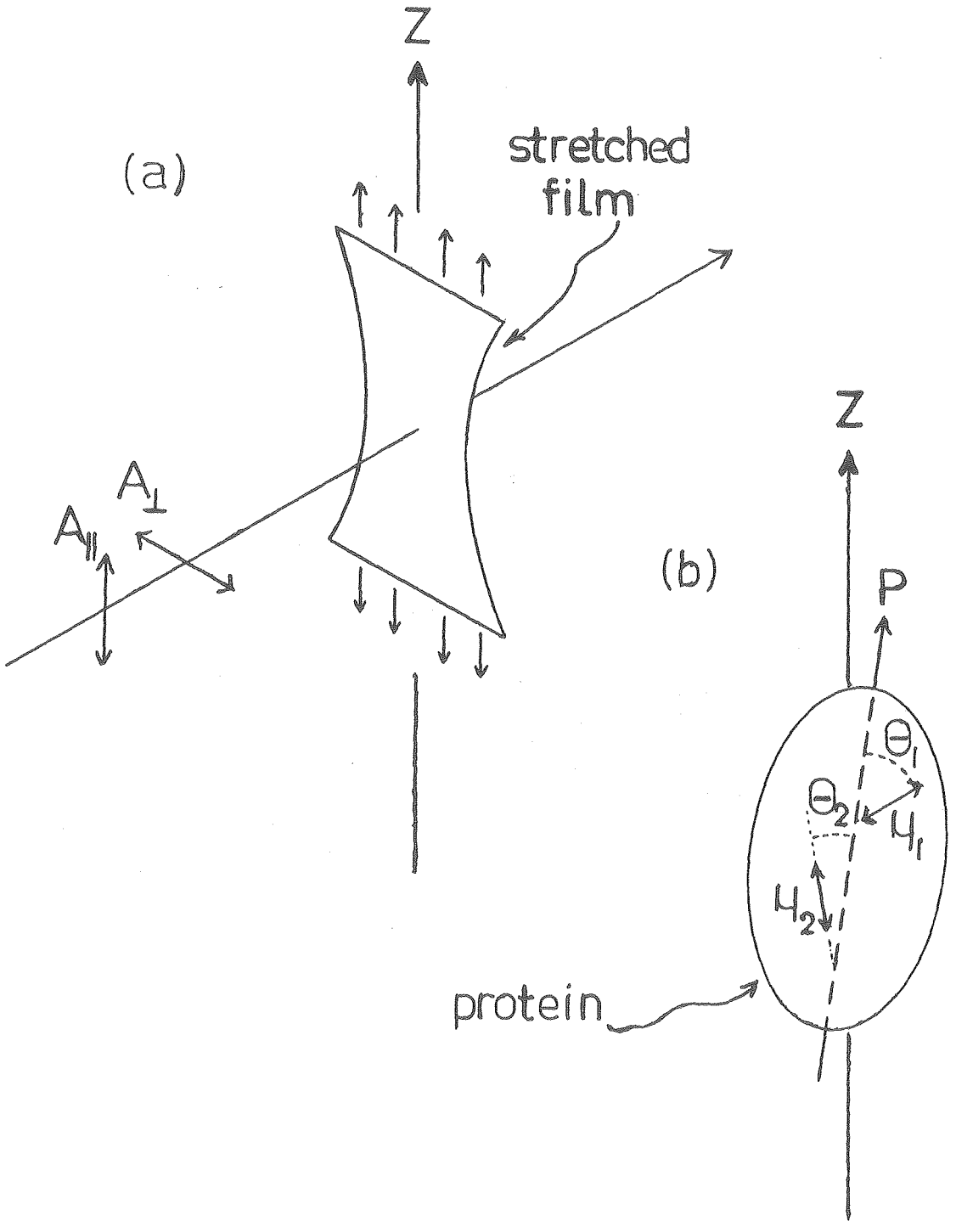


XBL 7912-13640

perpendicular, $A_{\perp}$, to the stretch direction can be determined using polarized measuring light. Within the protein particle there are chromophores at fixed positions with transition moments ($\mu_1$ and $\mu_2$) which have specific angles ($\theta_1$ and $\theta_2$) to the protein axis.

If the orientation of the proteins is perfect, all P's aligned along Z, the determination of the $\theta$'s is straightforward. However this is rarely the case. Treatment of the disorder or imperfect orientation is the most difficult problem of linear dichroism. Rafferty and Clayton (12) and this author chose to analyze the LD results with a useful model, after Fraser (18). The population of proteins is divided into a fraction, f, oriented perfectly and a fraction, 1-f, oriented entirely at random. The problem of imperfect orientation is then reduced to determining f. Although the model is artificial, it is easily perceived and formulated. Nairn, et. al. have developed an approach to LD in partially ordered systems (22). Using a model for the partial order, they develop a density of states function describing the orientation of incident polarized light within a fixed molecular axis system. Other techniques used to analyze linear dichroism utilize order parameters, integrals over the orientational distribution of molecules within a laboratory axis system (8,23). Unfortunately no analysis method can provide a completely quantitative description of the disorder of a partially ordered system on the basis of LD measurements alone. Nevertheless, much information is available from LD measurements.

For example if any LD is present, resolution of overlapping absorption bands is possible (see discussion section).

The LD measurements described here are for oriented BChl proteins LH-R26 and B800+850 from R-26 mutant and wild type Rps. sphaeroides. The LD of LH-R26 allows resolution of overlapping absorption bands. To confirm this resolution, the circular dichroism, CD, of the protein was reinvestigated and accurately quantitated. CD was reported previously by Austin (24). Also, LD measurements of LH-R26 reconstituted in lipid bilayers is reported and compared to native membranes.

Materials and Methods

a) Protein preparation: Light harvesting proteins LH-R26 and B800+850 were prepared as in reference (13) or as in Appendix I. The proteins were concentrated by dialysis against 10 mM Tris-HCl, pH 7.6, henceforth called buffer. After centirfugation, the proteins were resuspended in buffer containing 3.5 mM SDS to an absorbance of 25/cm at the near infrared maximum near 850 nm. Due to the labile nature of the 800 nm band 0.05 M dithioerythritol was included in the final solution of the B800+850 protein.

b) Reconstituted bilayer vesicles: Egg phosphatidyl choline was prepared from egg yolks by the method of Singleton et. al. (25). Commercial egg lecithin (Pierce) and dioleolyl lecithin (P-L Biochemicals) were also suitable. The reconstitution method was essentially that of Hong and Hubbell (26). In a test tube an aliquot from a stock solution of

lipid was dried under a stream of nitrogen. Residual solvent was removed under vacuum. An SDS solution in buffer was added to give a molar detergent:lipid ratio of 100:1. The mixture was sonicated at 0°C under nitrogen atmosphere until the lipid was dispersed, several minutes with the bath type sonicator or 60 seconds with the probe type. The SDS solution of the protein preparation was added to give a lipid to protein weight ratio of 1:1 to 3:1. Vesicles were formed by dialyzing the mixture against 2 liters buffer for 3 to 4 days with frequent changes of buffer. Dialysis was performed at 4°C in the dark with nitrogen bubbling through the buffer to prevent photooxidation of BChl. RCs were reconstituted using DDAO and egg phosphatidyl choline.

It was found that protein did not disperse evenly in the lipid phase. To remove extraneous lipid, the reformed bilayers were layered over a glycerol density gradient, typically 4 to 80% glycerol, and centrifuged at 150,000g for 5 hours. Protein-lipid bilayers sedimented into the gradient to a density of approximately 1.1 g/ml. Extraneous lipid remained at the top of the gradient. Glycerol was removed by dialysis.

Vesicles and chromatophores were negatively stained with uranyl acetate and examined in a Zeiss EM-9S2 electron microscope.

c) Linear dichroism in PVA: Low molecular weight polyvinyl alcohol (PVA) (Touzart et Matignon) was dissolved as a 35% solution in 50mM Tris-HCL to a final pH 7.0. One

half to 2 ml of the concentrated protein solution was mixed with 2.5 ml PVA solution at 20°C. After allowing the bubbles to rise over night, the solution was spread over a glass microscope slide, 25x76 mm, and dried in a nitrogen atmosphere at room temperature in the dark. The PVA film was peeled off the glass slide and hydrated at 100% humidity for 1 hour. A center portion was cut, clamped into a simple stretching device and stretched slowly to about half maximum. The film was rehydrated for 30 min. before stretching to the final value. The extent of stretching was measured by stretch ratio, Rs, as defined by Land (27). Stretch ratio is the axial ratio of the ellipse into which a hypothetical circle on the film is distorted.

Absorption measurements were performed using a Cary 14 recording spectrophotometer with a Hamamatsu R928 photomultiplier. Glan-Thompson prisms were mounted in sample and reference beams. The plane of the PVA film was mounted perpendicular to the beam with the stretch axis vertical. Absorption spectra with polarizations parallel and perpendicular to the stretch axis were measured by rotating the polarizing prisms for vertical and horizontal polarizations, respectively. Baselines with vertical and horizontal polarizations were measured separately. Absorption of films made and stretched with no proteins present was coincident with the baseline after correcting for the baseline shift at 930 nm. The baseline shift was attributed to reflection and a small amount of light scattering. The plane of the PVA film was

tilted by mounting dry films on a goniometer, with the rotation axis vertical and passing through the center of the beam.

Reconstituted lipid-protein bilayers and native chromatophore membranes were oriented in PVA films by the same techniques.

d) Circular dichroism (CD) measurements: CD spectra were recorded on an instrument described by Sutherland et. al. (28). The S-1 photomultiplier tube could not be standardized with camphor sulfonic acid (CSA) due to poor sensitivity to 290 nm light. The S-1 was standardized with a methanol solution of N-dithiocarbethoxy-L-alanine ($\Delta A$ $\lambda$ max = 340 nm) (29) which had been calibrated against CSA using a S-20 PM tube. Both CD and absorption spectra were digitized manually on a wavenumber scale with points every 20 cm-1 ($Q_y$) or 40 cm-1 ($Q_x$). Curve resolution was obtained using GAMET, a computer program using Gauss's method of non-linear least squares (30). Corresponding resolved absorption and CD components were set to have equal halfwidths and positions. Rotational and dipole strengths were calculated from the areas under the resolved curves using the equations of Schellman (31).

## Results

### LH-R26

The absorption and circular dichroism (CD) of the LH-R26 protein are presented in Figure II-2. The spectra show

FIGURE II-2

Abosrption (a) and circular dichroism (b) of the LH-R26 protein. Exciton induced CD is evident in both $Q_x$ (550-650 nm) and $Q_y$ (820-920 nm) regions.

A

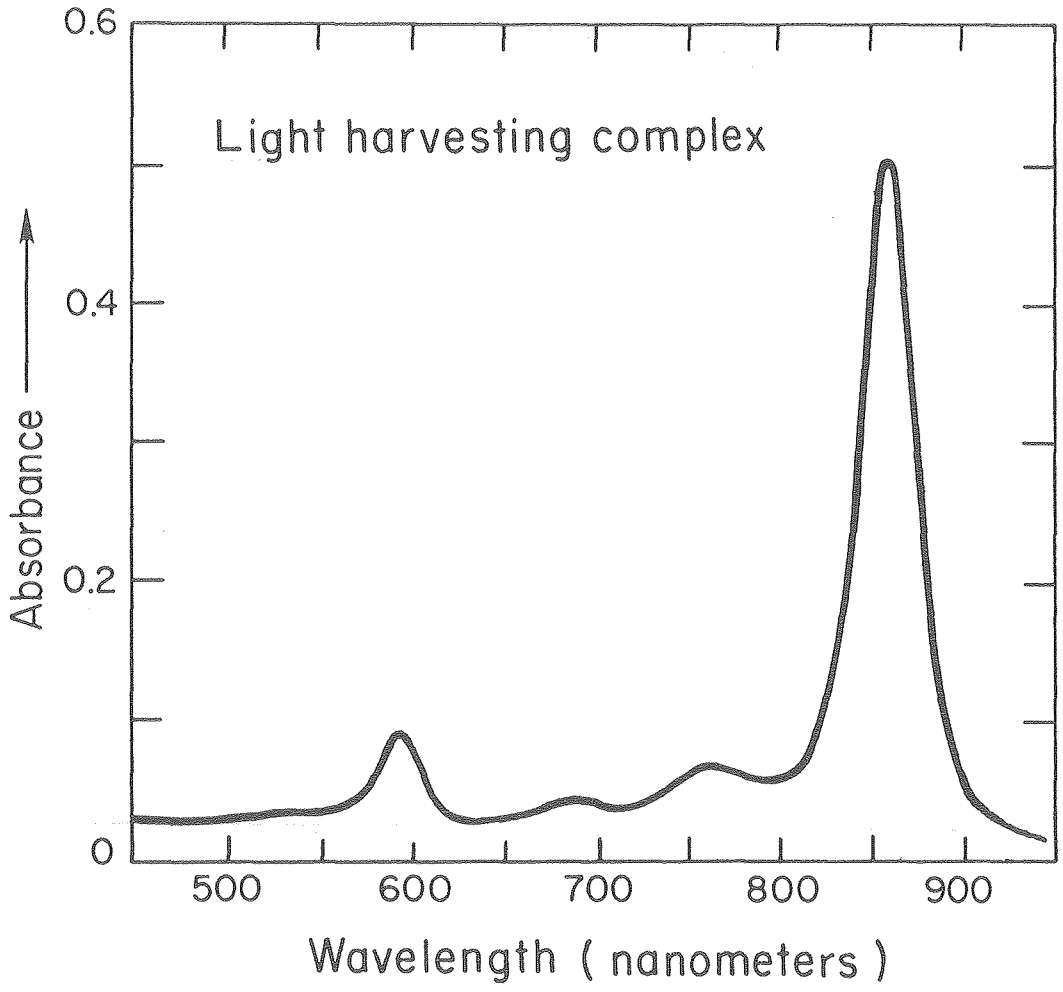


XBL 796-4865

B

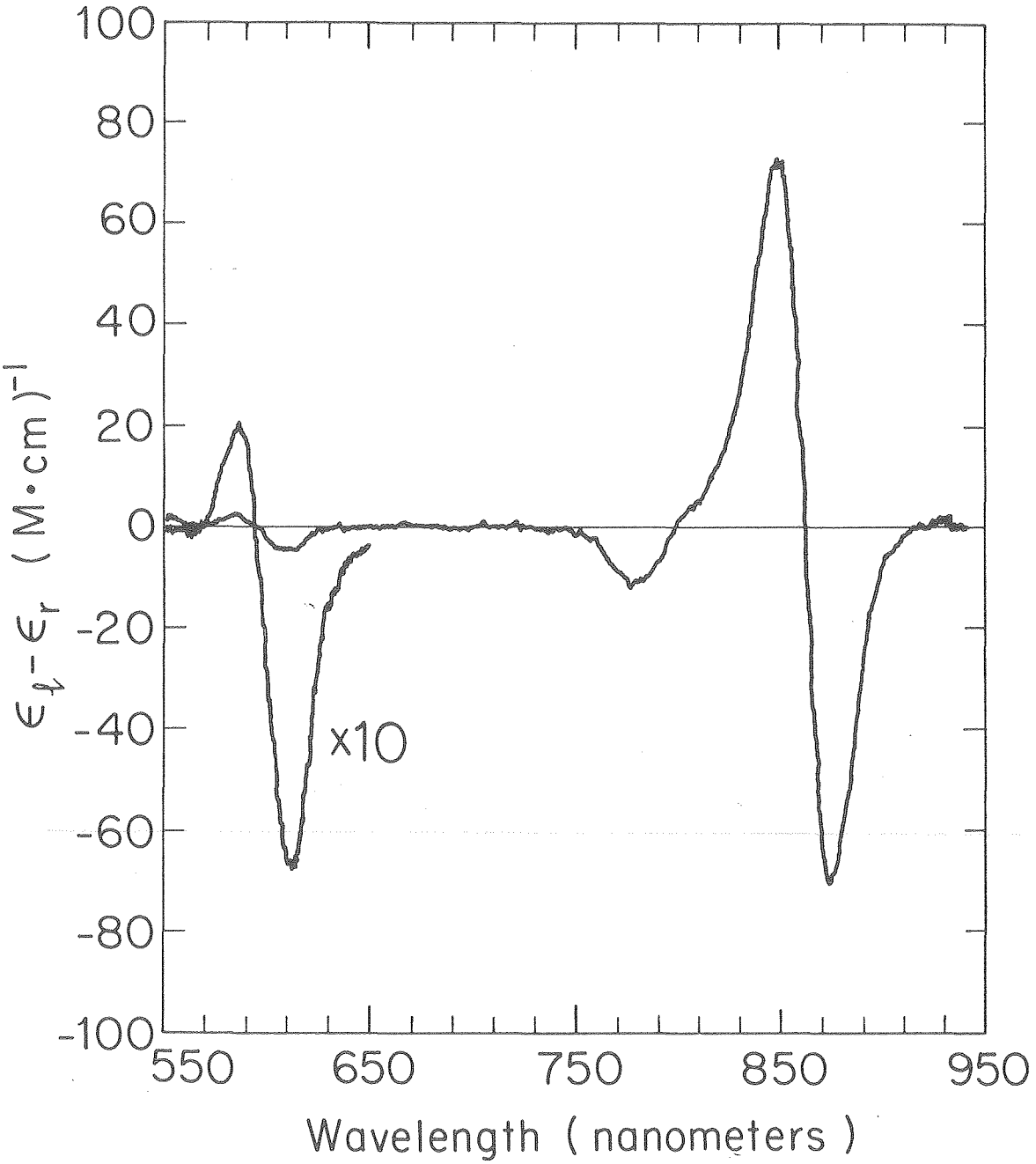


XBL795-4775

exciton induced CD in both $Q_x$ (550-650 nm) and $Q_y$ (820-920 nm) absorption bands. Linear dichroism (LD) of LH-R26 is induced by embedding the protein in PVA film and stretching the film. LD is positive ($A_{\parallel} > A_{\perp}$) in the $Q_y$ region and negative in the $Q_x$ region (Figure II-3). In the $Q_y$ region the dichroic ratio ($A_{\parallel}/A_{\perp}$) varies with wavelength. This suggests the presence of more than one transition of differing dichroic ratio in the absorption band. In the $Q_x$ region LD is constant within the estimated uncertainty of the measurement.

As described in the discussion section, both LD and CD can be used to resolve the $Q_y$ absorption band into its components $A_+$ and $A_-$. The results are presented in Table II-1.

B800+850

The light harvesting component B800+850 has a similar LD spectrum, Figure II-4, which is positive in $Q_y$ and negative in $Q_x$. In the $Q_y$ region the dichroic ratio is slightly greater in the long wavelength edge, as observed for LH-R26. However, in the B800+850 protein there is a dramatic change in dichroic ratio across the $Q_x$ absorption band. The dichroic ratio of carotenoid absorption band is constant from 440-520 nm.

The dependence of LD on extent of stretching was investigated. As shown in Figure II-5, dichroic ratios approach constant values at stretch ratios greater than three.

Reconstituted lipid protein vesicles

Linear dichroism of bilayer vesicles containing LH-R26 is presented in Figure II-6. Again LD is positive in $Q_y$ and

FIGURE II-3

Absorption parallel ($A_{||}$) and perpendicular ($A_{\perp}$) to the stretch axis is shown for the LH-R26 protein in stretched polyvinyl alcohol film. In the $Q_y$ region Rs = 2.5. A more concentrated sample was used for better precision in the $Q_x$ region, and Rs = 3.1.

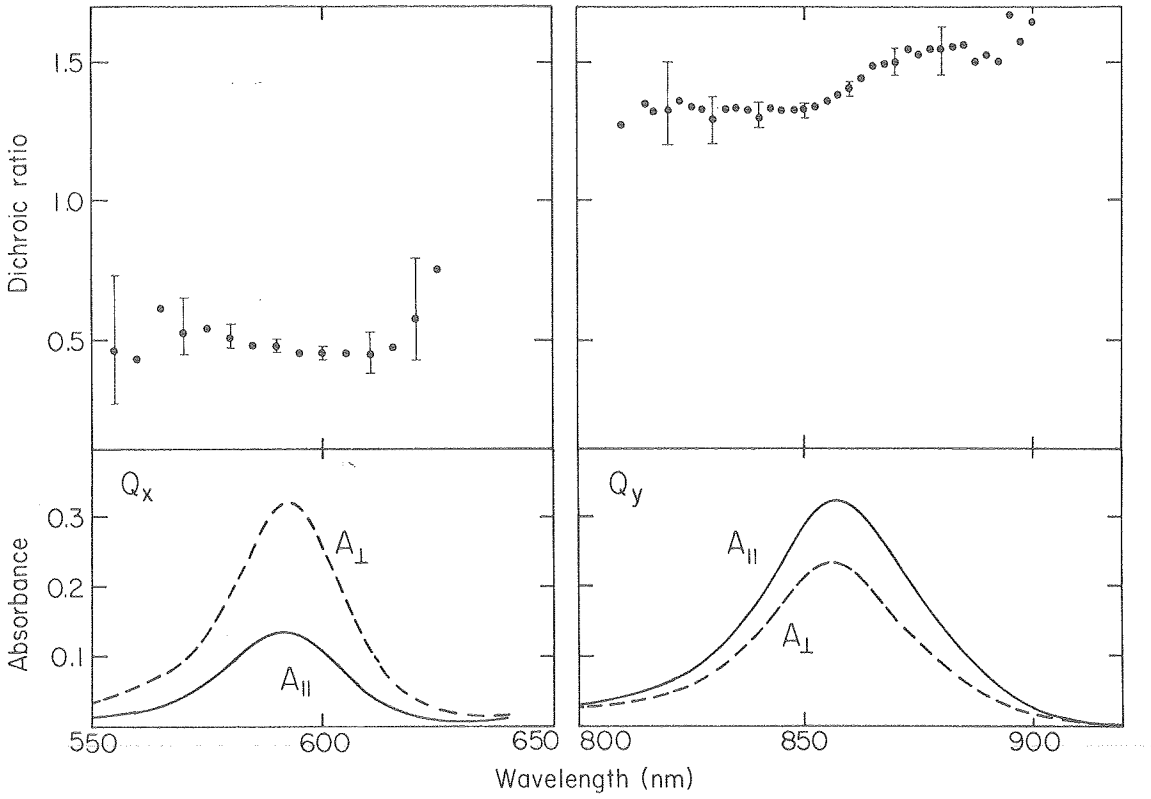


XBL 788-4099 A

FIGURE II-4

Absorption parallel and perpendicular to the stretch axis for the B800+850 protein in stretched polyvinyl alcohol. Rs = 2.9.

FIGURE II-4

Absorption parallel and perpendicular to the stretch axis for the B800+850 protein in stretched polyvinyl alcohol. Rs = 2.9.

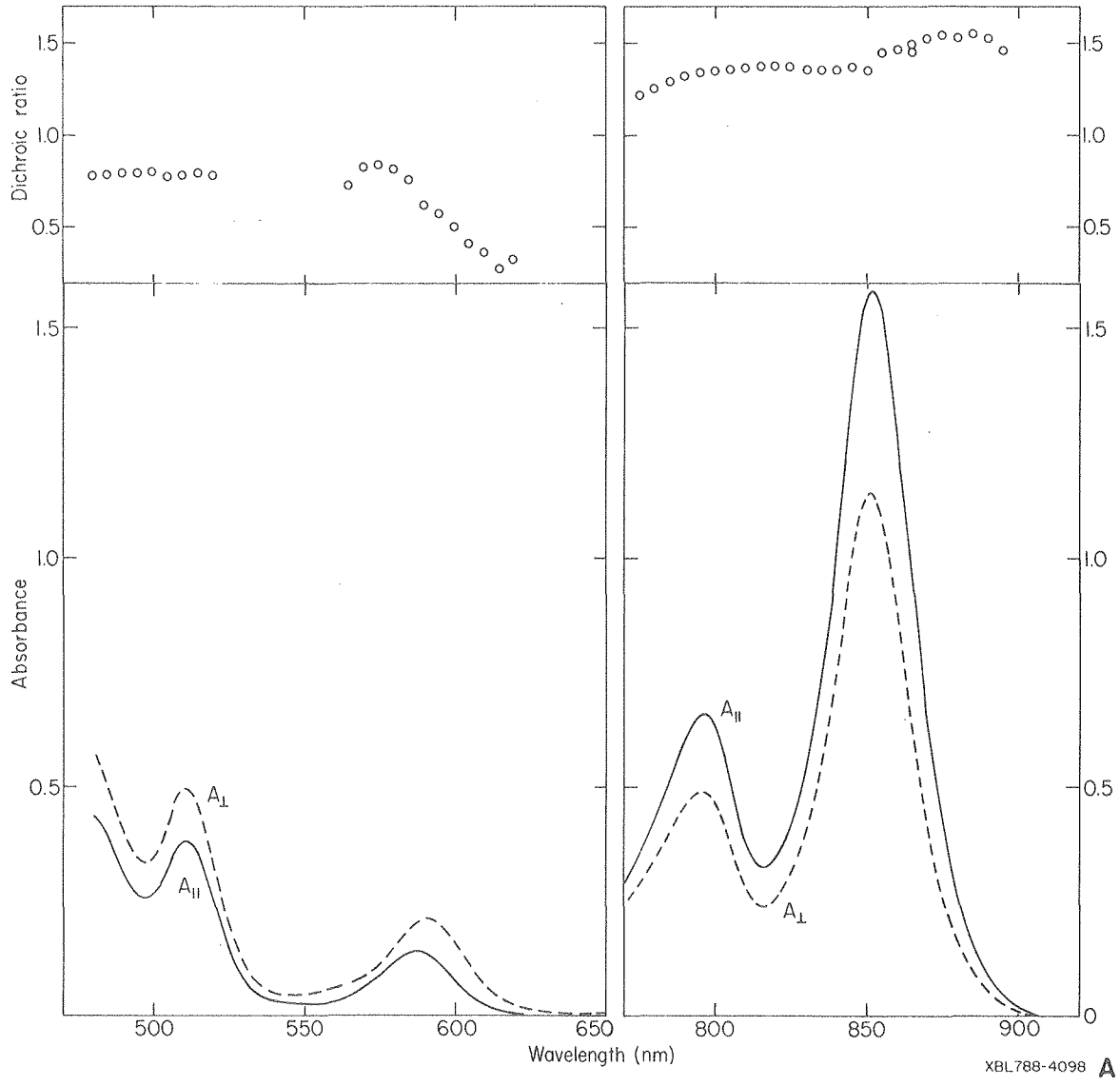
Dichroic ratio
1.5
1.0
0.5
Absorbance
1.5
1.0
0.5
A⊥
A∥
500
550
600
650
800
850
900
0
Wavelength (nm)
XBL788-4098 A

FIGURE II-5

The dependence of dichroic ratio on stretching. The sample is B800+850 in PVA. $A_{\parallel}/A_{\perp}$ is plotted versus stretch ratio at several wavelengths.

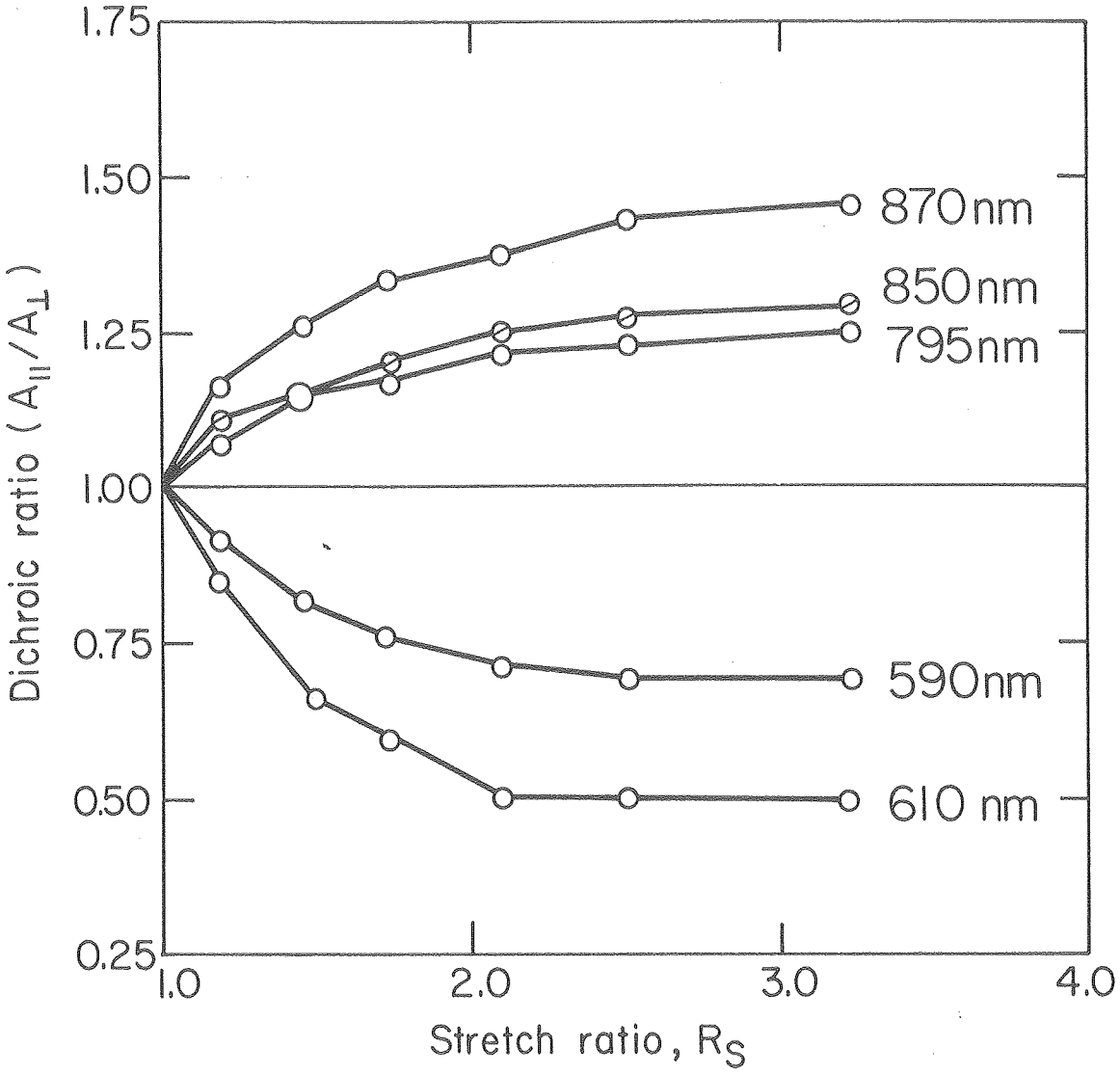
1.75
1.50
1.25
1.00
0.75
0.50
0.25
1.0
2.0
3.0
4.0
Dichroic ratio ( $A_{\parallel}/A_{\perp}$ )
Stretch ratio, $R_S$
870nm
850nm
795nm
590nm
610 nm

XBL 787-4092

FIGURE II-6

Linear dichroism of reconstituted lipid-protein vesicles containing LH-R26. Vesicles are oriented in PVA; Rs = 3.0.

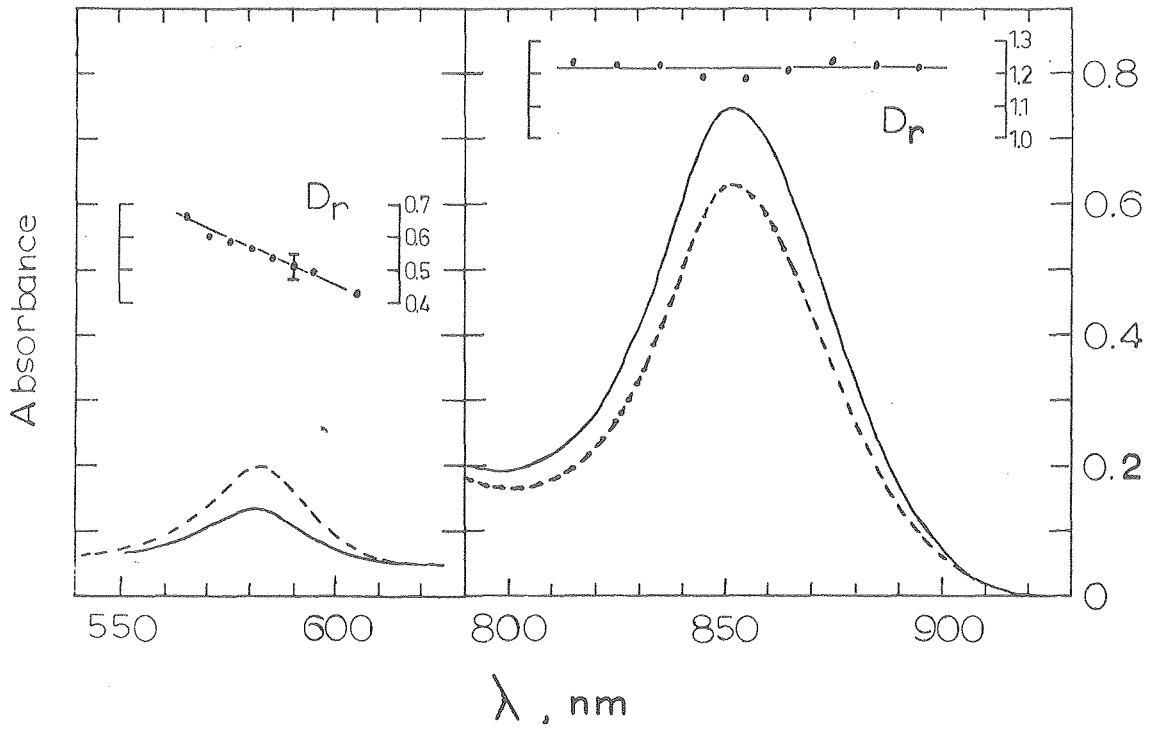


XBL 7912-13644

negative in $Q_x$. However the values of dichroic ratio are less than for oriented proteins. Also, no change in LD is observed across the $Q_y$ absorption band.

Electron micrographs of reconstituted LH-R26 protein showed flattened vesicles of 500 to 2000 Å in diameter. Chromatophores were typically 500 to 1500 Å in diameter. Reaction centers were also reconstituted. RC vesicles were 1500 to 4000 Å in diameter. Controlled dehydration by two freeze-thaw cycles fused RC vesicles into sheets of greater than 1 micron in diameter.

## Discussion

### LH-R26

As discussed by Sauer and Austin (24) the CD of LH-R26 (Figure II-2) reveals exciton coupling between the two BChls associated with the protein. Exciton interaction has been described by Tinoco, Kasha and others (32). For purposes of discussion, their results are presented here. The degenerate energy levels and allowed transitions of monomeric chromophores in molecular aggregates are split into nondegenerate levels and transitions by their mutual interaction. Figure II-7 gives a schematic representation of monomer and dimer energy levels. Exciton interaction is approximated by dipole-dipole interaction of the degenerate monomer transition dipole moments. The magnitude of energy level splitting ($2V_{12}$), the dipole strengths of exciton transitions ($D_{\pm}$) and the rotational strengths of induced circular dichroism ($R_{\pm}$) are given by equations [2-5]:

FIGURE II-7

Monomer and exciton dimer energy levels and transition frequencies. Exciton levels are split by $2V_{12}$.

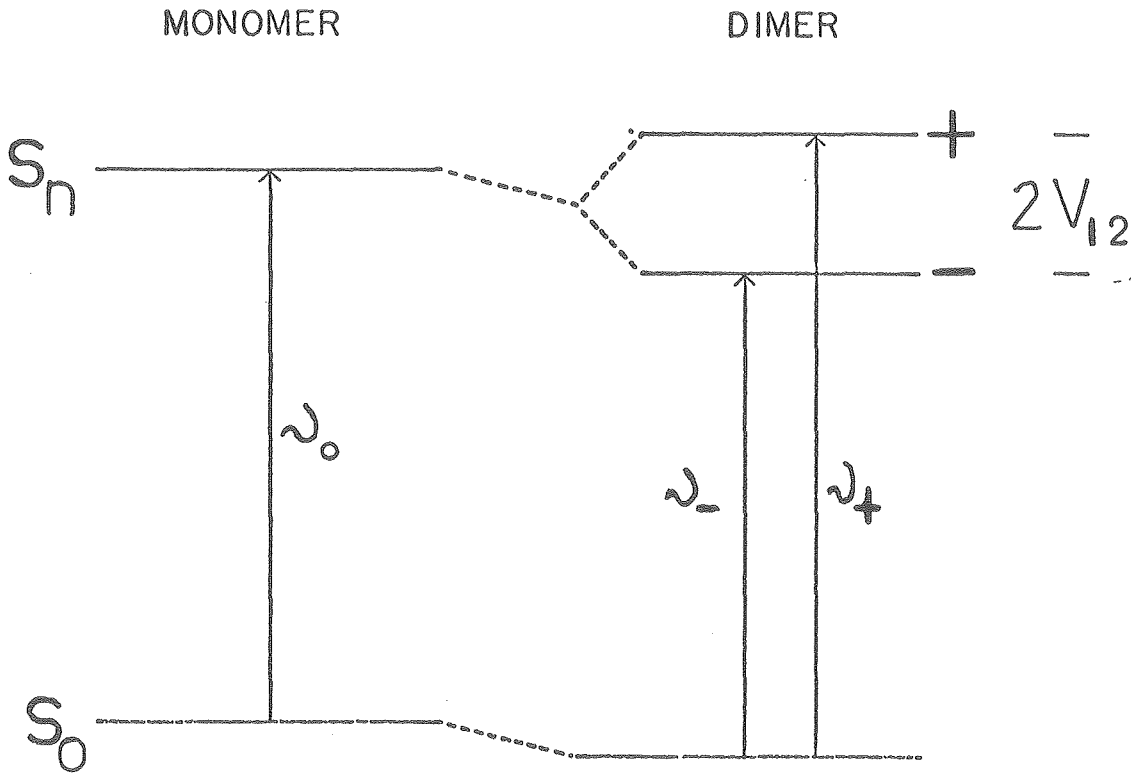


XBL 7912-13639

$$\nu_{\pm} = \nu_o \pm V_{12}/hc \qquad [2]$$

$$V_{12} = \frac{1}{r_{12}^3}\left[\underset{\sim}{\mu}_1 \cdot \underset{\sim}{\mu}_2 - 3\frac{(\underset{\sim}{r}_{12}\cdot\underset{\sim}{\mu}_2)(\underset{\sim}{r}_{12}\cdot\underset{\sim}{\mu}_2)}{r_{12}^2}\right] \qquad [3]$$

$$D_{\pm} = |\underset{\sim}{\mu}|^2 \pm \underset{\sim}{\mu}_1\cdot\underset{\sim}{\mu}_2 = D_o \pm \underset{\sim}{\mu}_1\cdot\underset{\sim}{\mu}_2 \qquad [4]$$

$$R_{\pm} = \mp \tfrac{1}{2}\pi\nu_o(\underset{\sim}{r}_{12}\cdot\underset{\sim}{\mu}_1 \times \underset{\sim}{\mu}_2) \qquad [5]$$

where $\nu_o$ and $D_o$ are the frequency and dipole strength of the monomer transition. $\underset{\sim}{\mu}_1$ and $\underset{\sim}{\mu}_2$ are the monomer transition dipoles, and $\underset{\sim}{r}_{12}$ is the vector connecting the centers of the two monomers. The two exciton transition moments are predicted to be mutually perpendicular. Ratios of dipole strengths or rotational strength to monomer dipole strength depend only on the geometry of the aggregate. For example:

$$\frac{D_+}{D_-} = \frac{1 + \cos\beta}{1 - \cos\beta} \qquad [6]$$

where $\beta$ is the angle between monomer transition dipoles.

The dimer CD spectra are predicted to have equal and opposite components at transition frequencies $\nu_+$ and $\nu_-$. The rotational strength, R, should sum to zero across the overall band. A CD of this type is termed "conservative". The CD of LH-R26 in the near infrared region, $Q_y$, Figure II-2, appears to be a convolution of overlapping bands of nearly equal magnitude and opposite sign. As discussed by Dratz, et. al. (33) monomeric contribution to CD will distort the conservative nature of exciton CD. In the $Q_x$ region of LH-R26 this is apparent.

The CD spectra of LH-R26 were used to deconvolute the absorption bands into their two exciton components. Each CD component has a corresponding component in the absorption spectrum. Furthermore the band shapes of CD and absorption are predicted to be the same (33). By simultaneously fitting the CD and absorption curves enough restrictions can be made to give a unique solution (30). First, the CD or absorption curves were restricted to only two absorption components each. Symmetrical gaussians were chosen to limit the number of parameters. Both gaussians had equal half widths; position and magnitude were allowed to vary. However, the position of corresponding absorption and CD gaussians are the same. CD gaussians were further restricted to equal magnitude and opposite sign. To remove the monomer CD contribution in the $Q_y$ region, the negative CD component was inverted about the zero crossing point (862 nm, 11,600 $cm^{-1}$) to generate the positive component. The resulting CD curve fitted the experimental curve very closely, leaving a residual monomer CD of about one-tenth the magnitude of the exicton-induced CD. In the $Q_x$ region, the monomer CD contribution is much larger. To subtract monomer CD, the absorption band was multiplied by a variable factor and subtracted from the experimental CD curve until the resulting CD curve was conservative. The deduced monomer CD contribution in both the $Q_x$ and $Q_y$ regions are similar in sign and magnitude to monomer CD of BChl in polar organic solvents (3). This agreement supports the validity of the approximations. However the recent work of

Wright and Boxer shows that the CD sign can change in a protein complex (36).

CD-Absorption band deconvolution is presented in Figure II-8. Given the restrictions placed on the fitting procedures, the fits are good. The fits deviate from experimental points at the higher energy side of the absorption bands where vibronic components contribute. The dipole and rotational strengths of the deconvoluted spectra are presented in Table II-1.

Linear dichroism may also be used to resolve the $Q_y$ absorption into two components. Fewer assumptions are involved than for CD convolution. Figure II-3 gives the LD of LH-R26 in stretched PVA film. Note that the dichroic ratio, $D_r$, is constant at short wavelengths, 800-850 nm, increases significantly, then levels out at higher wavelengths, 875-890 nm. This sigmoid shape suggests that there are two transitions in the absorption band, one with $D_{r+} = 1.30$ at higher energy and one with $D_{r-} = 1.57$ at slightly lower energy (longer wavelength). The midpoint of the sigmoid curve is 6 to 8 nm to the red of the wavelength maximum absorbance, $\lambda$ max. The presence of two apparent electronic transitions in the $Q_y$ region is best interpreted in terms of oscillators (transition moments) with unequal strengths. We identify these transitions as the exciton transition moments of the dimer. Alternatively, the two transitions could represent two monomeric BChls of slightly different environments and, therefore, at different energies. This would

FIGURE II-8

Simultaneous deconvolution of LH-R26 CD and absorption. Monomeric contributions to the CD have been subtracted as described in the text.

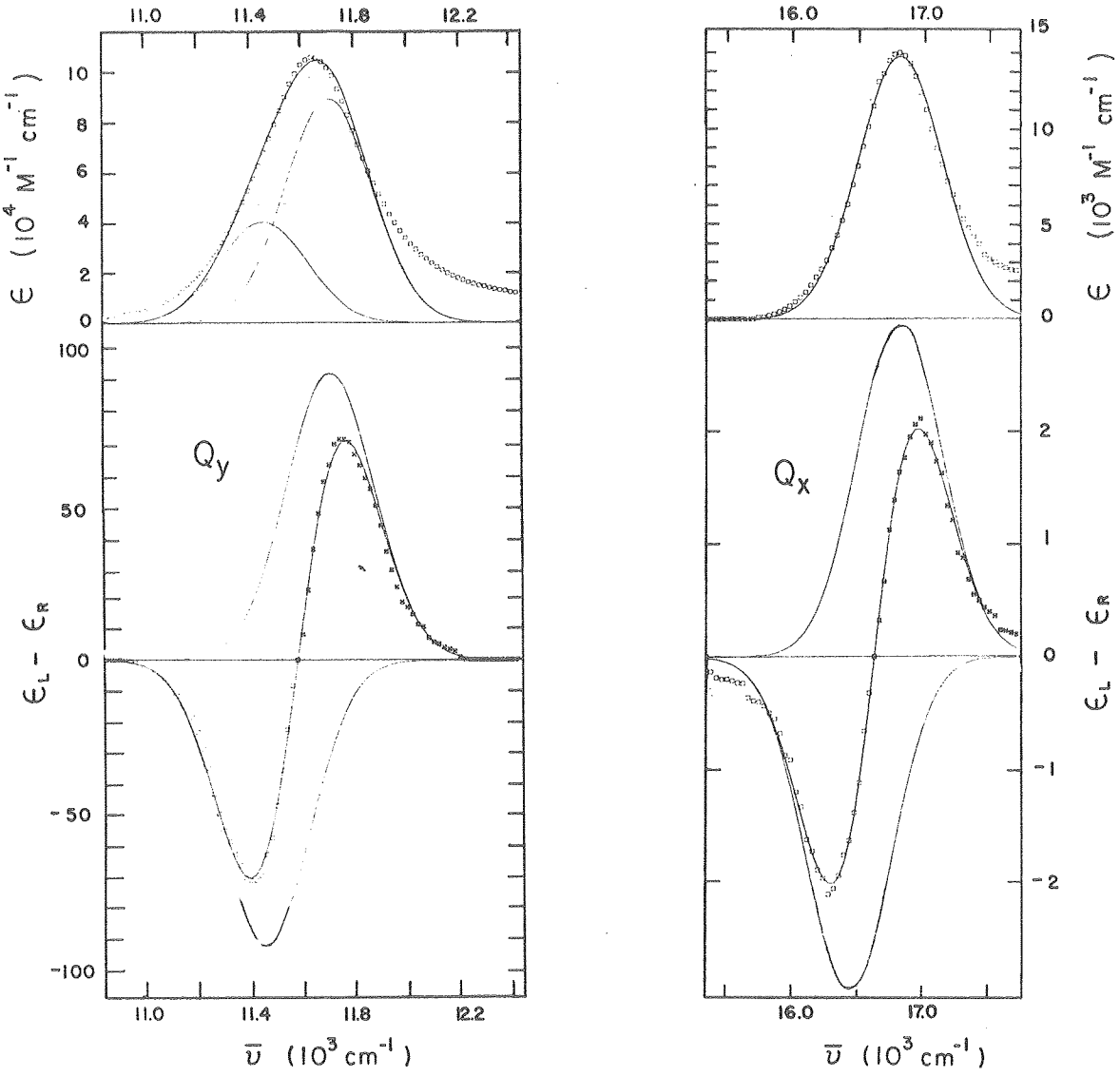
11.0
11.4
11.8
12.2
16.0
17.0
ε (10⁴ M⁻¹ cm⁻¹)
ε (10³ M⁻¹ cm⁻¹)
Qy
Qx
εL - εR
ν̄ (10³ cm⁻¹)
XBL 7912-13645

TABLE II-1

ABSORPTION AND CD PROPERTIES OF LH-R26 RESOLVED EXCITON BANDS

| Absorption Band | Method | | $\bar{\nu}(cm^{-1})$[a] | $2V_{12}$ ($cm^{-1}$) | Dipole Strength (Debye)$^2$ | Rotational Strength (Debye·Bohr magneton) | $\frac{R_{\pm}}{D_o}$ | $\frac{D_+}{D_-}$ | $\beta$[b] |
|---|---|---|---|---|---|---|---|---|---|
| LH-R26 | | | | | | | | | |
| $Q_y$ | CD | $D_+$[c] | 11708±25 | 252 | 67.1±2.0 | +1.64±1.0 | 0.033 | 2.16 | 68±3° |
| | | $D_-$ | 11456±25 | | 31.0±2.0 | -1.64 1.0 | | | |
| | LD | $D_+$ | 11730±30 | 208 | (59.3±3.5[d] | -- | -- | 1.53 | 78±4° |
| | | $D_-$ | 11527±30 | | (38.3±3.0 | | | | |
| $Q_x$ | CD | $D_+$ | 16622±40 | 404 | 12.0±0.6 | +0.17 | 0.014[e] | >19[e] | 0±25° |
| | | $D_-$ | 16420±40 | | 0±0.6 | -0.17 | | | |
| | LD[f] | | -- | -- | -- | -- | -- | -- | ~0° |
| BChl[h] | | | | | | | | | |
| $Q_y$ | | | 36.9 | | +0.054 | | | | |
| $Q_x$ | | | 14.9 | | -0.047 | | | | |

[a] From $\lambda$ max.

[b] From equation [6].

[c] Assuming $V_{12}$ is positive, equation [3].

[d] From $2D_o$ of CD Calculation and $D_+/D_-$ ratio from LD.

[e] D was found to be zero; ratio calculated from uncertainty.

[f] $Q_x$ not resolved.

[g] $Q_x$ monomers are parallel if all dipole strength is one exciton band.

[h] References (1) and (30).

result in a CD crossing and dichroic ratio transition with midpoint centered at the peak of the absorption curve, in conflict with the observed results.

To resolve the absorption band we must assume only that the limiting values of dichroic ratios, the plateau regions of the sigmoid curve, represent the dichroic ratios of the individual exciton transitions. For the perfect uniaxial orientation of proteins (see below) the isotropic absorption of the sample is given by:

$$A = A_{||} + 2A_{\perp} = A_{+} + A_{-}$$

and

$$A_{\pm} = A_{\pm||} + 2A_{\pm\perp} \qquad [7]$$

Absorption parallel and perpendicular to the stretching direction are given by:

$$A_{||} = A_{+}\cos^2\theta_{+} + A_{-}\cos^2\theta_{-}$$

$$A_{\perp} = \tfrac{1}{2}A_{+}\sin^2\theta_{+} + \tfrac{1}{2}A_{-}\sin^2\theta_{-} \qquad [8]$$

where:

$$\theta_{\pm} = \arctan[2/Dr_{\pm}]^{\frac{1}{2}}$$

Combining equations [7] and [8]:

$$A_{\pm} = \frac{2A_{\perp}D_{\pm} - A_{||}}{\tfrac{1}{2}D_{\pm}\sin^2\theta_{\pm} - \cos^2\theta_{\pm}} \qquad [9]$$

Using equation [9] the exicton components, $A_{+}$ and $A_{-}$ can be resolved at every wavelength. Equation [9] is a slight simplification of equation [4] of reference (13). The resolution of LH-R26 $Q_y$ is shown in Figure II-9. The resolution does not depend on either the degree of order (f) or the

FIGURE II-9

Deconvolution of $Q_y$ absorption of LH-R26 using linear dichroism.

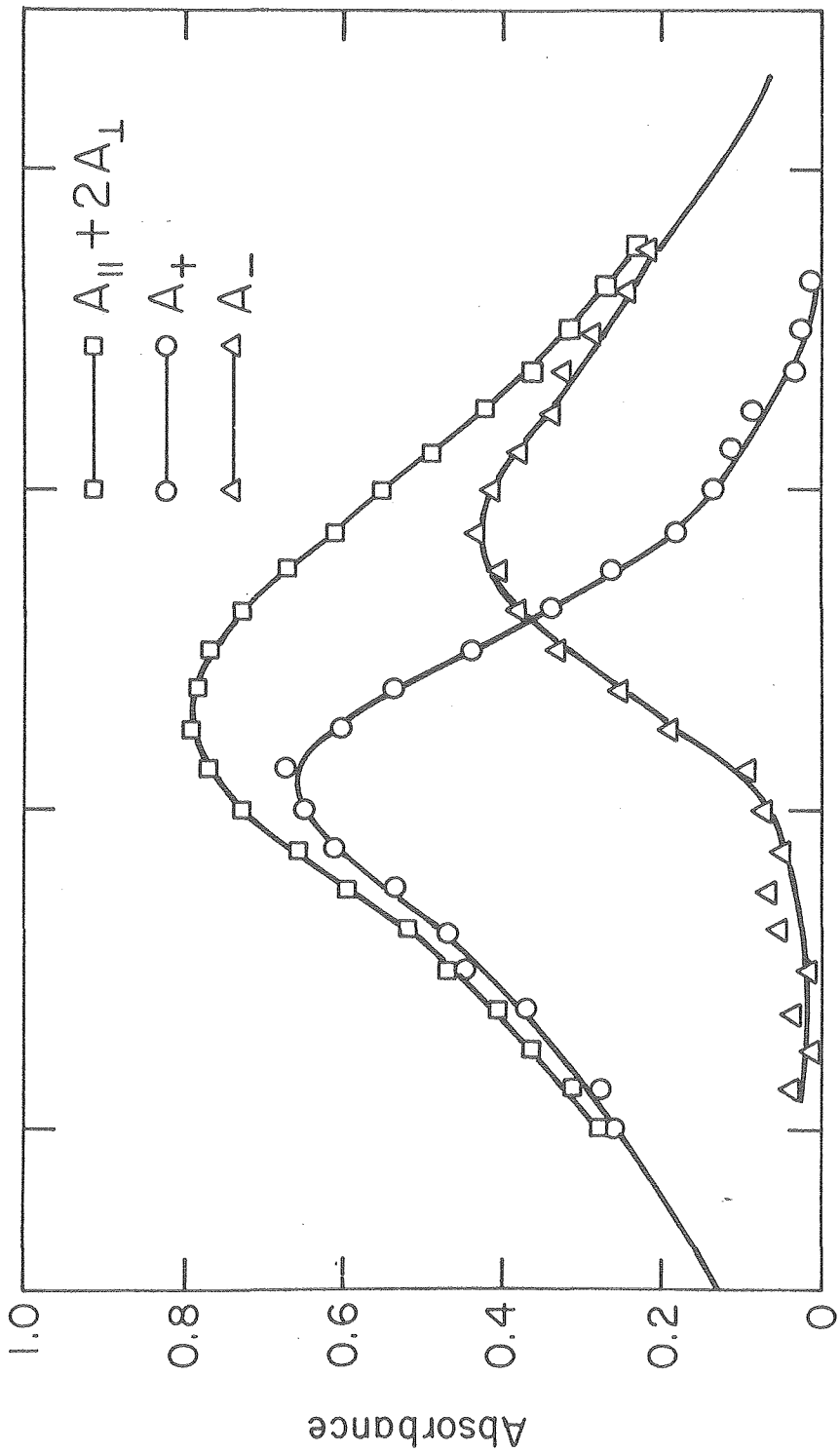


XBL 788-4094 A

choice of orientation (prolate or oblate protein shape); see below.

Several features of the resolution should be noted. First, the assignment of a + and - to the resolved transition bands represents the relative energies, not the absolute sign of the wavefunctions and, therefore, does not correspond directly with equations [2] - [5]. If $V_{12}$ is positive, the signs in Figure II-9 agree with equations [2] - [5]; if $V_{12}$ is negative, the signs should be reversed. From the relative areas under the absorption bands, the ratio of dipole strengths is 1.53. This corresponds to an angle of $78^{o}$ between the two $Q_y$ monomer transition dipoles, from equation [6]. This result agrees reasonably with $68^{o}$, derived from a ratio of 2.2 found using CD band resolution. The peak to peak separation is probably a valid representation of the exciton splitting. The splitting, $2V_{12}$, of 208 $cm^{-1}$ from LD resolution agrees reasonably with 251 $cm^{-1}$ from CD resolution. These results are summarized in Table II-1.

The shapes of the LD resolved bands are not gaussian. Both bands are skewed away from the center. The band shape is a direct result of the shape of the dichroic ratio curve, Figure II-3. The actual band shape of the exciton transition is important in theories which include the vibronic nature of exciton absorption bands. See reference (34) for one treatment. The band shape differences between the LD resolution and the gaussian CD resolution account, in part, for the differences in exciton splitting and dipole strength.

The lack of observable change in dichroic ratio in the $Q_x$ region of LH-R26 can be interpreted in two ways. The dipole strength of one of the exciton transitions is much greater than the other. The CD resolution suggests this possibility. In the CD resolution, no dipole strength was found for the lower energy CD band. In the vector model of exciton coupling (32), this predicts side-by-side $Q_x$ monomer orientation. Alternatively, the two $Q_x$ exciton transitions could make the same angle to the protein particle axis, resulting in identical dichroic ratios. The CD results favor the former interpretation.

To describe the orientation of LH-R26 in the stretched PVA film in a picture analogous to Figure II-1, quantitative values of the angles are needed. It is necessary to establish a model for the orientation phenomenon. First we will assume that the protein particle has a unique long axis which orients along the stretch direction (the prolate model). The aggregation state of LH-R26 in SDS solution is a simple dimer, 2 BCHls with two 10,000 dalton polypeptides (24). Unfortunately, the state of aggregation is not easily probed in the PVA glass. The absorption and CD spectra are unaffected by incorporation into PVA, and the films show no sign of particle aggregation and are optically clear. For these reasons we treat the LH-R26 protein as an individual unit. We cannot rule out the possible formation of small aggregates; the dichroism observed shows that such aggregation would not be random.

According to the model of Fraser, the degree or orientation can be described by a fraction, f, of particles aligned perfectly with the stretch axis and a fraction, 1-f, randomly oriented (18). The dichroic ratio, $D_r$, can be expressed as a function of f and $\theta$, the angle of the transition dipole to the particle axis:

$$D_r = \frac{A_{||}}{A_{\perp}} = \frac{f\cos^2\theta + 1/3(1-f)}{\frac{1}{2}f\sin^2\theta + 1/3(1-f)} \qquad [10]$$

Other choices for plausible distribution functions can be related to equation[10] (18).

Two approaches were used to assess the orientation parameter f. The first is based on the restrictions inherent in equation [10]. In figure II-10 f is plotted as a function of $\theta$ and $D_r$. Typical values for the dichroic ratio are 1.55 ($Q_y$) and 0.4 ($Q_x$), which restrict f to values greater than 0.15 and 0.5, respectively. Since f must be the same for all dipoles within the same sample, we restrict it to values greater than 0.5. For dichroic ratios close to 1, the choice of f is not critical; but for increasingly greater dichroism, the value of $\theta$ varies with f more significantly. Another approach is to plot the dichroic ratios as a function of amount of stretching. Figure II-5 plots $D_r$ versus $R_s$ at various wavelengths for a sample of the B800+850 protein. With stretch ratio greater than 3 the dichroic ratios approach limiting values. This implies that a maximum value of f has been reached, but it does not imply that f

FIGURE II-10

Dependence of $\theta$, angle between the unique particle axis and transition dipole moment for several values of dichroic ratio, $D_r$. Values of $D_r$ are labeled for each curve. Plotted from equation [10], (a) prolate and equation [11], (b) oblate. Unique axis is the long axis in (a) and the short axis in (b).

a) Prolate

b) Oblate

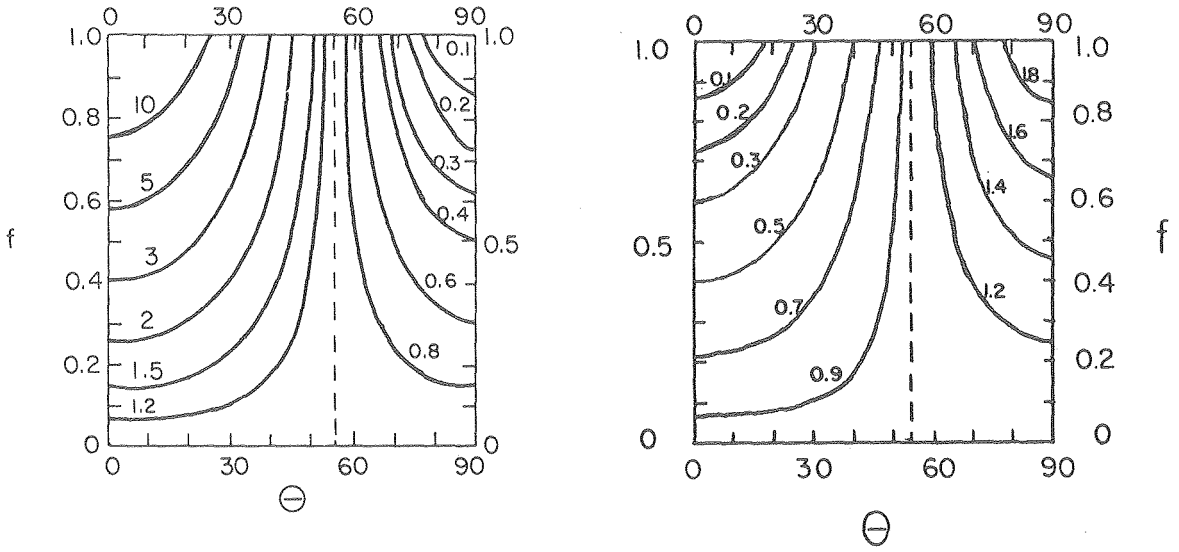


XBL 7912-13643

equals 1. The restrictions illustrated in Figure II-10a seem more definative. Table II-2 lists values of $\Theta$ based on observed dichroic ratios using several possible values of the orientation parameter.

Alternatively, the protein particle could be pictured as oblate shaped, with a unique short axis. For this model,

$$D_r = \frac{f\sin^2\Theta + 2/3(1-f)}{f\cos^2\Theta + f\tfrac{1}{2}\sin^2\Theta + 2/3(1-f)} \qquad [11]$$

where $\Theta$ is the angle between the unique, short axis and a transition moment. Equation [11] places restrictions on possible combinations of values for f and $\Theta$, as illustrated in Figure II-10b. For the oblate case, dichroic ratios greater than 1 are more restrictive of possible values for f. The dichroic ratios of 1.55 and 0.4 restrict f to values greater than 0.6 and 0.4 respectively.

It does not seem possible to distinguish between the prolate and oblate models at this time. However, the assumption of uniaxial orientation inherent in both models was tested. The plane of the stretched film was rotated about an axis perpendicular to the measuring beam and parallel to the vertical light polarization, $A_{||}$. Dichroic ratios measured on tilted specimens were the same as for untilted films. This confirms the presence of unidirectional orientation.

Rafferty and Clayton reported orientation of reaction centers in unstretched gelatin films (12). This was a result

TABLE II-2

ANGLES OF THE TRANSITION DIPOLES TO THE LONG AXIS OF LIGHT HARVESTING PROTEINS

The values are based on equation [10]. The dichroic ratio is given in parenthesis. See text for explanation of $Q_x$ absorption bands $A_{12x}$ and $A_{3x}$.

| | Wavelength (nm) | θ(degrees) | | |
|---|---|---|---|---|
| | | f = 0.5 | f = 0.25 | f = 1.0 |
| LH-R26 | 885 (1.57) | 42.3 | 46.4 | 48.5 |
| | 835 (1.30) | 47.6 | 49.9 | 51.1 |
| | 593 (0.43) | 81.8 | 69.3 | 65.1 |
| B800+850 | 885 (1.56) | 42.5 | 46.5 | 48.5 |
| | 835,800 (1.36) | 46.4 | 49.1 | 50.5 |
| | 610 (0.38) | -- | 71.4 | 66.4 |
| | 575 (0.84) | 59.5 | 57.8 | 57.1 |
| | 510 (0.78) | 61.5 | 59.1 | 58.0 |
| | $A_{12x}$ (0.33) | -- | 73.8 | 67.9 |
| | $A_{3x}$ (1.65) | 40.9 | 45.5 | 47.8 |

of the shrinkage in thickness by a factor of 30 on drying the gelatin film. The polyvinyl films shrink to no less than one-fourth the original thickness. As a result, no dichroism was detected in unstretched PVA film when $A_{||}$ and $A_{\perp}$ were recorded with the sample tilted by 45 degrees.

B800+850

The results of Austin and Sauer (24) suggested a similarity between B800+850 and the LH-R26 protein. The light harvesting complex from wild type Rps. sphaeroides has the conservative excitonic CD centered near 850 nm with the negative component at longer wavelengths, suggestive of a BChl dimer. The protein has a third BChl which does not appear to interact with this dimer. Selective bleaching of the absorption at 800 nm does not alter the 850 nm absorption and CD properties. Sauer and Austin suggested that the LH-R26 protein is an altered form of B800+850. This belief is supported by LD results.

The LD of B800+850 is presented in Figure II-4. A change in dichroic ratio is observed across the 850 nm band, similar to the LD of LH-R26. In the $Q_x$ region a distinct change across the absorption band is observed. When dithioerythritol is omitted from the PVA film, the 797 nm absorption bleaches (not shown). This also decreases the dichroic ratio on the short wavelength side of the 590 nm absorption band but not on the long wavelength side. In solution, the selective bleaching is accompanied by a shift of the $Q_x$ $\lambda$ max from 589 nm to 592 nm. Thus the increase in

$A_{||}$ at shorter wavelengths in the $Q_x$ region of the intact B800+850 protein is correlated with the presence of the 800 nm absorption band.

The dichoric ratio across the $Q_x$ band can be used to resolve the absorption into components of the coupled BChl dimer and the monomeric BChl absorbing at 800 nm. The ratio of dipole strengths (and the area under the absorption bands) should be 2:1. The choice of limiting dichroic ratios is more difficult than for the $Q_y$ band. We define $A_{12x}$ and $D_{r12x}$ as the absorption and dichroic ratio due to the coupled BChls; $A_{3x}$ and $D_{r3x}$ are similarly defined for the third BChl. On the long wavelength side D = 0.33 is chosen in accord with the LD-R26 values. The $A_{12x}$ and $A_{3x}$ are then calculated using different values for $D_{r3x}$ in equation [9] until the area under $A_{3x}$ is half the area under $A_{12x}$. ( + and - subscripts in equation [9] are substituted by 12x and 3x). The fit is plotted in Figure II-11. $D_{r3x}$ is found to be 1.65. The $\lambda$ max for $A_{12x}$ is 593 nm in agreement with the $\lambda$ max of the LH-R26 protein. From this result and the dichroic ratio of the 800 nm absorption the orientation of the third BChl may be deduced, Figure II-12.

Quantitative values for angles between the transition moments and the protein axis of B800+850 are included in Table II-2.

As discussed in the introduction to this chapter, the assignment of LH-R26 as either a B870 or a B800+850 type of BChl complex is unclear. The biochemical evidence supported

FIGURE II-11

Deconvolution of $Q_x$ region of the B800+850 protein using linear dichroism. $A_{12x}$ represents absorption attributed to the coupled BChl pair. $A_{3x}$ represents absorption attributed to the third BChl which absorbs at 800 nm.

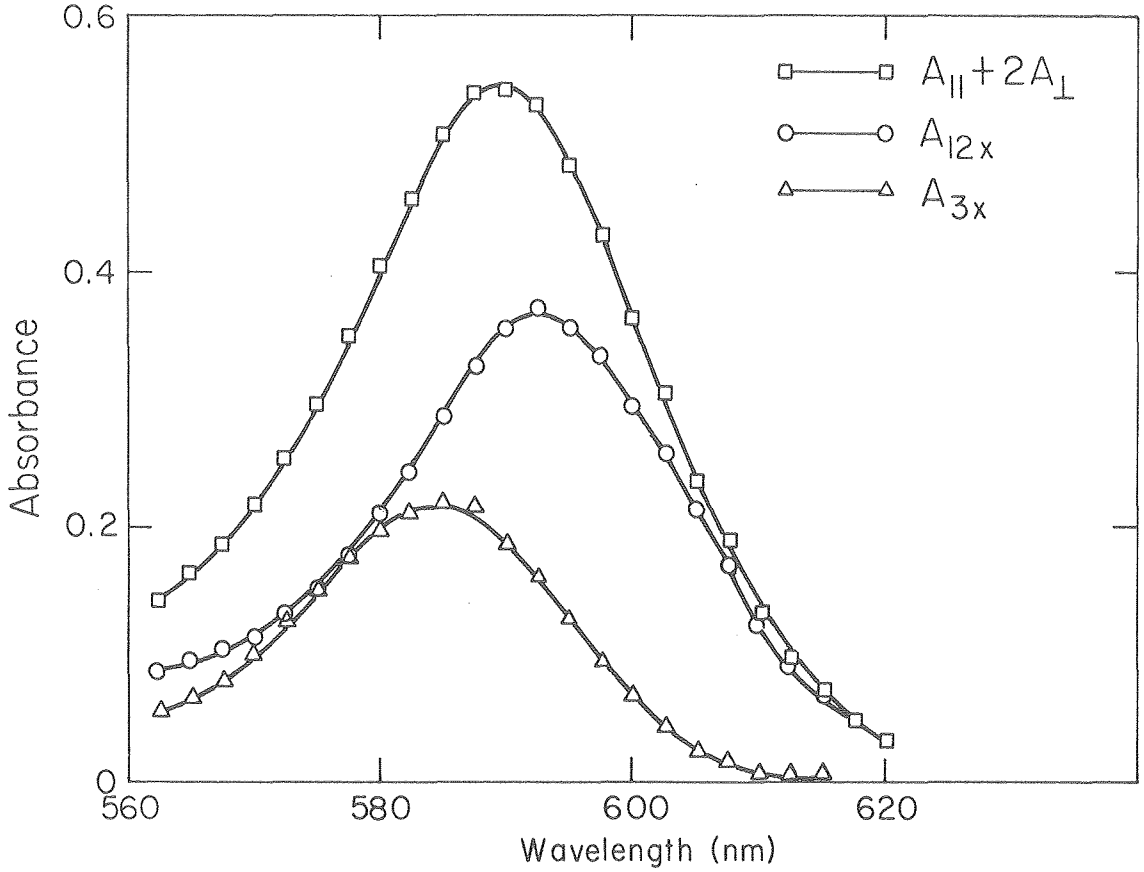


XBL 788-4097 A

FIGURE II-12

Orientations of the transition dipoles are sketched with respect to the particle stretch axis, z, using vector representation of the transition dipoles. (a) $A_+$ and $A_-$ represent the two exciton components of the 853 nm band of the LH-R26 protein. They are orthogonal, and the normal to the plane containing them makes an angle of 66 degrees with z. The exciton components of the $Q_x$ band make an angle of 65 degrees with z. (b) In the plane containing $A_+$ and $A_-$ the two monomeric transition dipoles, $A_1$ and $A_2$, are shown. (c) Additional components present in the B800+850 protein are shown. The square represents the plane of the third bacteriochlorophyll to which the 800 nm absorption is attributed.

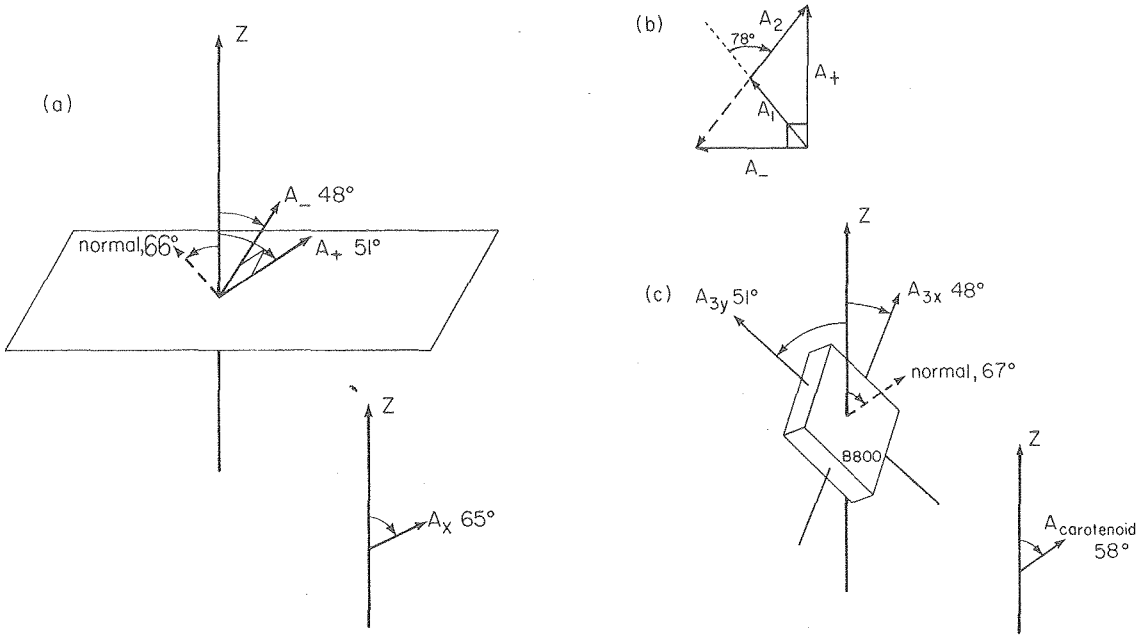


XBL 7912-13641

its assignment to the B870 class. If this assignment is correct then the LD and CD results summarized above indicate a strong similarity between the two protein complexes with respect to their BChl arrangement. Only a comprehensive biochemical characterization of the two classes of proteins will resolve the question.

Lipid-Protein Vesicles

Dichroic ratio of PVA oriented LH-R26 vesicles was 1.21 in the $Q_y$ absorption band. In the $Q_x$ region, $D_r$ varied from 0.43 at 605 nm to 0.66 at 865 nm. In an analysis similar to that of Figure II-5, it was found that maximum dichroic ratios are reached at Rs = 2.0. Assuming that the membrane planes align parallel to the stretching direction, the results can be analyzed by equation [11]. The unique axis is the normal to the membrane plane. The angle, $\gamma$ , between the membrane plane and a transition moment is:

$$\gamma = 90^{o} - \Theta$$

Assuming perfect orientation, f=1, we find the $Q_x$ transition tilted out of the plane by 49 degrees, and the $Q_y$ by 30 degrees. These results are in agreement with previous LD of native chromatophores oriented by other methods (7,9). The results suggest that the LH-R26 protein is oriented in reconstituted vesicles in a similar way to its orientation in chromatophores. LD of PVA oriented R-26 chromatophores (not shown) gave similar results to Figure II-6

In contrast to oriented proteins, the LD of oriented

LH-R26 vesicles shows no change in dichroic ratio across $Q_y$ absorption band. Since the orientation of membranes is probably different from that of the isolated proteins, the two $Q_y$ exciton transition moments may be tilted at a very similar angle to the membrane plane. Alternatively, the LH-R26 protein may orient in several inequivalent positions in the membrane. Such inhomogeneity could be sufficient to obscure small changes in the dichroic ratio.

Breton's results do show a change in dichroism across the absorption band of R-26 chromatophores. See Figure 3 of reference (7). The positive dichroism is greater on the long wavelength side of $Q_y$ $\lambda$ max. Breton did not comment on this change. Note that his results are presented in (7) as $\Delta$ A/A, which can be related to the dichroic ratio (22). The change is consistent with the LD results of the LH-R26 protein but could also be attributed to the presence of RCs in chromatophores.

The size of reconstituted LH-R26 protein-lipid vesicles is very similar to the size of native chromatophores. In contrast, vesicles reconstituted with RCs are much larger. The light harvesting proteins constitute about one-half of the membrane proteins in chromatophores (35). LH-R26 would influence the size of the chromatophore more than minor components such as RCs. The formation conditions for reconstituted vesicles may also affect their size.

Conclusions

Stretched polyvinyl alcohol film is a useful technique for orienting proteins and membranes for linear dichroism measurements. From these simple experiments we have been able to deduce information concerning the geometry of the transition dipoles in the light harvesting proteins. Figure II-12 summarizes the data. The LH-R26 protein contains two BChls; both $Q_x$ and $Q_y$ absorption transitions are coupled. The $Q_y$ absorption band is resolved into its exciton components, which are tilted at approximately 48 and 51 degrees to the particle axis (Figure II-12a). In the plane containing the two $Q_y$ exciton dipoles, the monomer dipoles can be found by using the simple point dipole theory for the exciton interaction (Figure II-12b). The $Q_x$ exciton transitions are tilted at 65 degrees to the particle axis but cannot be resolved. The B800+850 protein contains an additional BChl and a carotenoid (Figure II-12c). The carotenoid transition moment is tilted at 58 degrees to the particle axis. The $Q_x$ and $Q_y$ transitions of the third BChl are not coupled to the other two BChls; they are tilted by 48 and 51 degrees to the particle axis, such that the normal to the prophyrin plane is tilted by 67 degrees to that axis. More information is needed to obtain a complete picture of the geometry of the pigments. A detailed study of the fluorescence polarization presented in Chapter III is used to extend this picture of the BChl arrangement.

# REFERENCES


(1) Weiss, C., J. Mol. Spectr. 44, 37 (1972).

(2) Goedheer, J.C. in The Chlorophylls (L. Vernon and G.R. Seely, eds.) Academic Press, New York, N.Y. (1966).

(3) Sauer, K. in Bioenergetics of Photosynthesis (Govindjee, ed.) Academic Press, New York, N.Y. (1975).

(4) Pelke, J.D., Maggiora, G.M., Shipman, L.L. and Christoffersen, R.E. personal communication, and Abstracts to 7th Annual Meeting, American Society for Photobiology, 1979, p. 87.

(5) Hofrichter, J. and Eaton, W.A., Ann. Rev. Biophys. Bioenerg. 5, 511 (1976).

(6) Morita, S. and Miyazaki, T., Biochim. Biophys. Acta 245, 151 (1971).

(7) Breton, J., Biochem. Biophys. Res. Comm. 59, 1011 (1974).

(8) Paillotin, G., Vermeglio, A. and Breton, J., Biochim. Biophys. Acta 545, 249 (1979).

(9) Morita, S. and Miyazaki, T.J., Biochem. 83, 1715 (1978).

(10) Vermeglio, A. and Clayton, R.K., Biochim. Biophys. Acta 449, 500 (1976).

(11) Rafferty, C.N. and Clayton, R.K., Biochim. Biophys. Acta 502, 51 (1978).

(12) Rafferty, C.N. and Clayton, R.K., Biochim. Biophys. Acta 545, 106 (1979).

(13) Bolt, J. and Sauer, K., Biochim. Biophys. Acta 546, 183 (1979).

(14) Abdourakhmanov, I.A., Ganago, A.O., Erokhin, Y.E., Solov'ev, A.A. and Chugunov, V.A., Biochim. Biophys. Acta 546, 183 (1979).

(15) Whitten, W.B., Pearlstein, R.M., Phares, E.F. and Geacintov, N.E., Biochim. Biophys. Acta 503, 491 (1978).

(16) Jablonski, A., Acta Physica Polon. 3, 421 (1934).

(17) Beer, M., Proc. Roy. Soc. (London) A236, 136 (1956).

(18) Fraser, R.D.B., J. Chem. Phys. 21, 1511 (1953) and 28, 1113 (1958).

(19) Eckert, V.R. and Kuhn, H., Z. Electrochem. 64, 356 (1960).

(20) Dorr, F., Angew. Chem. Internal. Edit. 5, 478 (1966).

(21) Tanizaki, Y. and Kubodera, S., J. Mol. Spectr. 24, 1 (1967).

(22) Nairn, J.A., Friesner, R., Frank, H.A. and Sauer, K., submitted to Biophys. J., 1979.

(23) Chapoy, L.L. and DuPre, D.B., J. Chem. Phys. 70, 2550 (1979) and references therein.

(24) Austin, L.A., Ph.D. Thesis, University of California, Berkeley, 1976 and Sauer, K. and Austin, L.A. Biochemistry 17, 2011 (1978).

(25) Singleton, W.S., Gray, M.S., Brown, M.L. and White, J.L., J. Am. Oil Chem. Soc. 42, 53 (1965).

(26) Hong, K. and Hubbell, W.L., Biochemistry 12, 4517 (1973).

(27) Land, E.H., Jour. Opt. Soc. Am. 41, 957 (1951).

(28) Sutherland, J.C., Vickery, L.E. and Klein, M.P., Rev. Sci. Instrum. 45, 1089 (1974).

(29) DJerassi, C., Wolf, H. and Bunnenberg, E., J. Am. Chem. Soc. 84, 4552 (1962).

(30) Philipson, K.D., Ph.D. Thesis, University of California, Berkeley, 1972, p. 101.

(31) Schellman, J.A., Chem. Rev. 75, 323 (1975).

(32) Tinoco, I., Rad. Res. 20, 133 (1963), McRae, E.G. and Kasha M. in Physical Processes in Radiation Biology (L. Augenstein, ed.) Academic Press, New York, N.Y. (1964) p. 23, and Kasha, M., Rawls, H.R. and El-Bayoumi, M.A., Pure Appl. Chem. 11, 371 (1965).

(33) Dratz, E.A., Schultz, A.J. and Sauer, K., Brookhaven Symp. Biol. 19, 303 (1966).

(34) Hemenger, R.P., J. Chem. Phys. 66, 1795 (1977).

(35) Niederman, R.A. and Gibson, K.D. in The Photosynthetic Bacteria (R.K. Clayton and W.R. Sistrom, eds.) Plenum Press, New York, N.Y. (1978), p. 79.

(36) Boxer, S.G. and Wright, K.A., J. Am. Chem. Soc. 101, 6791 (1979).

# CHAPTER III

# FLUORESCENCE AND FLUORESCENCE POLARIZATION OF LH-R26

## Introduction

The use of fluorescence measurements in photosynthesis research is a topic which is much too broad to be considered here. The reader is refered to references (1)-(3) for a general introduction. This discussion is limited to those subjects which help to understand the fluorescence properties of LH-R26 and which provide information on the chromophore arrangement within the complex.

The fluorescence of BChl has been investigated previously by several laboratories (4)-(7). The fluorescence and fluorescence polarization of BChl are reported here to confirm the earlier measurements and to test the fluorimeter described below. The fluorescence spectrum of BChl shows a mirror image relation with the absorption spectrum of the lowest singlet excited state. This supports the belief that fluorescence originates from this excited state (8). Fluorescence polarization also supports this assertion.

The polarization of fluorescence is given by:

$$P = \frac{I_{||} - I_{\perp}}{I_{||} + I_{\perp}} \qquad [1]$$

where $I_{||}$ and $I_{\perp}$ are the intensities of fluorescence measured parallel and perpendicular to the excitation polarization. When a random, nonrotating sample is excited by plane polarized

light the polarization of fluorescence is given by:

$$p = \frac{3\cos^2\alpha - 1}{\cos^2\alpha + 3} \qquad [2]$$

where $\alpha$ is the angle between the absorption and fluorescence transition moments (9). Ideally p = +0.5 if the same transition moment absorbs and emits radiation. However, the limiting values of p (+0.5 for $\alpha = 0^{\circ}$ and -0.333 for $\alpha = 90^{\circ}$) are rarely achieved.

Depolarization of fluorescence can result from rotational motion of the chromophore. The relation between the polarization in the absence of rotational motion ($p_o$) and the observed value (p) was first given by Perrin (10):

$$\frac{1}{p} - \frac{1}{3} = \left(\frac{1}{p_o} - \frac{1}{3}\right)\left(1 + \frac{RT\tau}{V\eta}\right) \qquad [3]$$

where V is the molar volume, T is absolute temperature, $\tau$ is fluorescence lifetime and $\eta$ is viscosity. When rotational depolarization is eliminated (see Results), p becomes +0.42 with $Q_y$ excitation of monomeric BChl.

Depolarization can also arise from excitation transfer to molecules with different orientations. The calculation of fluorescence depolarization due to energy transfer is complicated by several factors, including back transfer to previously excited molecules and the dependence of transfer on orientation. See Knox (11) for discussions of the problem. This source of depolarization is considered unlikely in the case of dilute solutions of BChl in cyclohexanol

because (a), the concentrations are very low (~$10^{-6}$ M) and (b), chromophore aggregation would not be expected in cyclohexanol at these concentrations.

Some factors contributing to the incomplete polarization of BChl fluorescence may be intrinsic to the chromophore. Both absorption into and fluorescence from more than one vibrational-electronic state could lead to less than the theoretical values of p associated with a single isolated transition. The effect is clearly seen in the vibrational overtones of chlorophyll a (12). Overlapping transition moments leads to lesser values of p if the separate transitions have different polarization directions. In addition, excited state rearrangement of chromophore and solvent intra- and inter-atomic distances could lead to changes in transition moment direction. Albrecht (13) introduced a correction factor into the equations describing flourescence polarization to account for intrinsic depolarizations.

Fluorescence polarization is a special case of photoselection. In the method of photoselection as described by Albrecht (13), any photochemical event (fluorescence, bleaching of absorbance, phosphorescence, excited state absorption, etc.) can be used to probe relative orientations of the absorption transition moment and the vector representing the photochemical change. (For an interesting application of photoselection see Chapter IV.) The requirements are that the initial (ground) state population is not depeleted significantly and that energy transfer and rotational depolariza-

tion are suppressed.

In photosynthesis, fluorescence polarization has been used to study chlorophyll proteins (14), bacteriochlorophyll proteins (4,6), membranes (5,6) and oriented membranes (15-17). The study of fluorescence polarization of reaction centers by Ebrey and Clayton (4) is particularly interesting. When compensation for scattered light and fluorescence from contaminating pigments was made by subtracting the fluorescence of unreduced reaction centers from the fluorescence of dithionite ($Na_2S_2O_4$) reduced reaction centers, they found $p = +0.5 \pm 0.03$ with excitation into P870, the longest wavelength absorption band. The fluorescence polarization was measured at emission wavelengths of about 900 nm. Photoselection of absorption changes (18) confirmed this value. It is surprising that such a high value is reached in RCs when the polarization value found in BChl is +0.42.

In this chapter fluorescence polarization of LH-R26 is used to refine the model of BChl arrangement developed in Chapter II.

## Materials and Methods

The protein complex LH-R26 was isolated as described in the Appendix by either hydroxylapatite chromatography of SDS solubilized membranes or by DDAO solubilization and Sephadex chromatography. Although most experiments used the hydroxylapatite preparation, both methods gave the same fluorescence polarization values. The samples were equilibrated with

10 mM TrisHCL, pH 7.5, containing 0.1 to 0.5% SDS. For low temperature measurements the samples were in buffer with 55% glycerol or imbedded in unstretched polyvinyl alcohol (PVA) films described in Chapter II.

Fluorescence measurements were made on a home-built instrument diagrammed in Figure III-1. Excitation light from either a 650 W tungsten lamp or a 500 W Xenon dc arc lamp was passed through a Jarrel-Ash 0.25 meter monochromator with the grating blazed optimally at 600 nm. Normally, 1 mm slits were used, providing a 3.3 nm bandpass. Filters were inserted to remove stray and second order light. The light was focused through an 8 mm aperture Glan-Thompson polarizing prism ($25^{o}$ acceptance angle) and into the sample area. The prism was oriented to pass vertically polarized light. Typically, the sample was held in a 1 cm square cuvette equipped with a water jacketed holder for temperature control. Fluorescent light was collected at $90^{o}$. The first lens collimated the light which was then passed through a half wave plate (h.w.p.) and another Glan-Thompson prism, oriented to pass vertically polarized light. The h.w.p. could be rotated into two positions. When the h.w.p. fast axis is vertical (or horizontal) it has no effect on the polarization of fluorescent light. The instrument then measures fluorescence parallel ($I_{||}$) to the excitation light polarization (both vertical). When the h.w.p. fast axis is at $45^{o}$ to vertical, the electric vector of horizontally polarized light is rotated by $90^{o}$ such that it is now passed by the polarizing

FIGURE III-1

The instrument constructed to measure fluorescence polarization. PM = photomultiplier; h.w.p. = half wave plate; F = filter holders.

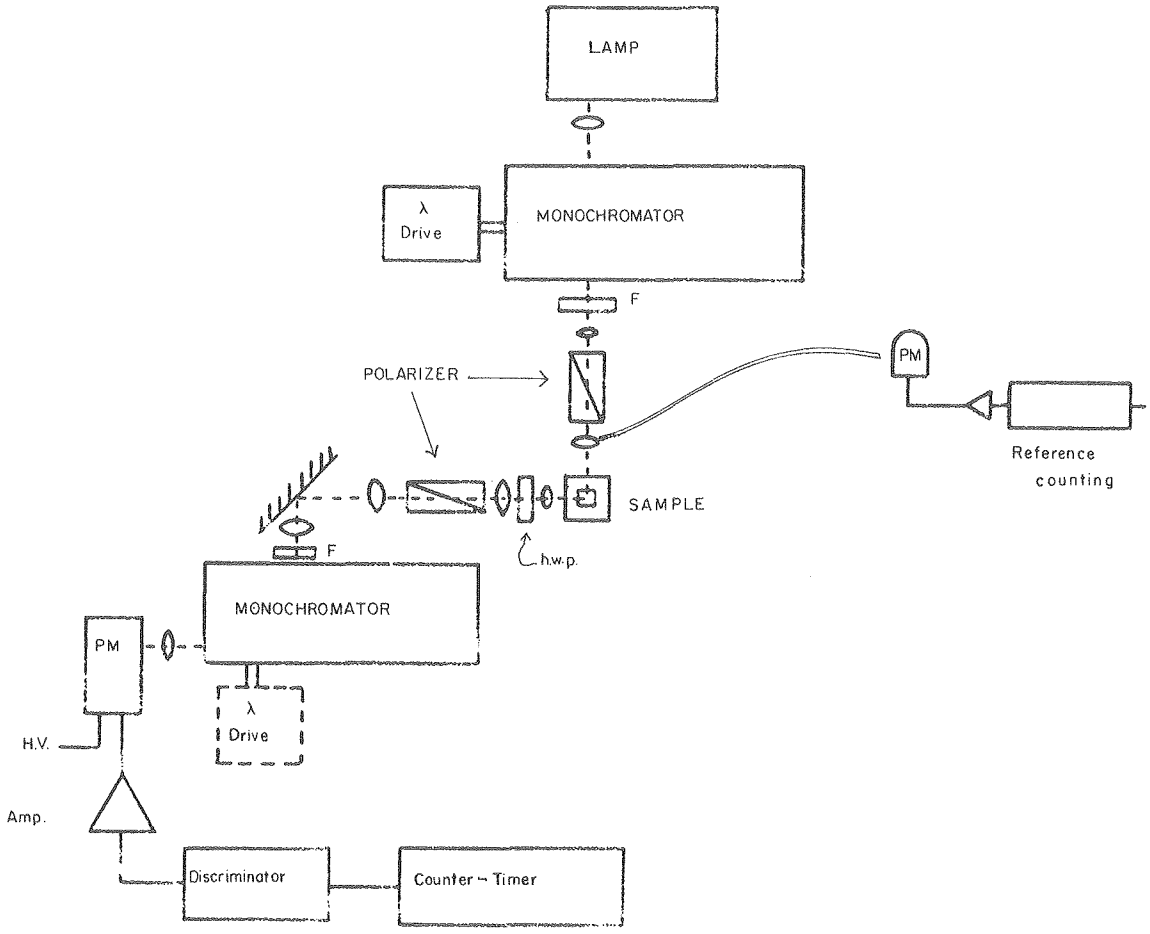
LAMP
λ Drive
MONOCHROMATOR
F
POLARIZER
PM
Reference counting
SAMPLE
h.w.p.
F
MONOCHROMATOR
PM
λ Drive
H.V.
Amp.
Discriminator
Counter – Timer

XBL 801-7723

prism and the instrument measures fluorescence perpendicular ($I_{\perp}$) to the excitation polarization. Use of the h.w.p. in this manner eliminated the effects due to preferential passage of one polarization in the subsequent optics and monochromator. Two wave plates with exactly half wave retardation at 895 and 694 nm were interchangeable. At wavelengths other than 895 or 694 nm the deviation of the measured polarization values from true values is easily calculated by Mueller calculus (19). When fluorescent light at significantly different wavelengths was measured, the wave plate was removed and correction for preferential polarization was made (8).

After passing through the second polarizer the fluorescent light was focused onto the slit of a 0.5 meter Bausch and Lomb monochromator with a grating blazed optimally at 750 nm. Slit width was variable; dispersion was 3.3 nm/mm. The light was then focused onto the photomultiplier (PM) cathode, normally an S-1 side-on tube (RCA C31004) cooled with dry ice. Signal intensity was measured by photon counting. The signal was amplified, and photoelectric pulses were counted using a Princeton Applied Research amplifier discriminator and counter (models 1121 and 1109). Noise, mostly from spontaneous electronic emission from PM dynodes, was rejected by the discriminator. Several references on photon counting techniques are available (20-22). The system had a dead time between photons of 10 ns resulting in maximum count rates of $2 \times 10^6$ per second. Normally,

counts were collected for a preset time period (typically 0.25 to 10 sec). To compensate for fluctuations in the lamp output, a reference PM was set up to detect a reflection from one of the lenses via a light pipe. Reference photons were counted with a PAR 1120 amplifier-discriminator. Fluorescence photon counts could then be collected over a period determined by a preset number of reference counts. This mode was particularly useful when scanning an excitation spectrum using the xenon arc lamp. An analog signal proportional to the counts could be fed to an X-Y recorder, or the counts could be read directly from the counter.

Emission spectra were corrected for the response of the detection system (PM and optics) and if necessary, for reabsorption as described by Parker (8).

Positioning of the polarizers and h.w.p. was optimized using Rayleigh scattering from a glycogen solution at the wavelength of the h.w.p. (895 or 694 nm); p should be 1.0 for the ideal case (22). Typically, p was 0.97 with the h.w.p. and 0.98, without the h.w.p., measured by rotating the polarizers. Checks were also made by measuring the fluorescence polarization of Rhodamine 6-G in gylcerol and BChl in cyclohexanol.

Bacteriochlorophyll was isolated by acetone/methanol (7/2) extraction of carotenoidless bacteria. Measurements of BChl fluorescence polarization were made in cyclohexanol. Measurements at several temperatures were made to correct for depolarization due to rotational diffusion. Viscosity

values were taken from Gray (23) and interpolated from a plot of $\eta$ versus 1/T ($^{o}$K). The limiting values of p ($p_o$ in equation [3]) were found from the intercepts of plots of 1/p against T/$\eta$.

For measurements at liquid nitrogen temperatures the sample was contained in a 5 mm square plexiglass cuvette inside a rectangular dewar clear on four sides. The cuvette and dewar were masked to reduce stray light effects. Cooling was achieved by passing $N_{2(g)}$ through copper coils immersed in $N_{2(l)}$ and into the dewar. The temperature at the sample was monitored by a thermocouple and could be varied by the rate of $N_2$ gas flow. For measurements at liquid helium temperatures, PVA films were immersed in $He_{(l)}$ which was pumped to reach the HeI to HeII transition point at 2.2 K where bubbling ceased.

Results

Figure III-2 displays the absorption, fluorescence and fluorescence polarization spectra of BChl. The fluorescence spectrum shows a mirror image of the $Q_y$ absorption band and a Stokes shift of 258±30 cm-1. In the $Q_y$ absorption band (570 nm) p is -0.21 at the peak. Limiting values of p are found to be +0.424 ($Q_y$) and -0.234 ($Q_x$) from the plot of 1/p against T/$\eta$ . Two bands overlap in the Soret region. The polarization suggests opposite directions of the respective transition moments.

Absorption and fluorescence of the light harvesting

FIGURE III-2

Abosrption of BChl in ether, solid curve. Corrected flour-escence of BChl in cyclohexanol, dashed curve, exicted by 575 nm light. Fluorescence polarization of BChl, above; solid points from this study, open circles from reference (4). Note that in cyclohexanol the $Q_x$ and $Q_y$ absorption bands are red shifted by about 12 nm.

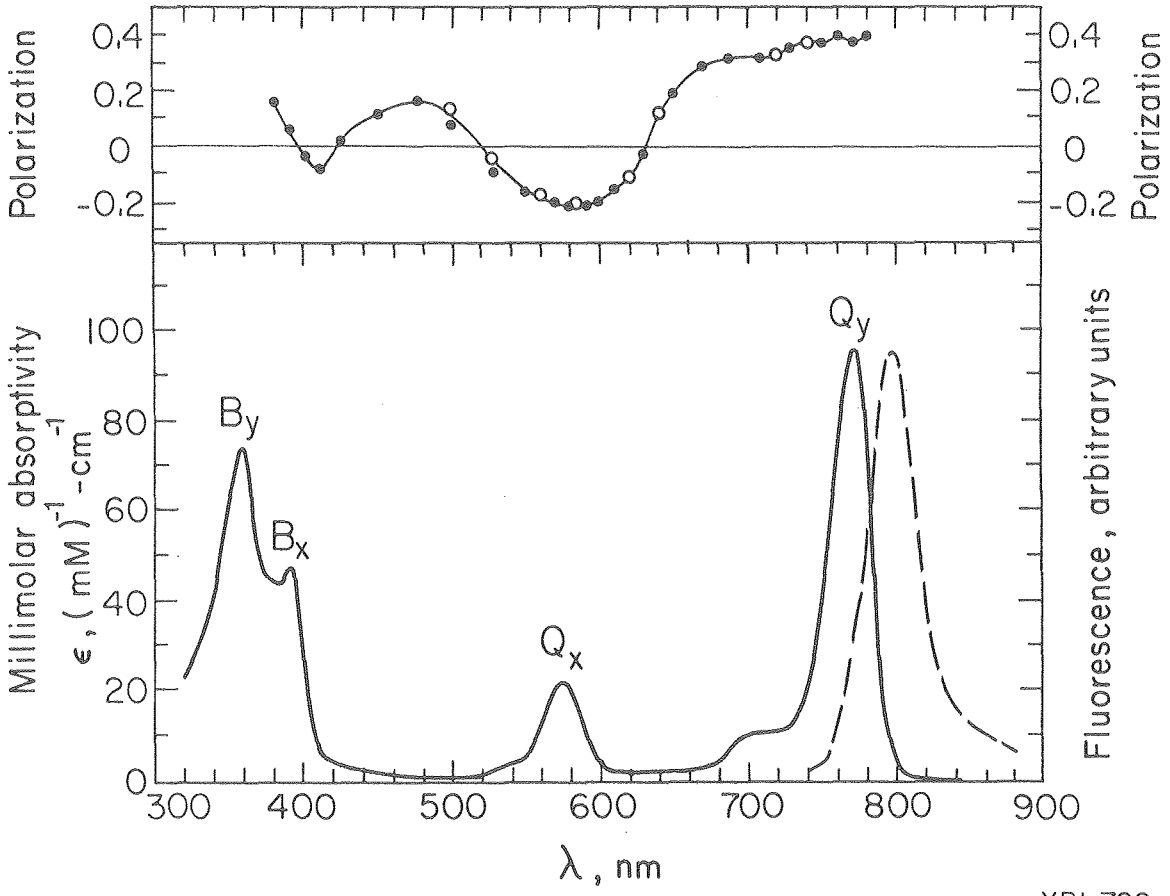
Polarization
0.4
0.2
0
-0.2
Millimolar absorptivity
ε, (mM)⁻¹-cm⁻¹
100
80
60
40
20
0
By
Bx
Qx
Qy
300
400
500
600
700
800
900
λ, nm
Fluorescence, arbitrary units

XBL799-4502

complex LH-R26 at 295° and 90°K are presented in Figure III-3. At 295°K the Stokes shift is 245±25 $cm^{-1}$; both absorption and fluorescence bands are featureless. At 90°K the absorption band ($\lambda$ max = 852 nm) has a distinct shoulder (866 nm) on the long wavelength side. Calculated Stokes shifts from the peak and shoulder are 520±35 cm-1 and 345±35 cm-1 respectively. In PVA at 77°K and 2°K the $Q_y$ absorption shoulder is less distinct but apparent from the overall band skew toward longer wavelengths.

The fluorescence polarization spectra of LH-R26 at 295° and 100°K are presented in Figure III-4. In the $Q_y$ region p is =0.12 to =0.14 at 295°K with the greater values at the red edge of the absorption band. At 100° K the red edge increase in p is more distinct, increasing to +0.20 at 895 nm. In the $Q_x$ absorption band p reaches -0.25 at the wavelength maxima. At 100°K only slight changes in the polarization spectra are observed. The $Q_x$ polarization increases from -0.25 to -0.23 at the lower temperature. In the Soret bands the polarization is negative on the long wavelength side and positive, but small, at the absorption maxima. The Soret band has shoulders on both sides of the absorption band. Light intensity was not sufficient to provide accurate polarization values at wavelengths less than 360 nm. All polarization values were independent of emission wavelength.

Fluorescence polarization in the $Q_x$ band of several different preparations, from the large aggregates expected in membranes to monomeric BChl, are compared in Table III-1.

FIGURE III-3

Absorption and corrected fluorescence of the LH-R26 protein in 0.1% SDS, 10 mM TrisHCl ph 7.5, 55% glycerol. Measurements at each temperature were made on the same sample; fluorescence samples were diluted ten-fold. Note the increase in fluorescence quantum yield of about three-fold.

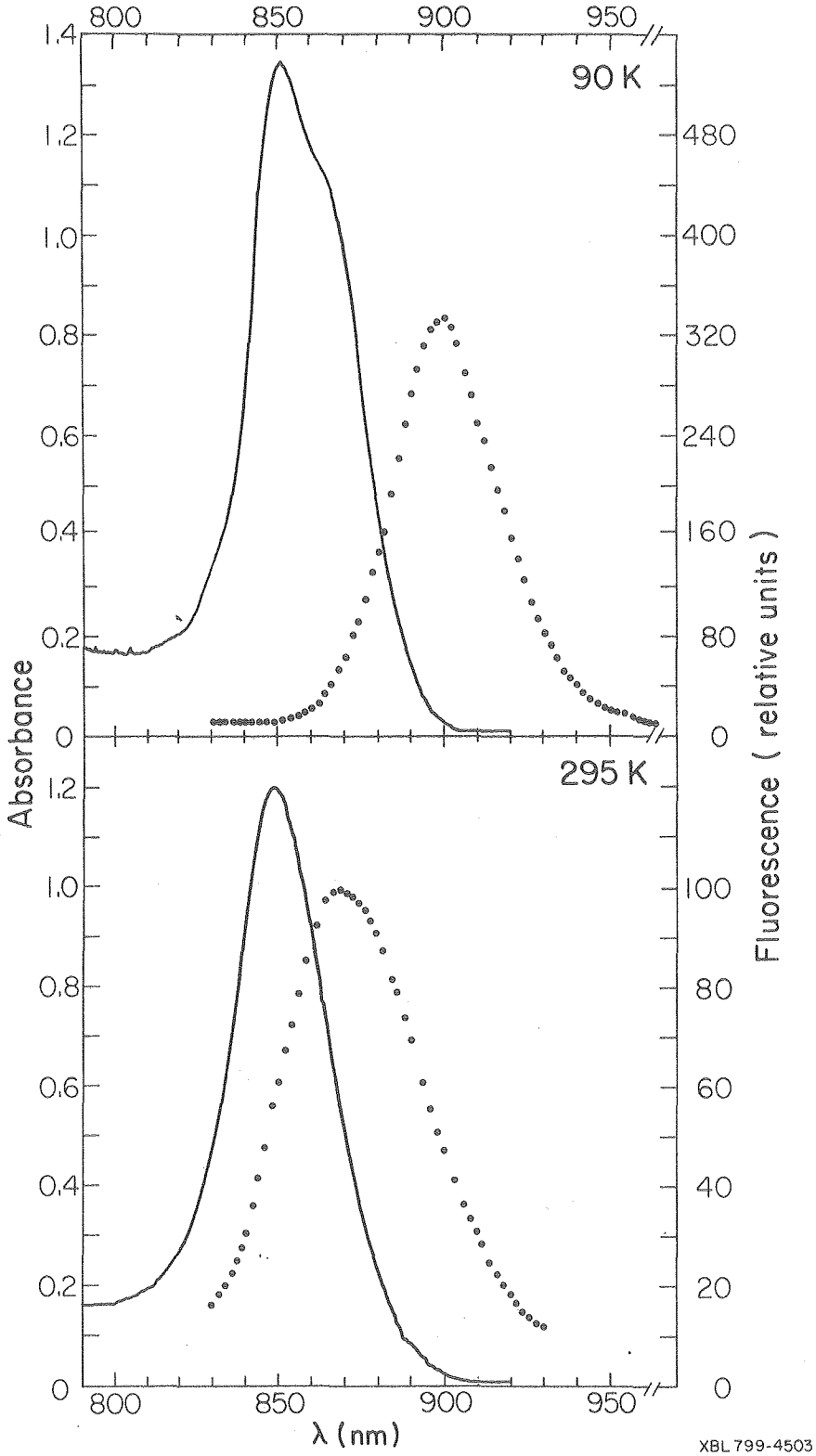
800
850
900
950
90 K
295 K
Absorbance
Fluorescence ( relative units )
λ (nm)
1.4
1.2
1.0
0.8
0.6
0.4
0.2
0
480
400
320
240
160
80
100
60
40
20

XBL 799-4503

FIGURE III-4

Absorption and fluorescence polarization of the LH-R26 protein in 55% glycerol/45% 10 mM TrisHCl, 0.4% SDS.

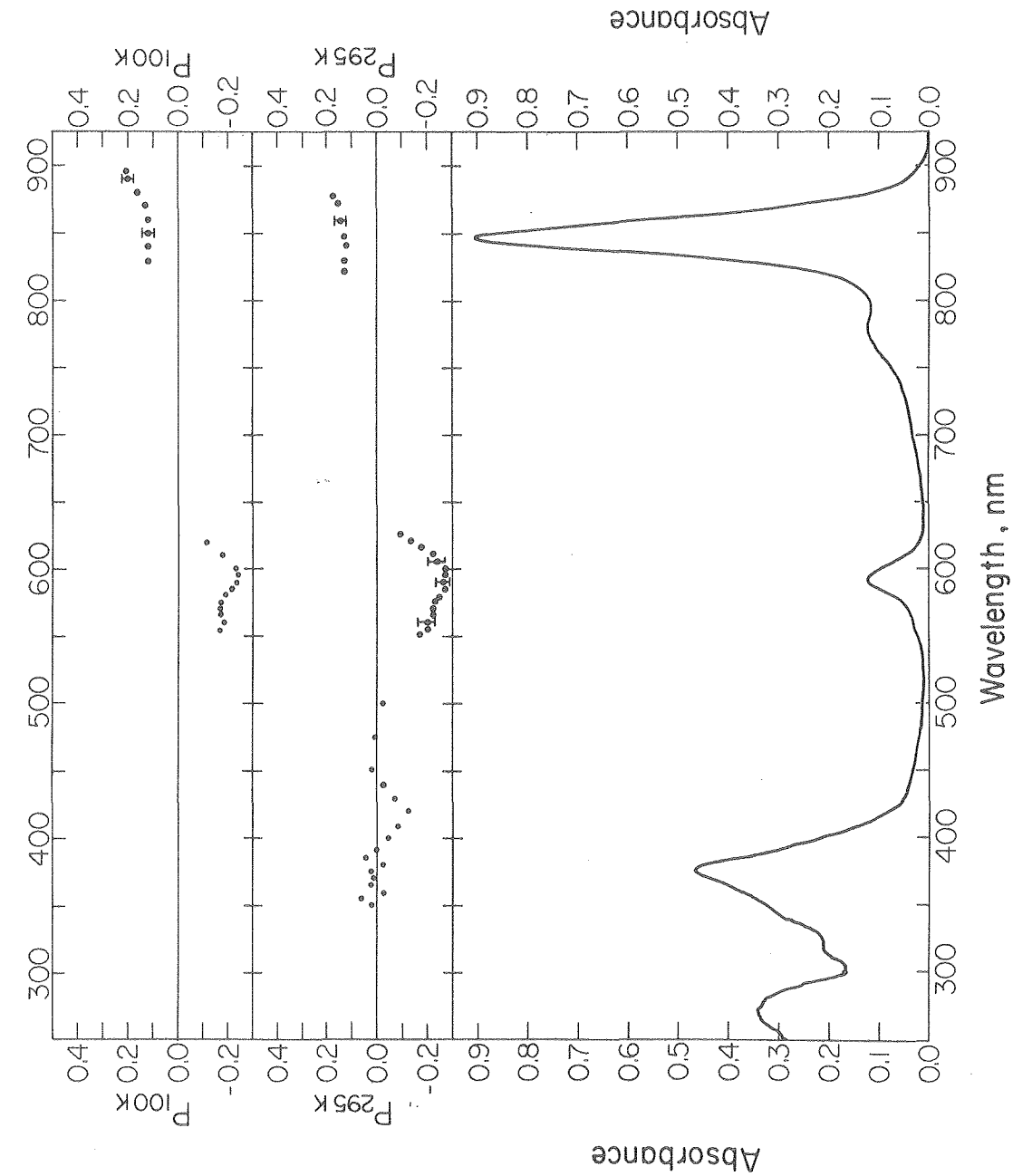
Absorbance
$P_{100K}$
$P_{295K}$
Absorbance
Wavelength, nm
XBL799-4501

TABLE III-1

$Q_x$ FLUORESCENCE POLARIZATION OF BCHL in VARIOUS STATES OF AGGREGATION

| Sample | Estimated number of BChls in aggregate | P[a] | Literature value (ref) |
|---|---|---|---|
| BChl in cyclohexanol | 1 | -0.23 | -0.17(6),-0.23(4)[c] |
| LH-R26 | 2 | -0.25 | -0.15(6) |
| LH-TX100 | 20 | -0.17 | -0.07(6) |
| Membranes | 200[b] | -0.15 | -0.16(4) |
| LH in PVA | --[b] | -0.18 | |

[a] All polarization values were determined with excitation in $Q_x$ maxima.

[b] See text.

[c] BChl in castor oil.

## Discussion

### Bacteriochlorophyll

The fluorescence polarization values of BChl, +0.42 ($Q_y$) and -0.23 ($Q_x$), are in agreement with the results of Ebrey and Clayton (4). Other investigators have reported slightly smaller values (5,6) but their measurements were probably affected by depolarization due to experimental factors. The moderately high polarization value, +0.42, supports the belief that fluorescence proceeds via the electronic transition responsible for the $Q_y$ absorption band. The Soret band fluorescence polarization supports the assignment of overlapping absorption bands in that region. The major transition moments can be assigned as represented in Figure I-1.

### LH-R26

The room temperature absorption of LH-R26 in the $Q_y$ region (820-920 nm) was attributed to the two exciton transitions of dimeric BChls (Chapter II). At temperatures below approximately 130$^{o}$K, Figure III-3, a shoulder is apparent on the lower energy exciton band. The LD and CD results of Chapter II resolved this band on the lower energy side of the absorption maxima with less oscillator strength. Lower temperatures often provide better resolution in absorption spectra. The narrowing of absorption spectra can occur by decreasing the available heterogenous sites (solute-solvent conformations) in which the chromophore may reside. Of course these postulated sites must lie at sufficiently low

energy to be populated at room temperature. In the LH-R26 complex the protein conformations must be included also. In polyvinyl alcohol films little absorption narrowing is observed, even at $2^{o}K$. The heterogeneity of sites may be "frozen in" even at room temperature, when the films are dried. The shoulder in low temperature absorption is in complete agreement with the assignments of exciton transition moments of Chapter II. The shoulder is also observed in chromatophore membranes at low temperature. In this way the isolated protein reflects the properties of the native state of the complex.

The Stokes shift of the fluorescence spectrum at room temperature ($245\pm25$ $cm^{-1}$) is within experimental error of the shift of monomeric BChl ($258\pm30$ $cm^{-1}$). At low temperature the Stokes shift is much greater (Figure III-3), even when calculated from the lower energy shoulder it is $345\pm35$ $cm^{-1}$.

We began the fluorescence polarization measurements with some naive assumptions. If the exciton picture of Figure II-7 is a good representation, one might expect flourescence from either or both energy levels. As the temperature is lowered the population would shift toward the lower energy level, resulting in a longer wavelength fluorescence. The results presented so far agree with the predictions. However, the fluorescence polarization values do not. The strong exciton picture presented in Chapter II predicts perpendicular orientations of the exciton transition moments. Thus, absorption into one $Q_y$ exciton level and fluorescence from

the other would result in a negative polarization ($\alpha = 90^{o}$ in equation [2]). Absorption into and fluorescence from the same exciton level would give a positive value, approaching +0.5 ($\alpha = 0^{o}$), or the maximum value achieved in monomeric BChl (+0.42). However, the value of p determined experimentally is low and positive (+0.12 to +0.20) regardless of excitation or emission wavelengths.

If the resolution of exciton bands from CD and LD is incorrect, the fluorescence polarization may be rationalized with a model which includes emission from exciton states. If the two exciton bands overlapped to a much greater extent than previously predicted, the fluorescence polarization would be essentially constant across the $Q_y$ absorption band. If the $Q_y$ monomer transition moments were also very nearly perpendicular to each other the exciton transitions would have oscillator strengths of almost identical magnitudes. In this case, the exciton absorption band is planar degenerate and fluorescence from one or both exciton states would have a value of about +0.14.

Trivial explanations of the low polarizations can be eliminated. Rotational depolarization can be ruled out. First, the size of the protein complex, a minimum of 20,000 daltons (6), increases V (equation [3]) to a value which predicts little rotation, assuming reasonable values for $\tau$. Increasing viscosity by adding glycerol to 80% w/v or lowering the temperature does not affect the value

of p. The molecular weight determinations of Austin (6) by several methods are all close to 20,000 daltons. This suggests no further aggregation beyond the dimeric BChl state which could lead to depolarization due to energy transfer. Furthermore, the $Q_x$ polarization with maximum values of -0.23 to -0.25, matches the polarization of monomeric BChl.

An explanation for the low $Q_y$ fluorescence polarization is that exciton states are responsible for absorption (and fluorescence excitation spectra) but that fluorescence occurs from molecular states of BChl. The possibility that exciton states may not exist long enough to contribute to the fluorescence has been suggested previously by Kenkre and Knox (24,25). In their terminology, the delocalized (exciton) states will decay into localized (monomer) states by coupling to vibrational modes. The LD analysis of LH-R26 (Chapter II) leads to the conclusion that BChl molecules are oriented with the $Q_y$ axis of one BChl at $78^{\circ}$ to the other, or nearly planar degenerate. In this model both exciton and molecular transition moments are confined to a single plane, Figure II-12b. Planar degenerate transitions lead to an ideal polarization value of +0.14 ($\alpha = 45^{\circ}$, equation [2]). Since the fluorescence polarization of BChl monomer approaches but does not reach +0.5, planar degenerate transition moments might be expected to have values slightly lower than +0.14. Indeed, the observed values, +0.12 to +0.14 at $295^{\circ}K$, are slightly lower than the theoretical value. In the model of Chapter II,

one exciton component makes angles of $39^{o}$ to the monomers and the other makes angles of $51^{o}$. At present the best explanation of the observed $Q_y$ fluorescence polarization is that the momomeric, molecular states are responsible for the fluorescence. The alternative explanation, that the exciton absorptions overlap very strongly, conflicts with the observed absorption shoulder resolved at low temperature (Figure III-3) and with the absence of significant change in fluorescence polarization at $90^{o}$ and $2^{o}K$.

Our previous interpretations of CD and LD have been based on the strongly coupled exciton model for the BChl dimer. It may be better to consider the dimer coupling as intermediate between the strong and very weak (Forster type) limits (24). Strong exciton theory predicts an $r^{-3}$ dependence on the interaction energy ($V_{12}$, equation [3], Chapter II). Forster theory predicts an $r^{-6}$ dependence. Recently a paper has appeared which presents a theoretical approach to fluorescence polarization in any intermediate case (25). Tests of this theory include measurement of the time dependence of p following excitation into the lowest energy absorption bands ($Q_y$ in our case). We hope to measure the lifetime of LH-R26 in this laboratory using $Q_x$ excitation very soon. Extension of these measurements to $Q_y$ excitation would be useful.

An unusual result appeared when fluorescence emission spectra were recorded at low temperatures ($100^{o}K$) with $Q_y$ excitation. The fluorescence emission maxima depended upon

the wavelength of excitation. Excitation at 880 nm resulted in emission maxima at wavelengths 15 nm longer than excitation at 840 nm in extreme cases. However, the actual magnitude of this shift differed from sample to sample. (With low temperature $Q_x$ excitation or either $Q_x$ or $Q_y$ excitation at room temperature the emission spectra widths and maxima were constant with respect to wavelength of excitation.) This variability suggested than an inhomogeneity arose at the lower temperatures. To my relief, I found that when the low temperature spectra were taken in 50% ethylene glycol glasses instead of glycerol, emission spectra were identical irregardless of excitation wavelength. It is suggested that all future low temperature absorption spectra be made in ethylene glycol glasses. The $90^{o}$K absorption spectrum of LH-R26 in 50% ethylene glycol is essentially identical to that shown in Figure III-3. The long wavelength shoulder is slightly less prominent.

Several other results are worth noting. The three-fold increase in fluorescence yield at lower temperature is rather large. The change in yield or emission wavelength maxima is not drastic until the temperature is less than $150^{o}$ K. These results may be related to the appearance of the absorption shoulder at temperatures below $130^{o}$ K (see above). It will be useful to confirm the fluorescence yield changes by measurements of fluorescence lifetimes at various temperatures.

The Soret band fluorescence polarization values of LH-R26 (Figure III-4) are similar to the values of BChl

monomer (Figure III-2). A negative dip at the red edge suggests x-oriented polarization of this shoulder. The Soret peak fluorescence polarization is slightly positive. The value of p is not so positive as monomeric BChl, probably due to the planar degeneracy of the fluorescence transition moments. These results are in basic agreement with the polarizations found by Breton from LD of oriented R-26 membranes (26).

Influence of Aggregation on Fluorescence Polarization

The effect of aggregation can be observed by measuring fluorescence polarization on different preparations. Aggregation leads to depolarization due to energy transfer. As seen in Table III-1, excitation into the $Q_x$ band gives large p values (-0.23 to -0.25) for LH-R26 or monomers (BChl in cyclohexanol). For larger arrays of pigments (LH-TX100) (6) or native membranes, somewhat weaker polarization is observed. It is interesting to note that in the membrane the excitation may visit seven or more photosynthetic units (27), each consisting of a reaction center and its associated antenna, or a total of about 100 LH-R26 aggregates. Despite this extensive energy transfer, the fluorescence still has significant polarization. This result suggests significant order within the light harvesting arrays. With $Q_x$ excitation p = +0.08 (4). The primary source of depolarization (with respect to BChl monomers, p = +0.42) is within the LH-R26 dimer unit.

When LH-R26 is embedded in PVA the polarization values

are somewhat less than those for solutions of the same complex (see Table III-1; also with excitation at 840 nm p is +0.12 in solution and +0.10 in PVA). This may arise from aggregation within the PVA matrix.

A Model for BChl Arrangement in LH-R26

As discussed above, the best hypothesis is that the $Q_y$ fluorescence transition moments are nearly planar degenerate. The $Q_x$ fluorescence polarization, -0.25, indicates angles of $74^o$ to $90^o$ with the fluorescing dipoles and, therefore, with the plane containing the $Q_y$ monomer and exciton transition moments. The lower value, $74^o$, is calculated from equation [2]. The upper value, $90^o$, is based on the fluorescence polarization of monomeric BChl (-0.23) and the assumption that the monomeric $Q_x$ transition moment is exactly perpendicular to the monomeric $Q_y$ transition moment. This arrangement agrees with the model developed from LD. Look again at Figure II-12 a and b. For the $Q_x$ transition moment to be perpendicular to the plane of $A_1$, $A_2$, $A_-$, and $A_+$ (Figure II-12) it must be at an angle of $65^o$ to the protein long axis ---- precisely the value found for the angle of the dominant $Q_x$ exciton transition moment!

From the CD/absorption curve resolution (Chapter II) we concluded that the $Q_x$ absorption band consisted of one major exciton transition centered at the absorption maxima and one exciton transition with vanishing oscillator strength at lower energy. These relative exciton dipole strengths are produced by parallel monomer transition moments. The

presence of exciton induced CD requires that the monomer transition moments are not exactly parallel. Thus, the lower energy transition must have a finite oscillator strength.

Figure III-5 summarizes these arguments in a model for the BChl arrangement in LH-R26. Solid vectors represent the directions of monomeric BChl transition dipole moments. Dashed vectors represent the absorptions in the strong coupling exciton limit. + and - designate relative energy of transitions, not the absolute sign of wavefunctions. $Q_{y1}$, $Q_{y2}$, $Q_{y+}$, and $Q_{y-}$ are in the YZ plane; $Q_{x1}$, $Q_{x2}$, and $Q_{x+}$ are along the X axis of the reference coordinate system, upper left. The very weak $Q_{x-}$ exciton transition moment lies somewhere within the YZ plane. The molecules are super-imposed for this representation. A complete geometry would specify, in magnitude and orientation, the position vector from molecule 1 to molecule 2.

We may now make some rough calculations of the BChl-BChl inter-molecular distance. Based on the protein molecular weight and the density of proteins, a spherical particle would have a diameter of about 35 Å. Based on the known cyrstal structure of the water soluble BChl protein from green bacteria (29) we would expect the protein to enclose the two BChls of LH-R26. The greater stability of the protein-contained BChls to oxidation and $Mg^{++}$ loss relative to monomeric BChl supports the speculation that the protein encloses (and protects) the chromophore. Therefore we can

FIGURE III-5

Schematic view of the mutual orientations of absorption transition dipoles for LH-R26. Solid vectors represent the directions of monomeric BChl transition dipoles. Dashed vectors represent the absorptions in the strong coupling exciton limit. + and - designate relative energy of transitions, not the absolute sign of the wavefunctions. $Q_{y+}$, $Q_{y-}$, $Q_{y1}$, and $Q_{y2}$ are in the yz plane; $Q_{x1}$, $Q_{x2}$ and $Q_{x+}$ are along the x axis of the reference coordinate system upper left. The molecules are superimposed for this representation. A complete geometry would specify, in magnitude and orientation, the position vector from molecule 1 to molecule 2.

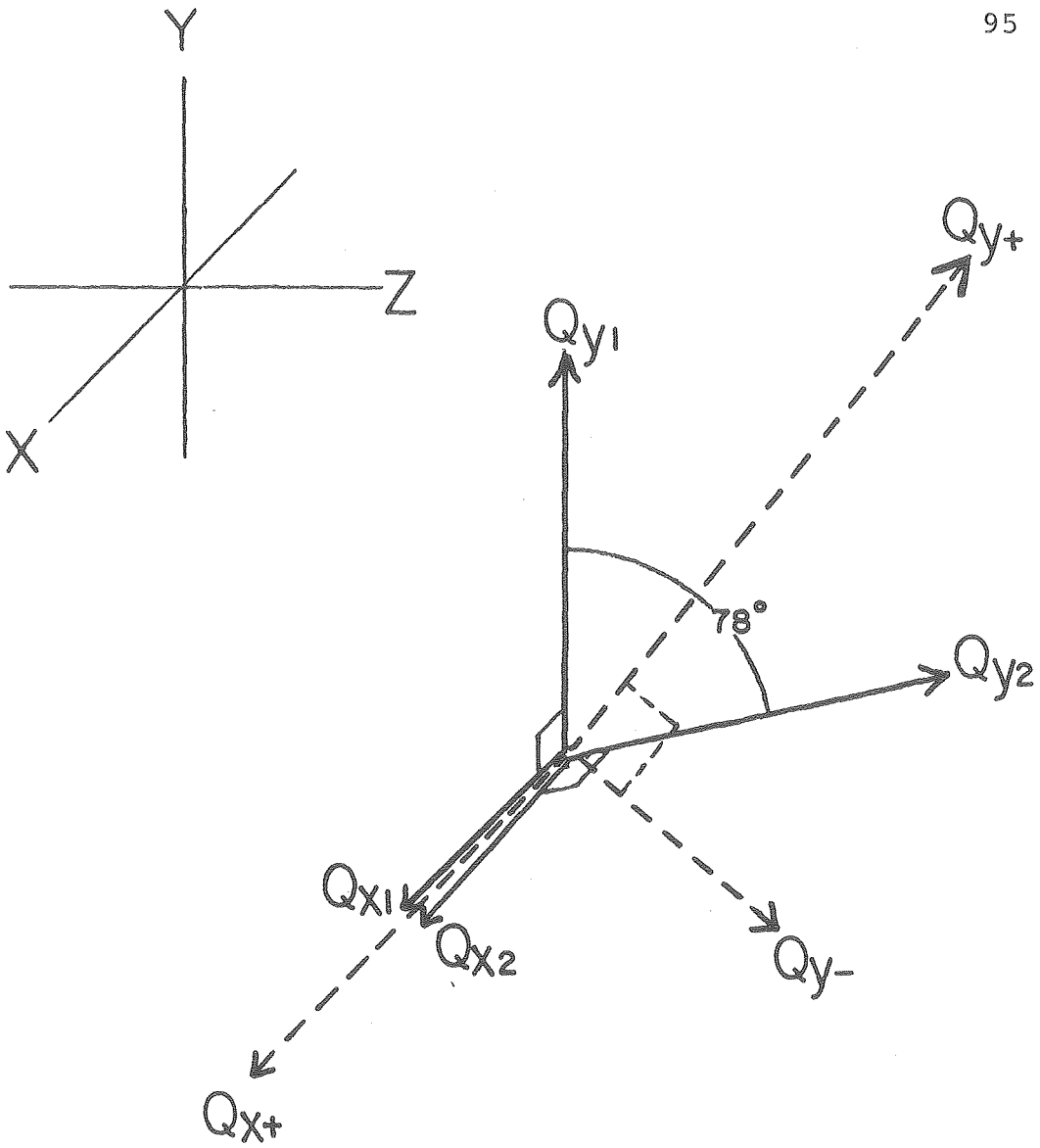


XBL 799-5017

expect to find an intermolecular distance of 20 Å or less.

The exciton equations of Chapter II should provide a complete geometry of the dimer. The $Q_x$ dipoles are nearly parallel and provide a convenient simplification. Based on the $Q_x$ exciton splitting (Table II-1) and equation [3] of Chapter II as simplified by Kasha, et. al. (30), and assuming that the $Q_x$ monomer transition moments are side-by-side parallel, a distance of 6.7 Å is calculated. (The monomer transition moments must be closer to side-by-side than end-to-end parallel to give the allowed $Q_x$ exciton transition a greater energy than the forbidden transition.) Unfortunately, this distance, 6.7 Å, is close enough for the point dipole approximation to break down. Chang and Knox have used monopoles to better approximate transition moments in calculating chlorophyll interactions (11). The point dipole approximation deviates seriously at distances of 20 Å or less. From calculations using the $Q_y$ exciton bands and Kasha's simplified models (30), a distance of about 16 Å is predicted.

A consistent geometrical calculation must include the rotational strengths (CD) of each exciton band. Attempts by Richard Friesner (unpublished results) to calculate the geometry of LH-R26, using the monopole approximations, have been unsatisfactory. The primary pitfall of exciton theory presented in Chapter II is the exclusion of molecular vibrations. Theoretical treatments which include the vibronic character of aggregate electronic transitions must be consistent with LD, CD and fluorescence polarizations presented here.

Other approaches to the structure of LH-R26 may also be useful. These include nuclear magnetic resonance spectroscopy, electron paramagnetic resonance spectroscopy of the triplet state of LH-R26, and direct structure determination by x-ray or electron diffraction.

## Conclusions

The fluorescence and fluorescence polarization of the LH-R26 BChl protein have been presented. The results are interpreted as follows: Because exciton coherence rapidly decays in the excited state, fluorescence probably originates from monomer excited states. The $Q_y$ monomer transition moments are nearly planar degenerate, roughly $90^{\circ}$ to each other, in agreement with the value of $78^{\circ}$ from LD. The $Q_x$ monomer transition moments are almost parallel and side-by-side. A model for the geometry of the BChl dimer is presented in Figure III-5. The model lacks specification of the vector connecting the centers of the two monomers.

# REFERENCES


(1) Clayton, R.K. and Sistrom, W.R., editors, The Photosynthetic Bacteria (Plenum Press) New York, N.Y., 1978, chapters by Borisov, A. Yu., Amesz, J. and Zankel, K.L.

(2) Papageorgiou, G., in Bioenergetics of Photosynthesis, Govindjee, ed. (Academic Press) New York, N.Y., 1975.

(3) CIBA Foundation Symposium 61, Cholorphyll Organization and Energy Transfer in Photosynthesis, (Exerpta Media) Amsterdam, 1979, numerous articles.

(4) Ebrey, T.G. and Clayton, R.K., Photochem. Photobiol. 10, 109 (1969).

(5) Goedheer, J., Biochim. Biophys. Acta 16, 471 (1955).

(6) Austin, L.A., Ph.D. Thesis, University of California, Berkeley, 1976.

(7) Tumerman, L.A. and Rubin, A.B., Dokl. Akad. Nauk. SSSR 145, 202 (1962).

(8) Parker, C.A., Photoluminescence of Solutions (Elsevier) New York, N.Y., 1968.

(9) Jablonski, A., Z. Phys. 96, 236 (1935).

(10) Perrin, F., Ann. Phys. (Paris) 12, 169 (1929).

(11) Knox, R.S., in Bioenergetics of Photosynthesis, Govindjee, ed. (Academic Press) New York, N.Y., 1975, pp. 183-221.

(12) Gouterman, M. and Stryer, L., J. Chem. Phys. 37, 2260 (1962).

(13) Albrecht, A.C., J. Mol. Spect. 6, 84 (1961).

(14) Van Metter, R.L., Biochim. Biophys. Acta 462, 642 (1977) and Knox, R.S. and Van Metter, R.L., CIBA Symposium 61, 177 (1979).

(15) Breton, J. and Geacintov, N.E., CIBA Symposium 61, 217 (1979).

(16) Geacintov, N.E., Van Nostrand, F., Becker, J.F. and Tinkel, J.B., Biochim. Biophys. Acta 267, 65 (1972).

(17) Breton, J., Becker, J.F. and Geacintov, N.E., Biochem. Biophys. Res. Comm. 54, 1403 (1973).

(18) Vermeglio, A., Breton, J., Paillotin, G. and Cogdell, R., Biochim. Biophys. Acta 501, 514 (1978).

(19) Shurcliff, W.A., Polarized Light (Harvard Press) Cambridge, Mass., 1962.

(20) Longworth, J.W., Photochem. Photobiol. 36, 665 (1977).

(21) Aoshima, R., Iriyama, K. and Asai, H., Appl. Optics 12, 2748 (1973).

(22) Jameson, D.M., et. al., Rev. Sci. Instrum. 49, 510 (1978).

(23) Gray, D.E., editor, Am. Inst. Phys. Hdbk. (McGraw-Hill) New York, N.Y., 1963.

(24) Kenkre, V.M. and Knox, R.S., Phys. Rev. Lett. 33, 803 (1974).

(25) Rahman, T.S., Knox, R.S. and Kenkre, V.M., Chem. Phys. 44, 197 (1979).

(26) Breton, J., Biochem. Biophys. Res. Comm. 59, 1011 (1974).

(27) Clayton, R.K., J. Theor. Biol. 14, 173 (1967).

(28) Aagaard, J. and Sistrom, W.R., Photochem. Photobiol. 15, 209 (1972).

(29) Fenna, R.E. and Matthews, B.W., Brookhaven Symp. Biol. 28, 170 (1976).

(30) Kasha, M., Rawls, H.R. and El-Bayoumi, M.A., Pure Appl. Chem. 11, 371 (1965).

# CHAPTER IV

# ELECTRON PARAMAGNETIC RESONANCE STUDIES OF TRIPLET STATES IN PHOTOSYNTHETIC BACTERIA

## Introduction

Results presented in this chapter have been reported in reference (1) (magnetophotoselection) and in a paper recently submitted for publication (2) (carotenoid triplet states).

Reaction centers of photosynthetic bacteria contain a primary electron donor consisting of a BChl dimer (sometimes called the "special pair"), an initial electron acceptor thought to be a bacteriopheophytin (BPheo) and one or two quinones which act as secondary acceptors (3). After absorption of light, initial charge separation begins from the excited singlet state of the primary donor. The donor becomes oxidized and the acceptors reduced in a rapid sequence:

$$\mathrm{BChl_2BPheo\ Q_AFeQ_B} \xrightarrow{h\nu} {}^{1}\mathrm{BChl_2}^{*}\mathrm{BPheo\ Q_AFeQ_B} \longrightarrow$$

$$\mathrm{BChl_2}^{+}\mathrm{BPheo}^{-}\ \mathrm{Q_AFeQ_B} \longrightarrow \mathrm{BChl_2}^{-}\mathrm{BPheo\ Q_A}^{-}\mathrm{FeQ_B} \longrightarrow$$

$$\mathrm{BChl_2}^{+}\mathrm{BPheo\ Q_AFeQ_B}^{-} \qquad [1]$$

At room temperature under ambient redox conditions, the charge on the second quinone ($Q_B$) proceeds to other acceptors in the electron transport cycle. At low temperature, secondary electron transport is inhibited, and the RC remains in the charge separated state for seconds before charge recombina-

nation occurs. If the reaction center quinone is removed or if it is reduced prior to light excitation, the primary photochemistry if blocked and the charge separated state $BChl_2^+BPheo^-$ undergoes a rapid back reaction (~10n sec). Not all reaction centers return directly to the initial ground state; many proceed via a triplet state which develops on the special pair, $BChl_2$. The overall scheme is:

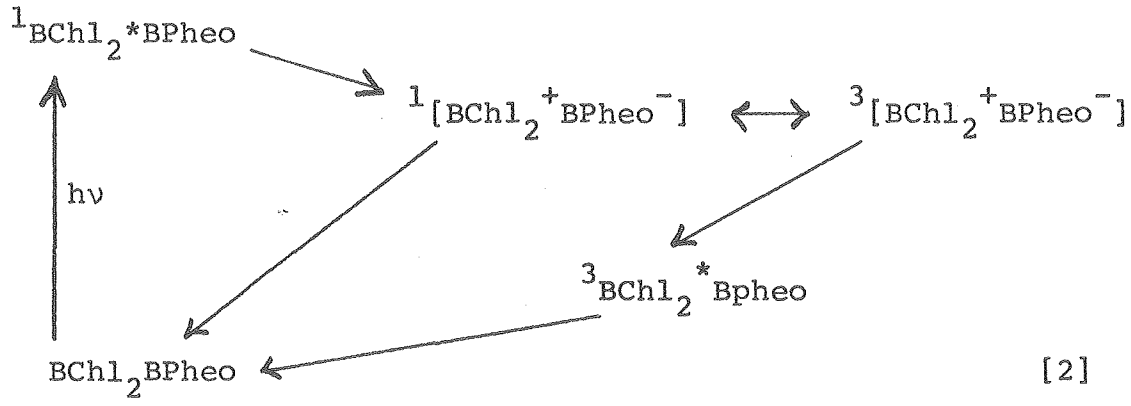


[2]

At low temperatures the $BChl_2$ triplet yield is near unity (3). We have investigated this triplet state by the method of magnetophotoselection (1).

Magnetophotoselection combines the optical photoselection and electron paramagnetic resonance (EPR) experiments (4,5). A randomly ordered system of molecular species is excited with polarized light and its light-induced EPR spectrum is recorded with light polarized parallel and perpendicular to the static EPR field direction. The technique has been used extensively in assigning the principal magnetic axes of the photoexcited triplet states of aromatic molecules (6-9) including chlorophylls (10) and in the study of triplet-triplet

energy transfer between different aromatic molecules (8, 11-13).

Thurnauer and Norris performed magnetophotoselection experiments on membranes from Rhodospirillum rubrum and offered a qualitative interpretation of the results (10). We have extended this application and treated the information quantitatively (1). The method is used to locate the optical transition moments within the magnetic axis system of the $BChl_2$ triplet state. Also, the method can serve to link optical photoselection studies on oriented bacterial cells (15) to EPR experiments performed on the same systems (16). We believe that the determination of mutual orientations of the primary photoreactants in bacterial photosynthesis and their orientations within the membrane as deduced from optical and from EPR experiments must be consistent with magnetophotoselection results.

Using photoselection of optical changes Vermeglio, et. al. (17) have calculated the relative orientations of transition moments within RCs of Rhodoseudomonas sphaeroides, R-26. They found that the transition moments for absorption at 870 nm, which belongs to the BChl "special pair", and absorption at 546 nm, which is attributed to a BPheo, make an angle of $60^{o}$ to each other. A magnetophotoselection study of the R-26 reaction center is presented in this chapter. Light-induced triplet state EPR spectra excited by 882 nm and 550 nm light polarized parallel and perpendicular to the static EPR field are presented and analyzed.

Following the procedure outlined in another publication (16), the observed triplet state spectra were computer simulated. The orientations of the 870 nm and 546 nm transition moments with respect to the principal magnetic axes of the triplet state are calculated. A distribution function $D(\theta,\phi)$ is derived which is used to calculate the triplet state EPR intensity, $\bar{I}(|\underset{\sim}{H}|)$ for broadband unpolarized or polarized narrow band excitations. EPR intensities are calculated from:

$$\bar{I}(|\underset{\sim}{H}|) = \int_0^{\pi}\int_0^{2\pi} I(\theta,\phi,|\underset{\sim}{H}|)D(\theta,\phi)d\theta d\phi \qquad [3]$$

where $I(\theta,\phi,|\underset{\sim}{H}|)$ is the intensity of the triplet signal at field $|\underset{\sim}{H}|$, when the static EPR field is specified by angles $\theta$ and $\phi$ (see Discussion). The expression for $I(\theta,\phi,|\underset{\sim}{H}|)$ is taken from standard texts (4).

In addition to the orientation of the transition moments, zero-field splitting parameters and relative rate constants of intersystem crossing for the triplet state are calculated.

The R-26 RC contains no carotenoids. In the investigation of the triplet states in reaction centers from wild type (2.4.1) Rps. sphaeroides which contain a carotenoid, a new EPR signal was observed. We have assigned this signal to the triplet state of the carotenoid. In doing so, we report for the first time EPR observation of triplet states in carotenoids. Several arguments in support of this assignment are presented.

Carotenoids serve important functions in photosynthesis. They act as light harvesting pigments which transfer their excitation energy to BChl and to the reaction centers (18). Their role as protective agents against irreversible photodestruction by singlet oxygen is well known in photosynthetic bacteria, green plants and algae (19).

The triplet states of carotenoids are poorly understood. This is due in part to the fact that direct population of the triplet states of isolated carotenoids via singlet-triplet intersystem crossing is not very efficient (20,21). Population of the triplet states has been possible only through photosensitization in optical flash photolysis experiments (20-22). We show here that in pigment protein complexes, in vivo or as isolated entities, BChl can photosensitize the formation of carotenoid triplet states.

The impetus for this study came from an unidentified triplet observed in green plants which may have been a carotenoid triplet (23) and from the abundance of literature on the optical detection of carotenoid triplet states in photosynthetic preparations (24-28).

Reaction centers from carotenoid containing bacteria produce the special pair BChl dimer triplet described in scheme [2], above. However, the triplet energy can be transferred to the carotenoid associated with the RC. Parson and Monger (29) have proposed that an equilibrium triplet energy exchange occurs between the $BChl_2$ and the carotenoid which can be illustrated as follows:

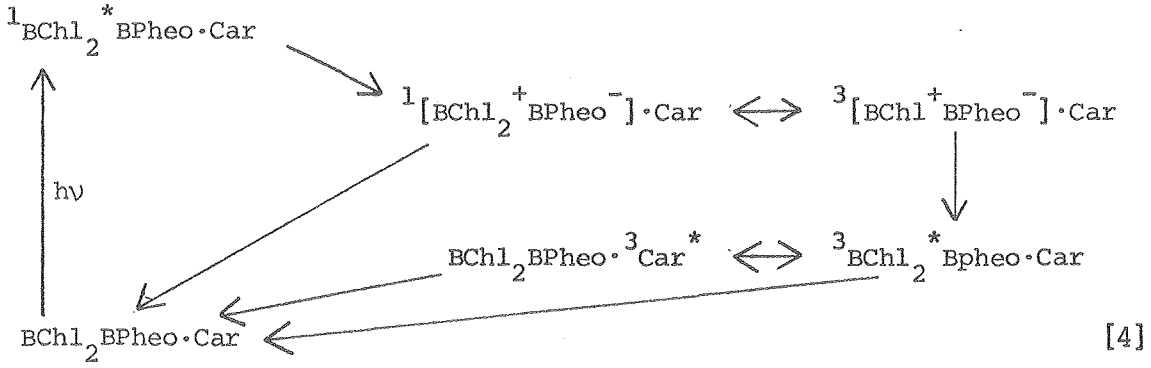


[4]

It has been suggested that the predominant triplet is $^3BChl_2^*$ at temperatures below 77°K. We have tested these ideas by examining the effect of temperature and the state of reduction on the triplet state EPR spectra of carotenoid-containing and carotenoidless photosynthetic bacteria. In addition, the triplet state EPR spectrum of β-carotene has been observed in non-ionic detergent micelles and in phospholipid bilayers.

## Materials and Methods

Reaction centers were prepared as described in the Appendix. The final ammonium sulfate precipitates were dialyzed against 0.01 M TrisHCl (pH 7.6), reprecipitated and suspended in 2% Triton X-100, 0.025 M Tris HCl (pH 8.0). Solid $Na_2S_2O_4$ was added to about 10 mg/ml and the solution was diluted with an equal volume of ethylene glycol. The final concentration of reaction centers ranged from $10^{-4}$ to $10^{-5}$M. Careful cooling to 77°K gave clear glasses in sample tubes (2 mm I.D.). The samples could be stored in liquid nitrogen for several months.

Photosynthetic bacteria used in the carotenoid experi-

ments were grown as described previously. Initial samples of the light harvesting protein, B800+850, were a gift of Richard Cogdell. Other samples of the protein were prepared as described in the Appendix. All biological samples contained 50% ethylene glycol. Untreated samples were prepared at ambient redox potential. Reduced samples were treated with 0.02 M sodium dithionite and $1.0 \cdot 10^{-5}$ M methyl viologen in 0.025 M Tris HCl buffer, pH 8.0.

β-carotene, obtained from Sigma, was suspended in micelles by dropwise addition of 50 μL of carotenoid solution in THF to 2 mL phosphate buffer containing 0.10 M detergent. The non-ionic detergent IGEPAL-CO-630 (nonylphenoxypoly (ethylenoxy) ethanol, from GAF) was used. The detergent solution was vigorously stirred and gently heated to remove THF. Carotenoids were incorporated in phospholipid vesicles by injection of a known volume of THF or ethanol solution containing both lipid and carotenoid into rapidly vortexing buffer solution. Egg phosphatidyl choline was purified by published procedures (30). β- carotene was obtained from Sigma. The samples were purged of oxygen by bubbling nitrogen through the solutions for a few minutes before freezing.

EPR measurements: EPR measurments were performed on a Varian E109 spectrometer at X-band (~9 GHz) microwave frequencies. Magnetic field was modulated 16 gauss peak-to-peak at 100 KHz. Light-induced triplet states were produced as described below and modulated by a 33.5 or 11 Hz light beam

chopper. The output of the EPR detection system was fed through a selective amplifier into a lock-in amplifier (Princeton Applied Research models 210 and 220) referenced to the chopper. Output from the lock-in amplifier was plotted on the EPR spectrometer recorder.

Triplet state spectra presented in the carotenoid study were produced by excitation from a mercury-xenon 1000 W arc lamp filtered through pyrex and 5 cm of $H_2O$. In the magneto-photoselection study braodband excitation was produced by a tungsten lamp filtered through 5 cm of $H_2O$ at intensities below 25 $mW/cm^2$. For excitation at 882 nm, light from a 900 W xenon or a 1000 W mercury-xenon dc arc lamp was filtered through 5 cm of a 6% w/v aqueous solution of chromium potassium sulfate ($Cr_2(SO_4)_3 \cdot K_2SO_4 \cdot 24\ H_2O$) and a Baird-Atomic interference filter with a bandwidth of 10 nm at half maximum transmittance. Immediately prior to the cavity was located a Polaroid type HN-7 sheet polarizer which could be rotated through $360^o$. The amplitude ratios given in Table IV-1 were corrected for incomplate polarization (at 882 nm the principal transmittance ratio is 27). For excitation at 550 nm light from the mercury xenon lamp was filtered by 5 cm of a 0.2% w/v solution of para-nitrophenol in 2% w/v sodium bicarbonate and focused through a Corning glass filter 1-69, an interference filter (550 nm) and a Polaroid type HN-38 sheet polarizer.

In the magnetophotoselection studies light was focused into an open ended flange constructed from waveguide and affixed to the front of a Varian TE microwave cavity to allow

100% transmission of light. In the carotenoid study, excitation from a 1000 W mercury-xenon dc arc lamp was filtered through 5 cm of water in a pyrex container and focused through the 75% transmitting grid of a Varian $TM_{110}$ (E-238) microwave cavity. Measurements at $10^{o}K$ and $100^{o}K$ utilized an Air Products Helitron cryostat. Measurements at $160^{o}K$ were made using a Varian Associates nitrogen gas flow dewar.

## Results

### Magnetophotoselection

The experimental results are summarized in Table IV-1. The triplet state EPR spectra were quantitated by measuring amplitudes at key field positions as indicated in Figure IV-1 and normalized to the amplitude of the Z± peaks.

### Calculation of Magnetophotoselection Distribution Functions

When polarized light is absorbed by a random sample of molecules a non-random distribution of excited states is produced. To calculate the EPR spectrum intensities we must specify this distribution in terms of the location of the absorption transition moment, $\underset{\sim}{\mu}$, and the location of the static EPR field, $\underset{\sim}{H}$, in the triplet state principal magnetic axis spectrum. First we write the dot product of $\underset{\sim}{\mu}$ and $\underset{\sim}{H}$:

$$\underset{\sim}{\mu} \cdot \underset{\sim}{H} = |\underset{\sim}{\mu}||\underset{\sim}{H}| \cos\beta \qquad [5]$$

where $\beta$ is the angle between $\underset{\sim}{\mu}$ and $\underset{\sim}{H}$. For light excitation polarized parallel to $\underset{\sim}{H}$ the probability of exciting $\underset{\sim}{\mu}$ is $\cos^2\beta$. Squaring equation [5] and rearranging:

FIGURE IV-1

Experimental triplet state spectrum of Rhodopseudomonas sphaeroides R-26 generated by broadband unpolarized light. Spectrum of reduced reaction centers was taken with the following conditions: sweep time, 16 min; field modulation frequency, 100 kHz; field modulation amplitude, 16 G; receiver gain, 32; temperature, 11°K; microwave power, 50 μw; microwave frequency, 9.069 GHz; light modulation frequency 33.5 Hz; recorder time constant, 10 s; tungsten lamp excitation. The light induced free radical signal at g = 2.0 has been omitted.

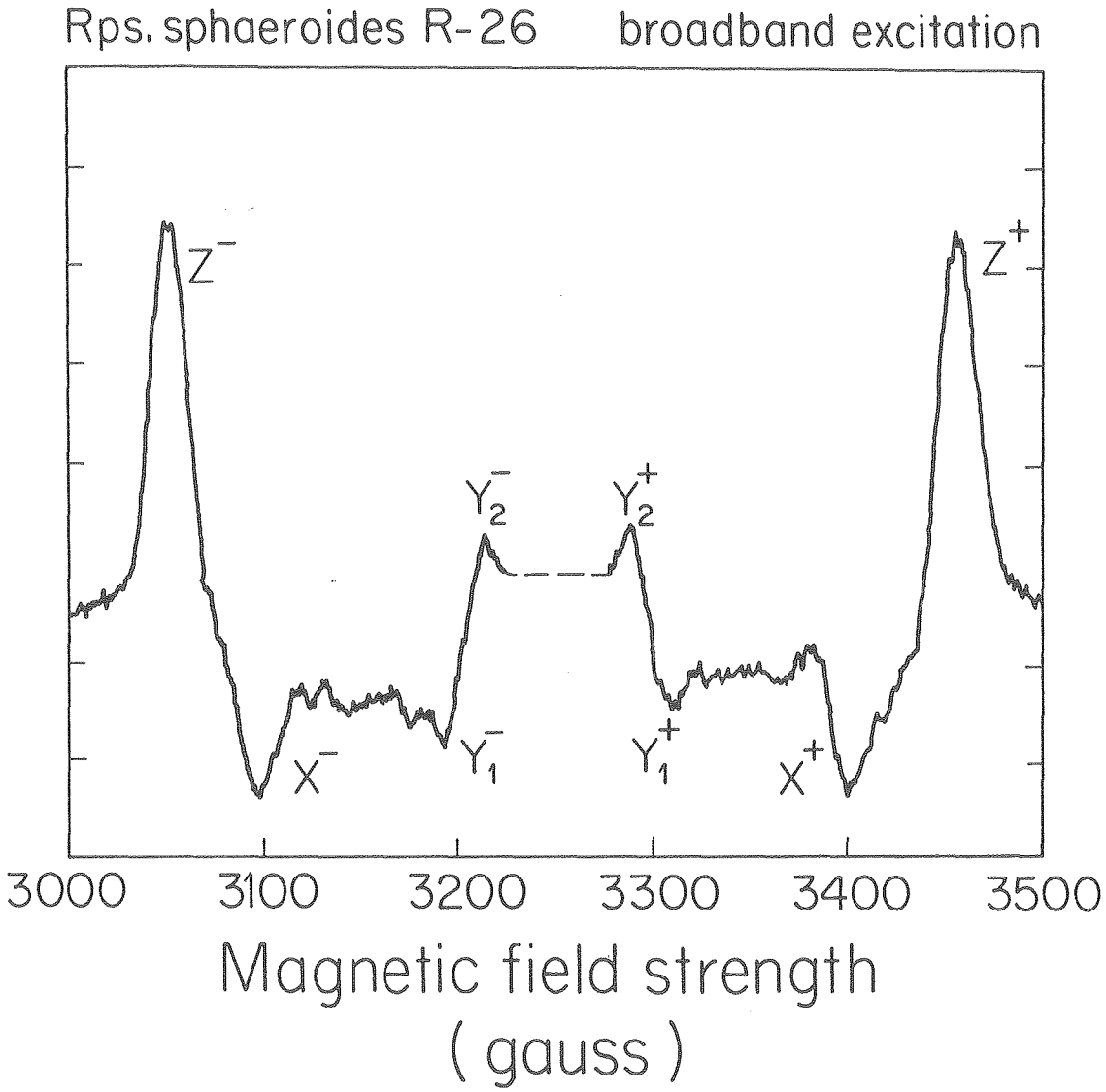


XBL 7812-13056

$$\cos^2\beta = \frac{|\underset{\sim}{\mu}\cdot\underset{\sim}{H}|^2}{|\underset{\sim}{\mu}|^2\,|\underset{\sim}{H}|^2} \qquad [6]$$

Decomposing H into its components along the principal magnetic axes gives:

$$\underset{\sim}{H} = |\underset{\sim}{H}| \begin{vmatrix} \sin\theta\cos\phi \\ \sin\theta\sin\phi \\ \cos\theta \end{vmatrix} \qquad [7]$$

where $\theta$ is the angle between $\underset{\sim}{H}$ and the z magnetic axis and $\phi$ is the angle between the component of $\underset{\sim}{H}$ in the xy plane and the x magnetic axis. Similarly for $\underset{\sim}{\mu}$ we have:

$$\underset{\sim}{\mu} = |\underset{\sim}{\mu}| \begin{vmatrix} \sin\theta'\cos\phi' \\ \sin\theta'\sin\phi' \\ \sin\theta' \end{vmatrix} \equiv |\underset{\sim}{\mu}| \begin{vmatrix} P_x \\ P_y \\ P_z \end{vmatrix} \qquad [8]$$

where $\theta'$ and $\phi'$ locate $\underset{\sim}{\mu}$ in the magnetic axis system of the triplet. $P_x$, $P_y$ and $P_z$ represent the projections of $\underset{\sim}{\mu}$ onto the three axes. The proper distribution function for excitation polarized parallel to $\underset{\sim}{H}$ is obtained by substituting [7] and [8] into equation [6] and considering the appropriate solid angle element:

$$D_{||}(\theta,\phi) = (P_x \sin\theta\cos\phi + P_y \sin\theta\sin\phi + P_z\cos\theta)^2 \sin\theta \qquad [9]$$

For light excitation polarized perpendicular to $\underset{\sim}{H}$ the probability of $\underset{\sim}{\mu}$ being excited is proportional to $\frac{1}{2}\sin^2\beta$. This leads to the distribution function,

$$D_{\perp}(\theta,\phi) = \tfrac{1}{2}[1 - (P_x \sin\theta\cos\phi + P_y \sin\theta\sin\phi + P_z\cos\theta)^2]\sin\theta \qquad [10]$$

Photoselected triplet state spectra were calculated by substituting equation [9] and [10] into equation [3]. $P_x$, $P_y$, and $P_z$ were varied until the best fit to the observed experiment spectra was found.

Broadband Excitation

Braodband light excites numerous transition moments of the RC producing a random distribution of triplets. This is evidenced by the fact that the broadband spectrum agrees with a "random" spectrum generated by monochromatic polarized light by summing one "parallel" spectrum plus two "perpendicular" spectra. The random triplet spectrum produced by broadband light is shown in Figure IV-1. This spectrum was computer simulated using equation [3] with $D(\theta,\phi) = \sin\theta$ (16). The zero-field splitting parameters, $|D|$ and $|E|$, and relative rate constants for intersystem crossing, $k_x$, $k_y$ and $k_z$, were varied until a good fit to the experimental spectrum was obtained (1,16). The values which best fit the observed spectrum are given in Table IV-2. The calculated spectrum is shown in Figure IV-2.

Photoselected Triplet State Spectra

The absorption at 870 nm represents a pure electronic transition of the BChl special pair. At low temperatures the absorption maximum is shifted to lower energy (31). Photo-

TABLE IV-1

EXPERIMENTAL TRIPLET STATE SIGNAL AMPLITUDE RATIOS
R-26 REACTION CENTERS

The amplitudes were measured at the key field positions indicated in Figs. IV-1, -3, and -5. The pairs of measured intensities (e.g. $X^+$ and $X^-$) were found to be equal within experimental error. The amplitudes are therefore designated by a superscript $\pm$ (e.g. $X^{\pm}$). Numbers in parenthesis indicate the range of acceptable ratios calculated from a fixed value for the uncertainty in the experimental amplitude determination.

| | $Z^{\pm}/X^{\pm}$ | $Z^{\pm}/Y_1^{\pm}$ | $Z^{\pm}/Y_2^{\pm}$ |
|---|---|---|---|
| Broadband | -2.4 (-2.7,-2.2) | -4.0 (-4.6,-3.5) | 6.2 (7.7,5.2) |
| 882 cm | | | |
| 1) parallel | -0.28 (-.35,-.22) | 3.7 (13.0,1.8) | 2.2 (4.3,1.3) |
| 2) perpendicular | -6.0 (-8.2,-4.0) | -3.6 (-4.3,-3.1) | 9.0 (14.0,6.5) |
| 550 nm | | | |
| 1) parallel | -2.8 (-3.6,-2.2) | -8.8 (-23.5,-5.1) | --* |
| 2) perpendicular | -1.6 (-2.4,-1.1) | -3.2 (-7.3,-1.8) | 1.6 (2.4,1.1) |

*$Y_2^{\pm}$ amplitude was approximately zero

FIGURE IV-2

Computer simulated triplet state spectrum of Rhodopseudomonas sphaeroides R-26. The spectrum was calculated assuming a random distribution of triplet states with respect to the EPR field direction. The parameters used to calculate this spectrum are given in Table IV-2.

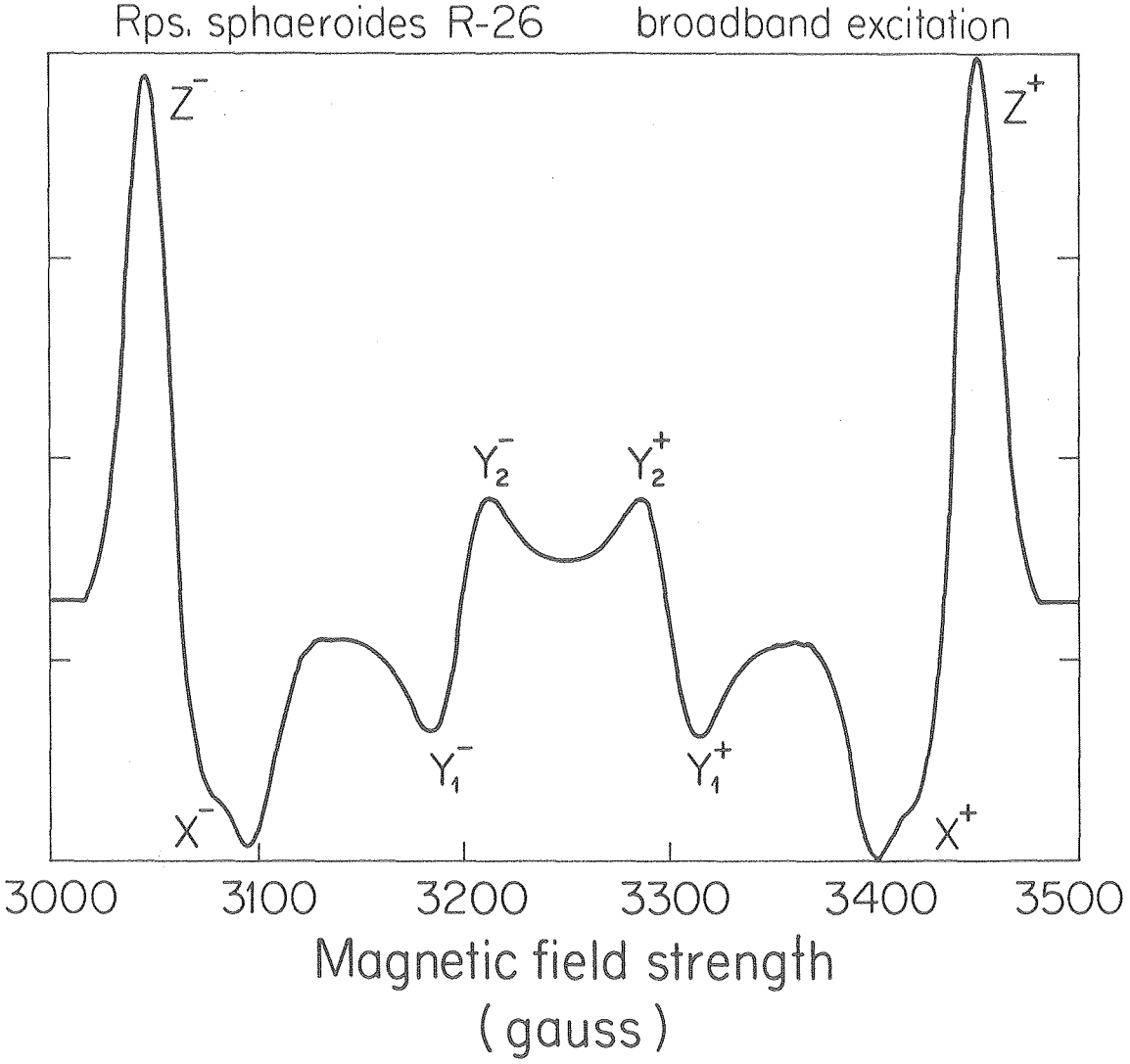


XBL7811-13039

TABLE IV-2

ZERO-FIELD SPLITTING PARAMETERS AND RELATIVE RATE CONSTANTS FOR INTERSYSTEM CROSSING

The $|D|$ and $|E|$ zero-field splitting parameters are given in $cm^{-1}$ units. $k_x$, $k_y$, and $k_z$ refer to rate constants for depopulation of the triplet spin sublevels associated with the $X^{\pm}$, $Y^{\pm}$, and $Z^{\pm}$ triplet peaks. A comparison of the present results with published values is given.

| Rps. sphaeroides R-26 | $\|D\|$ | $\|H\|$ | $k_x:k_y:k_z$ |
|---|---|---|---|
| The present work | .0187 ± .0002 | .0031 ± .0002 | 8.3:7.1:1.0 |
| Reference (34) | .0187 ± .0002 | .0031 ± .0001 | 1.7:2.0:1.0 |
| Reference (33) | .01872 ± .00002 | .00312 ± .00002 | 6.4:5.7:1.0 |

selected spectra using 882 nm excitation are shown in Figure IV-3. We assume that $|D|$, $|E|$, $k_x$, $k_y$, and $k_z$ remain constant, at the values found by simulation of the broadband spectra, Figures IV-1,2. $P_x$, $P_y$ and $P_z$ were varied in equations [9] and [10] in simulating the photoselected spectra. The best fit to the experimental spectra is given in Table IV-3 and the calculated spectra are shown in Figure IV-4.

At low temperatures the $Q_x$ absorption bands associated with the two BPheos are resolved at 530 nm and 546 nm (17,31). Light at 550 nm selects primarily the latter BPheo. Triplet state spectra photoselected at 500 nm are presented in Figure IV-5. Computer simulation found the best fit, which is shown in Figure IV-6 and summarized in Table IV-3.

Carotenoid Studies

Reaction Centers from Rps. sphaeroides wild type produce a triplet state spectrum at 160°K which is significantly different from the triplet from RCs of the carotenoidless mutant, R-26 (Figure IV-8). It is useful to compare the zero-field splitting parameters and polarization patterns. The wild type RC is characterized by the polarization pattern eaa eea, where e and a denote signals in emission and absorption respectively. The zero-field splitting parameters are: $|D| = 0.0290 \pm 0.0005$ and $|E| = 0.0044 \pm 0.0006$ $cm^{-1}$. For the R-26 RC triplet $|D| = 0.0189 \pm 0.0004$ and $|E| = 0.0032 \pm 0.0004$ $cm^{-1}$ and the polarization pattern is aee aae. Under the conditions initially used, the zero-field splitting para-

FIGURE IV-3

Experimental triplet spectra of Rhodopseudomonas sphaeroides R-26 generated by 882 nm polarized light. a) Spectrum taken with $\tilde{E} \parallel \tilde{H}$. b) Spectrum taken with $\tilde{E} \perp \tilde{H}$. Other conditions are as follows: sweep time, 1 h; field modulation frequency, 100 kHz, field modulation amplitude, 16G; receiver gain, 63, temperature, 11°K; microwave power 50 μ w; microwave frequency, 9.109 GHz; light modulation frequency 33.5 Hz; recorder time constant, 30 s; xenon lamp excitation. The light-induced free radical signal at g = 2.0 has been omitted.

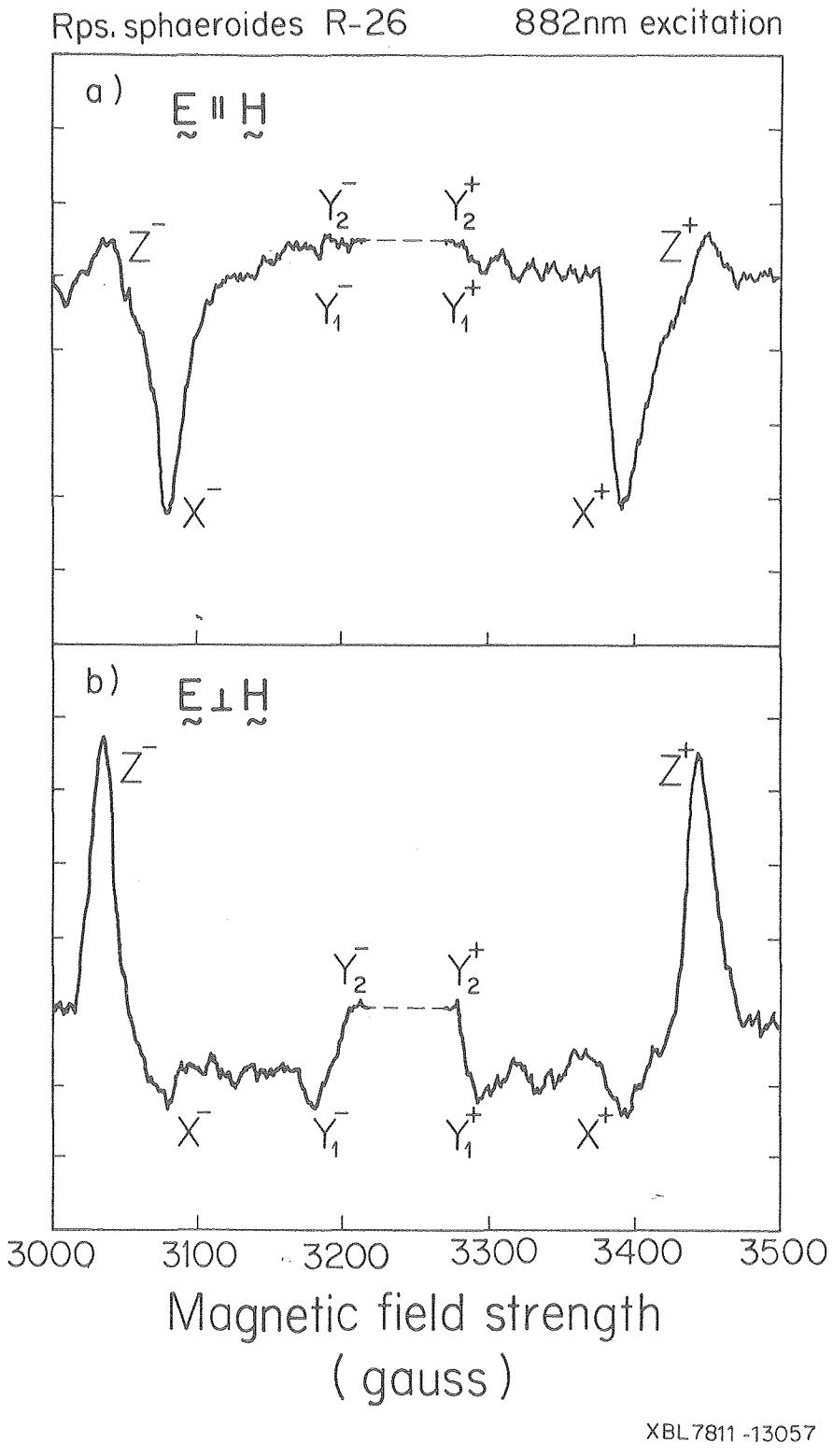


XBL 7811 -13057

FIGURE IV-4

Computer simulated 882 nm excited triplet state spectra of Rhodopsuedomonas sphaeroides R-26. The spectra were calculated assuming a) $\underset{\sim}{E} \parallel \underset{\sim}{H}$ and b) $\underset{\sim}{E} \perp \underset{\sim}{H}$. The parameters used to calculate these spectra are given in Tables IV-2 and -3. All computer simulations are normalized to the $|Z\pm| + |X\pm|$ peak amplitudes.

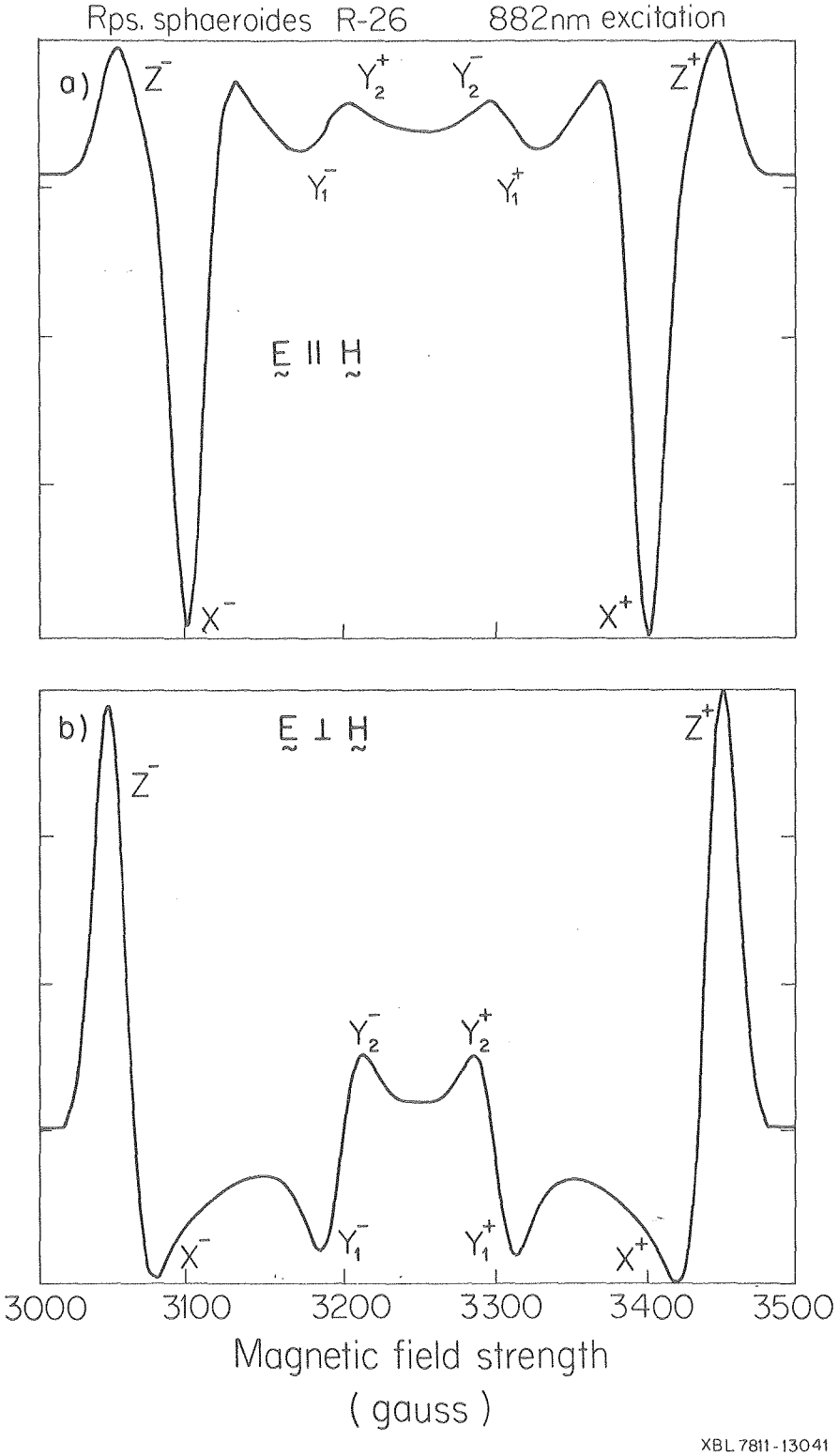


XBL 7811-13041

FIGURE IV-5

Experimental triplet state spectrum of Rhodopseudomonas sphaeroides R-26 generated by 550 nm polarized light. a) Spectrum taken with $\underset{\sim}{E} \parallel \underset{\sim}{H}$. b) Spectrum taken with $\underset{\sim}{E} \perp \underset{\sim}{H}$. Other conditions are as follows: sweep time, 1 h; field modulation frequency, 100 kHz; field modulation amplitude, 16 G; receiver gain, 80; temperature, 11°K; microwave power, 50 μ w; microwave frequency, 9.117 GHz; light modulation frequency 33.5 Hz; recorder time constant, 30 s; mercury-xenon lamp excitation. The light induced free radical signal at g = 2.0 has been omitted.

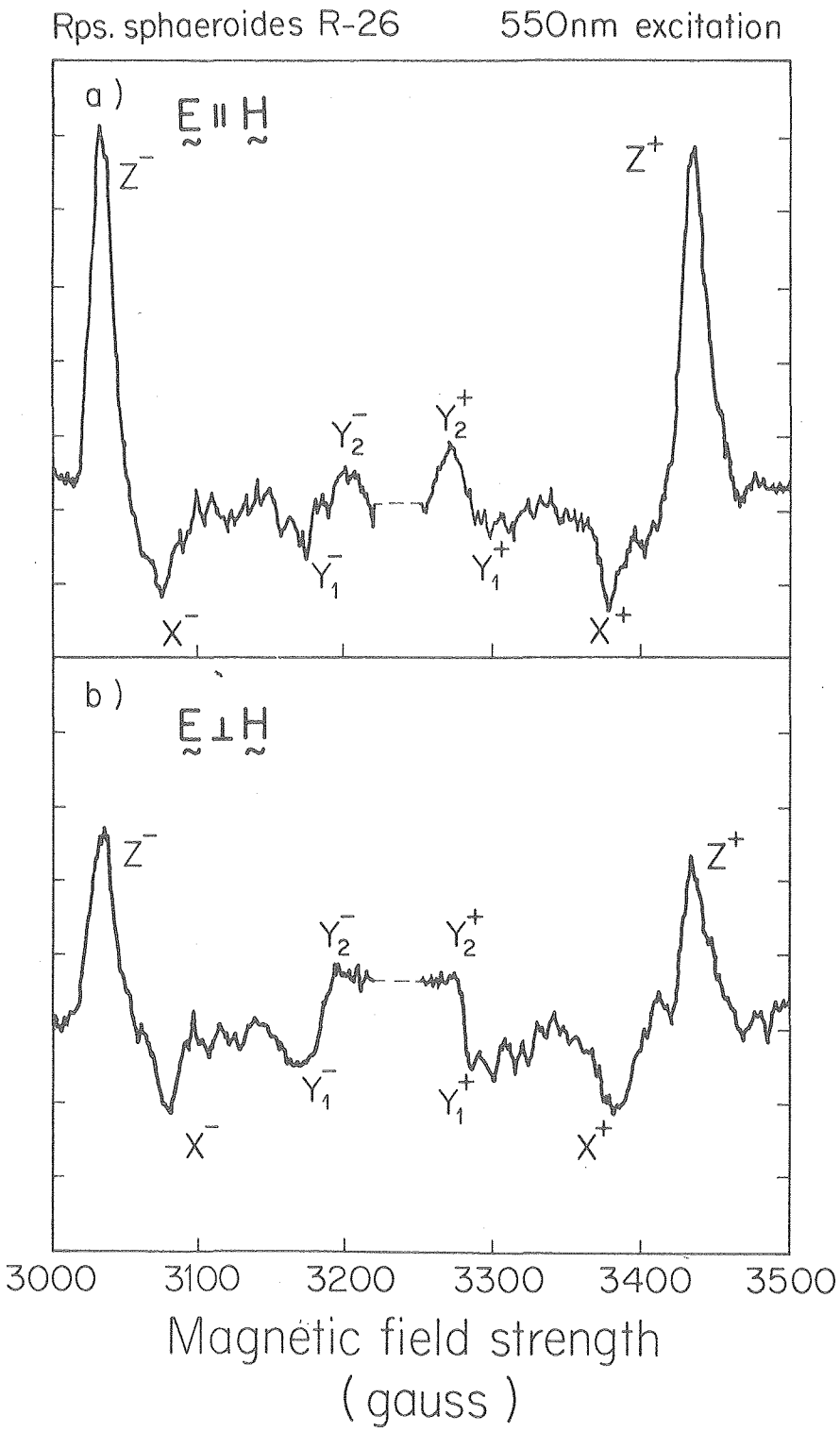


XBL 7812-13058

FIGURE IV-6

Computer simulated 550 nm excited triplet state sepctra of Rhodopseudomonas sphaeroides R-26. The spectra were calculated assuming a) $\underset{\sim}{E} \parallel \underset{\sim}{H}$ and b) $\underset{\sim}{E} \perp \underset{\sim}{H}$. The parameters used to calculate these spectra are given in Tables IV-2 and -3.

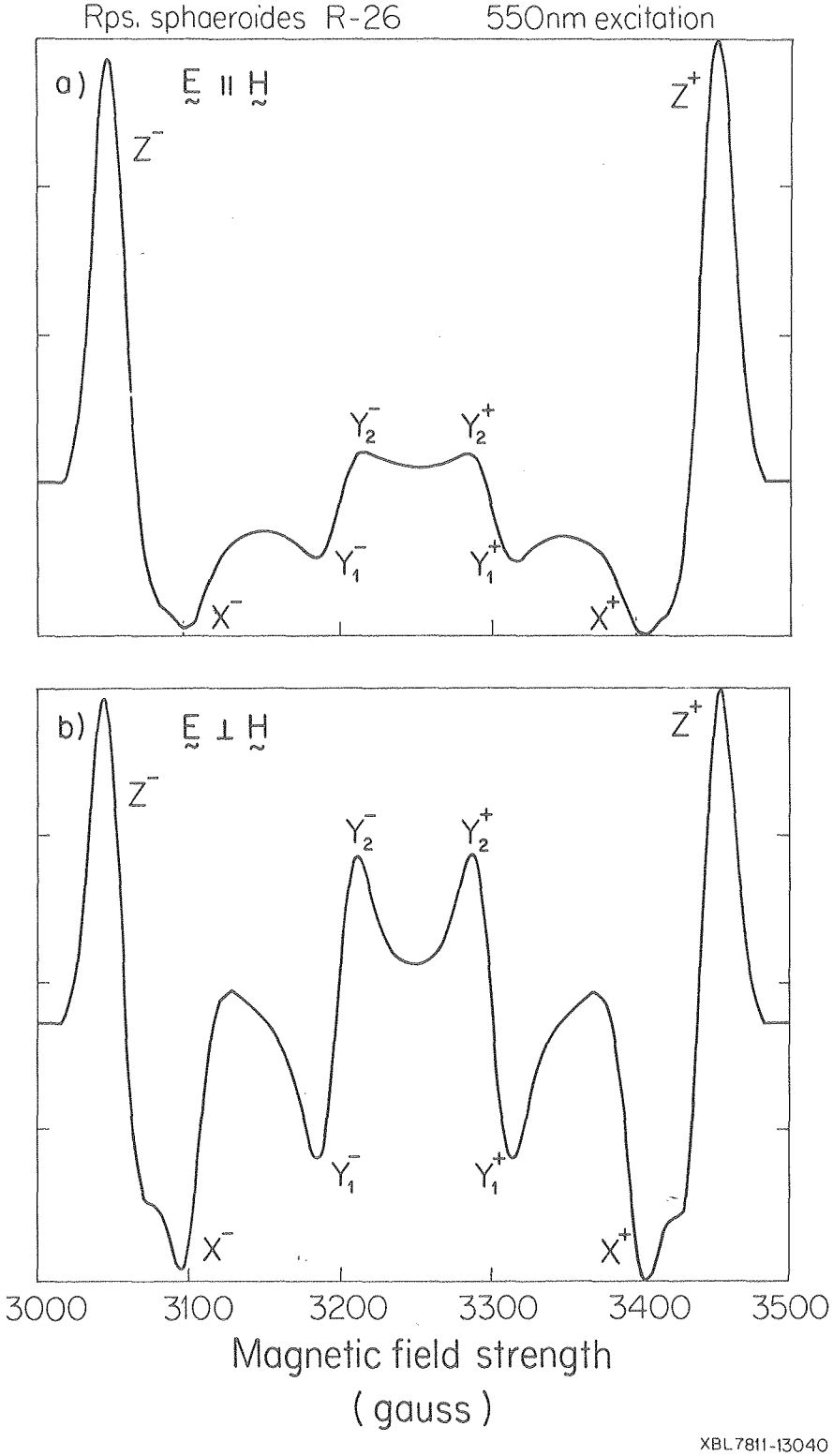


XBL7811-13040

FIGURE IV-7

The orientation of the transition moments at 546 nm and 870 nm with respect to the principal magnetic axis system (x,y,z) of the triplet state. The angles were calculated from the projections given in Table 3 using the relations $\theta_x$ = arccos $P_x$, etc. $\gamma$ was calculated from equation [11] in the text.

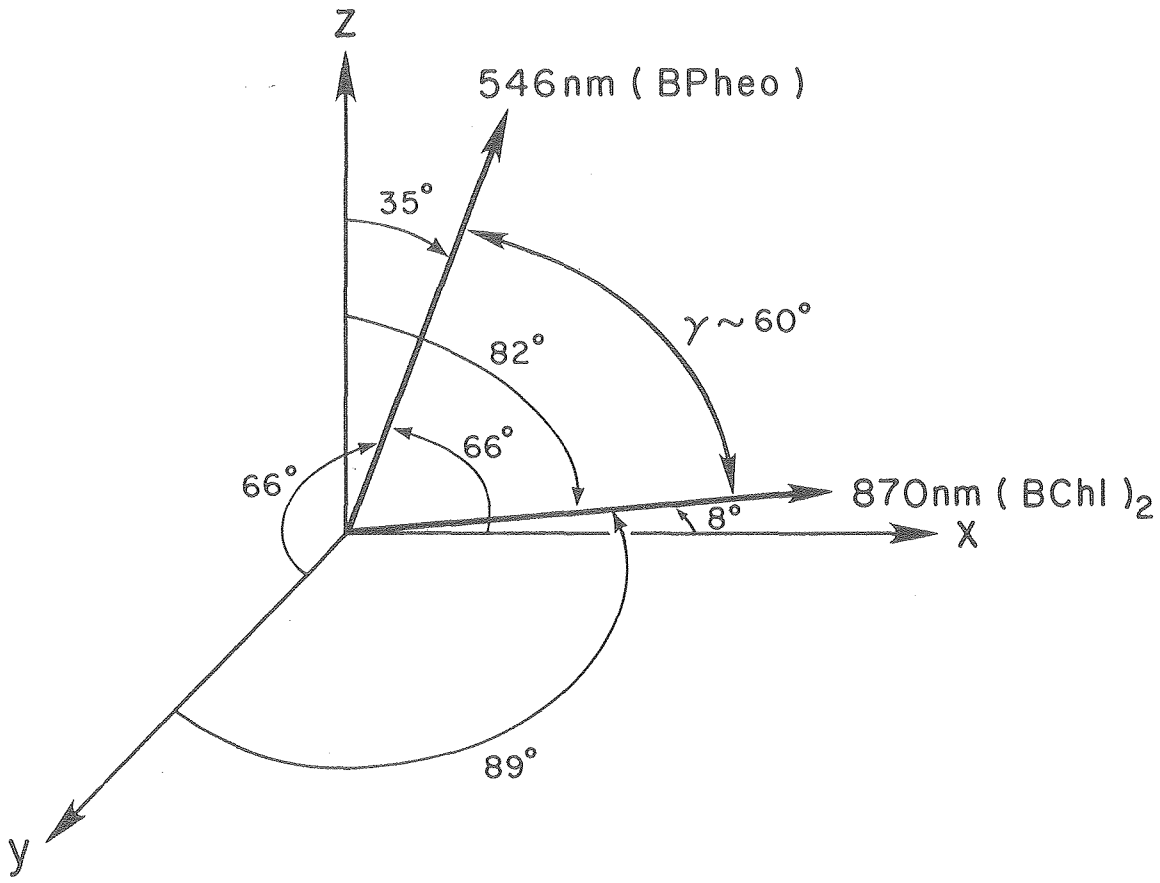


XBL7811-13055

TABLE IV-3

PROJECTION OF THE OPTICAL TRANSITION MOMENTS ONTO THE PRINCIPAL MAGNETIC AXES OF THE TRIPLET STATE

The best fit of the calculated spectra to the experimental results are given by the projections $P_x$, $P_y$, and $P_z$.

| | $P_x$ | $P_y$ | $P_z$ |
|---|---|---|---|
| 870 nm | .99 | .014 | .14 |
| 546 nm | .405 | .405 | .82 |

TABLE IV-4

BOUNDARY CONDITIONS FOR THE RECTANGULAR REGION OF SOLUTION

The regions of solution are given by rectangles, the dimensions of which are determined by $P_x$ and $P_z$ which are the projections of the transition moments onto the x and z principal magnetic axes, respectively.

| | | |
|---|---|---|
| 870 nm | $.98 < P_x < 1.00$ | $.10 < P_z < .16$ |
| 546 nm | $.33 < P_x < .63$ | $.73 < P_z < .85$ |

FIGURE IV-8

(a) Rps. sphaeroides wild type reaction center, triplet state spectrum taken with the following conditions: temperature, 160°K; receiver gain, 50; microwave power, 5 mW; light modulation frequency, 33 Hz; sweep time, 1 hour; recorder time constant, 30 sec.

(b) Rps. sphaeroides R-26 reaction center, triplet state spectrum. The conditions are the same as in (a) except: receiver gain, 32, sweep time, 8 min; recorder time constant, 3 sec.

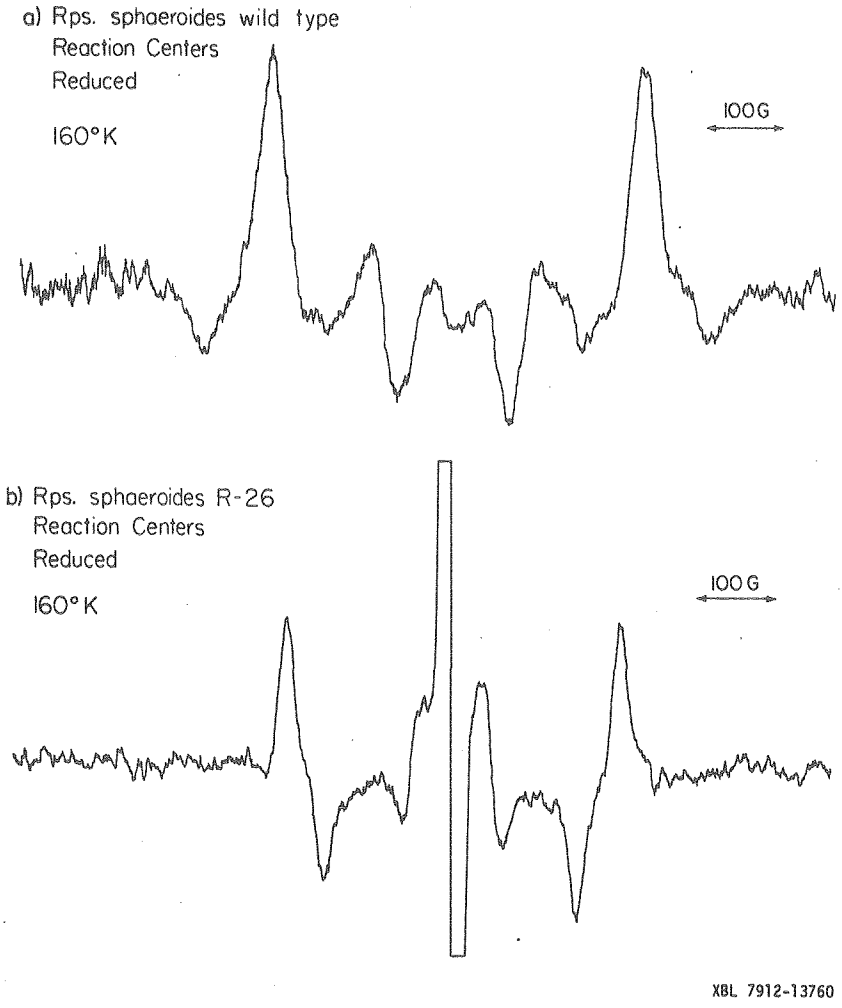


XBL 7912-13760

FIGURE IV-9

Rps. sphaeroides wild type light harvesting protein, triplet state spectrum. Experimental conditions were: temperature, 160°K; receiver gain, 63; microwave power, 5 mW; light modulation frequency, 11 Hz; sweep time, 1 hour; recorder time constant, 30 sec.

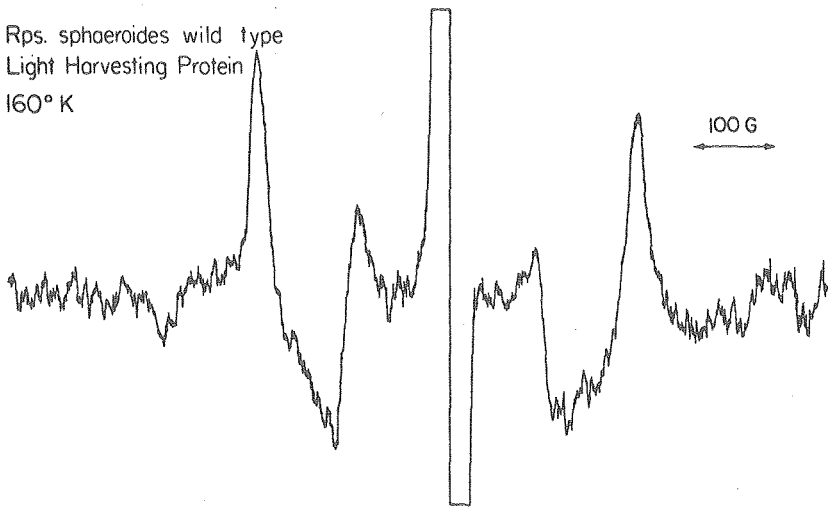


XBL 7912-13763

FIGURE IV-10

Rps. sphaeroides wild type untreated whole cells, triplet state spectra taken with the following conditions: receiver gain, 25; microwave power 1 mW; light modulation frequency, 33 Hz; sweep time, 30 min; recorder time constant, 30 sec; temperature (a) 100°K, (b) 10°K.

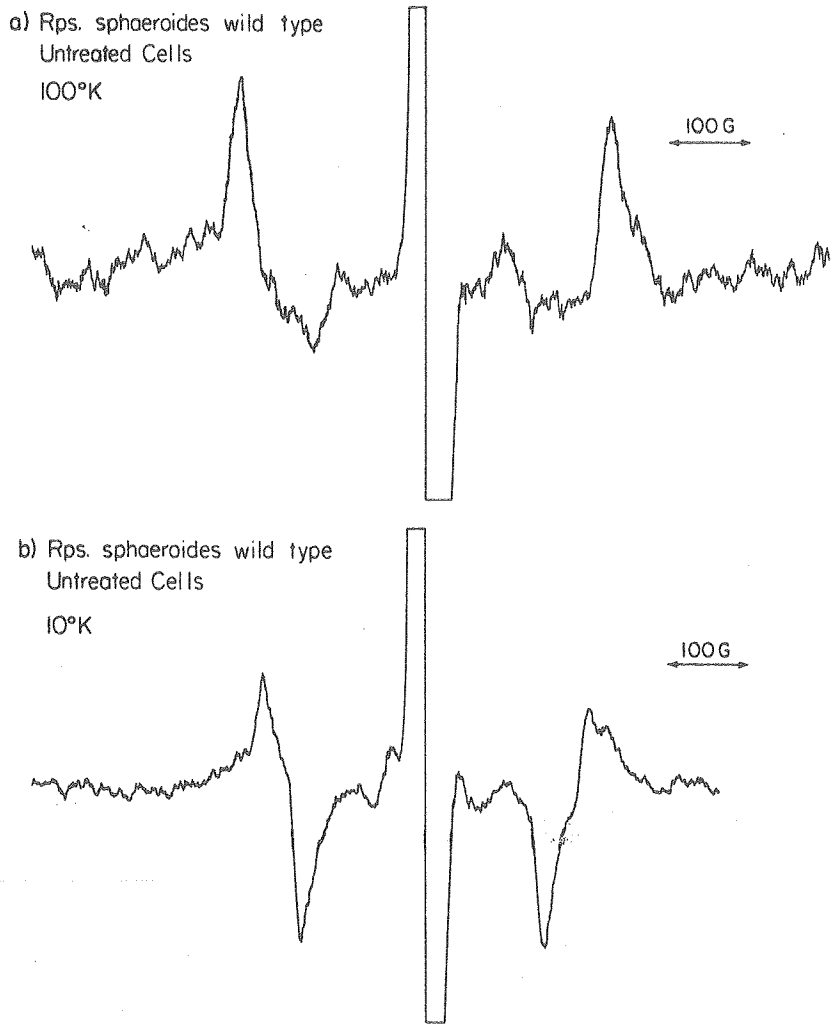


XBL 7912-13761

FIGURE IV-11

(a) Rps. sphaeroides wild type reduced whole cells, triplet state spectrum taken with the following conditions: receiver gain, 80; microwave power 1 mW; light modulation frequency, 33 Hz; sweep time, 8 min; recorder time constant, 10 sec; temperature, 100°K.

(b) Rps. sphaeroides wild type reduced whole cells, triplet state spectrum taken with the experimental conditions of (a) except: receiver gain, 63, sweep time, 16 min, temperature, 10°K.

(c) Rps. sphaeroides R-26 reduced whole cells, triplet state spectrum taken with the experimental conditions of (b).

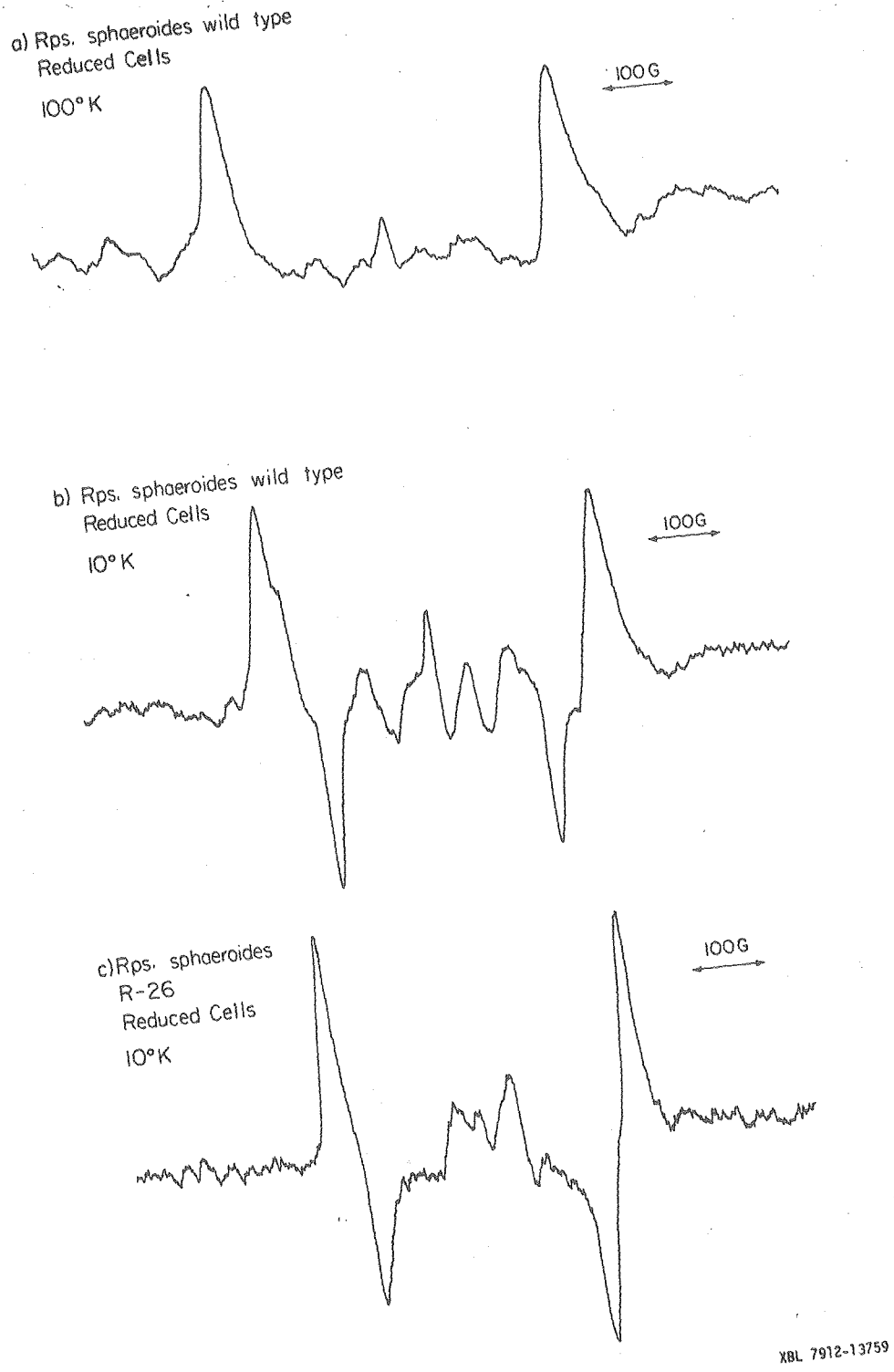
a) Rps. sphaeroides wild type
Reduced Cells
100° K
100 G
b) Rps. sphaeroides wild type
Reduced Cells
10° K
100G
c)Rps. sphaeroides
R-26
Reduced Cells
10°K
100G
XBL 7912-13759

meters and polarization patterns of both spectra (Figure IV-8) were unchanged at $10^{o}K$. When the Hg-Xe lamp was attenuated, the wild type RCs gave a spectrum at $10^{o}K$ which appeared to be a convolution of the $160^{o}K$ spectrum and the spectrum of R-26 RCs. At $160^{o}K$ light intensity did not affect the shape of the spectrum.

The triplet spectrum of the light harvesting protein B800+850, from wild type Rps. sphaeroides is shown in Figure IV-9. The zero-field splitting parameters are $|D| = 0.0326 \pm 0.0007$, $|E| = 0.0036 \pm 0.0007$ $cm^{-1}$ and the polarization pattern is eae aea. The same spectrum is observed at $10^{o}K$.

Whole cells of Rps. sphaeroides wild type which are prepared at ambient redox potential exhibit a market temperature dependence in triplet state EPR spectra (Figure IV-10). At $10^{o}K$ a spectrum is observed with identical zero-field splitting parameters and polarization pattern as the spectrum of R-26 whole cells or reaction centers. At higher temperatures the lineshape is transformed into a triplet spectrum which has parameters and polarizations which are very similar to those of the light harvesting complex shown in Figure IV-9.

Reduced whole cells of Rps. sphaeroides wild type show a change in the triplet state spectra upon raising the temperature from $10^{o}K$ to $100^{o}K$ (Figure IV-11). At $100^{o}K$ the parameters and polarization closely resemble the spectrum of reduced RCs at $160^{o}K$ (Figure IV-8a). At $10^{o}K$ the spectrum (Figure IV-11b) appears to be a convolution of the spectrum

at 100°K and the spectrum observed in the carotenoidless mutant, R-26 (Figure IV-11c). The spectra observed from cells of Rps. sphaeroides R-26 (carotenoidless mutant) under all conditions display the same zero-field splitting parameters and polarization pattern, corresponding to the values observed for reduced reaction centers (Figure IV-8b).

The effects of temperature and reduction on the triplet state spectra of Rhodospirillum rubrum wild type were also studied. Untreated cells, Figure IV-12, show one triplet signal and it is independent of temperature. The polarization pattern is eae aea and $|D| = 0.0233 \pm 0.0007$, $|E| = 0.0026 \pm 0.0007$ $cm^{-1}$. Reduced cells exhibit one triplet spectrum at 100°K, characterized by $|D| = 0.0180 \pm 0.0004$ and $|E| = 0.0040 \pm 0.0004$ $cm^{-1}$ and a polarization pattern of eaa eea. At 10°K the lineshape appears to be a convolution of two triplet species.

We also observed triplet state spectra from cells of the carotenoidless mutant of Rsp. rubrum G-9, from Rps. viridis and from Rps. palustris. Only Rps. palustris showed an effect upon variation of temperature and reduction.

We failed to observe triplet state spectra of β-carotene dissolved in numerous organic solvents (e.g., 2-methyltetrahydrofuran, hexane, EPA and cyclohexane). However, a spectrum was observed when β-carotene was suspended in phospholipid vesicles or non-ionic detergent micelles. Its polarization pattern was eae aea and $|D| = 0.0333 \pm 0.0010$, $|E| = 0.0037 \pm 0.0010$ $cm^{-1}$. All of the experimental results are

FIGURE IV-12

Rsp. rubrum wild type, triplet state spectra of (a) untreated cells. The spectrum was taken with the following conditions: temperature, 10°K; receiver gain, 125; microwave power, 1 mW; light modulation frequency, 33 Hz; sweep time, 16 min; recorder time constant, 10 sec. (b) Reduced cells. The spectrum was taken with the experimental conditions of (a) except: temperature 100°K; receiver gain, 20; sweep time, 8 min; recorder time constant, 3 sec. (c) Reduced cells. The spectrum was taken with the experimental conditions of (a) except, receiver gain, 25.

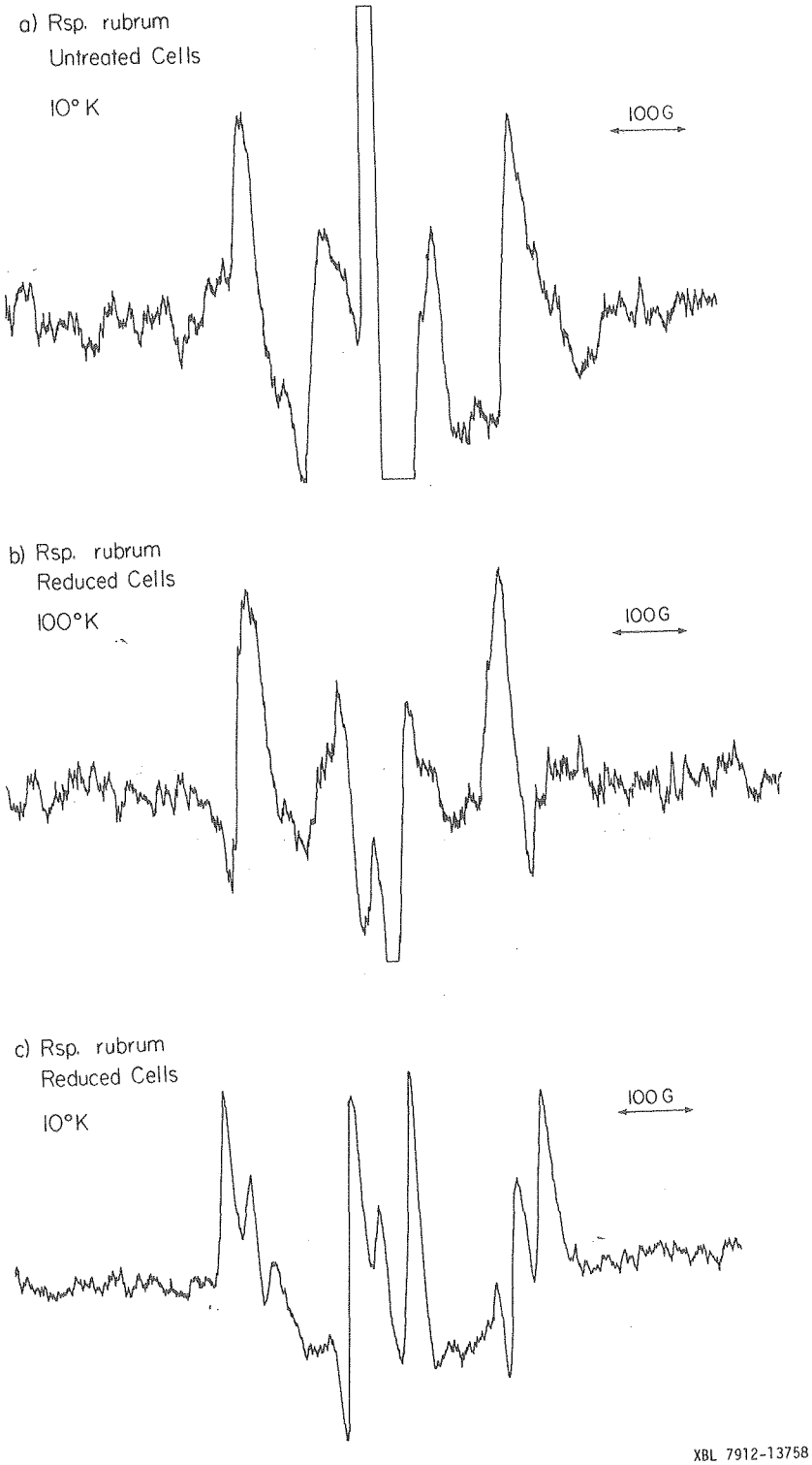


XBL 7912-13758

FIGURE IV-13

β-Carotene in micelles, triplet state spectrum taken with the following conditions: temperature, 160°K; receiver gain, 200; microwave power, 5 mW; light modulation frequency, 11 Hz; sweep time, 30 min; recorder time constant, 30 sec.

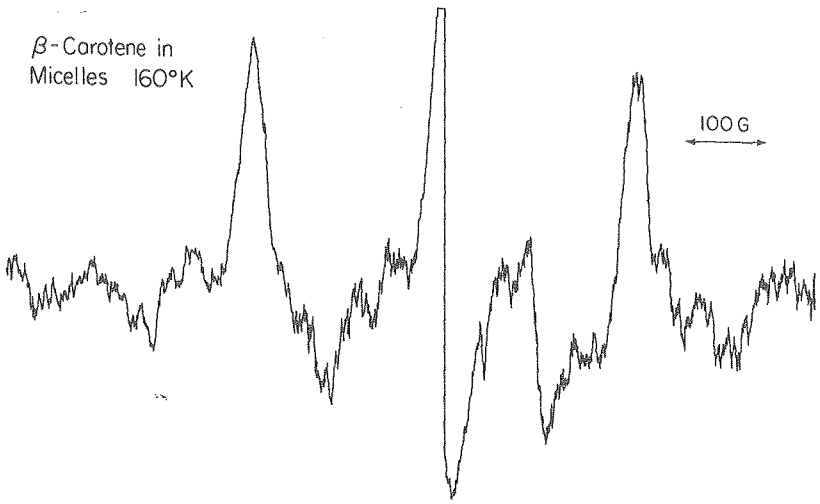


XBL 7912-13764

TABLE IV-5 Zero-field splitting parameters, polarization patterns and assignments of the observed triplet states. $|D|$ and $|E|$ are given in $cm^{-1}$ units.

| Sample | Temp. (K) | $\|D\|$ | $\|E\|$ | Polarization Pattern | Triplet Assignment |
|---|---|---|---|---|---|
| Rhodopseudomonas sphaeroides wild type | | | | | |
| Reduced reaction centers | 160,100,10 | .0290±.0005 | .0044±.0006 | eaa eea | Reaction center carotenoid |
| Light harvesting protein (LHP) | 160,100,10 | .0326±.0007 | .0036±.0007 | eae aea | Light harvesting carotenoid |
| LHP pigment extract | 160 | .0220±.0005 | .0053±.0005 | eea eaa | Bacteriochlorophyll monomer |
| Reduced cells | 100 | .0289±.0010 | .0044±.0010 | eaa eea | Reaction center carotenoid |
| | 10 | convoluted | | | RC carotenoid and $BChl_2$ |
| Untreated cells | 100 | .0323±.0010 | .0033±.0010 | eae aea | Light harvesting carotenoid |
| | 10 | .0189±.0005 | .0030±.0005 | aee aae | $BChl_2$ |
| Rhodopseudomonas sphaeroides R-26 | | | | | |
| Reduced reaction centers | 160,100,10 | .0189±.0004 | .0032±.0004 | aee aae | $BChl_2$ |
| Reduced cells | 100,10 | .0189±.0003 | .0030±.0003 | aee aae | $BChl_2$ |
| Untreated cells | 100,10 | .0189±.0003 | .0030±.0003 | aee aae | $BChl_2$ |
| Rhodospirillum rubrum wild type | | | | | |
| Reduced cells | 100 | .0180±.0004 | .0040±.0004 | eaa eea | Reaction center carotenoid |
| | 10 | convoluted | | | RC carotenoid and $BChl_2$ |
| Untreated cells | 100,10 | .0233±.0007 | .0026±.0007 | eae aea | Light harvesting carotenoid |
| Rhodospirillum rubrum G-9 | | | | | |
| Reduced cells | 100,10 | .0192±.0004 | .0033±.0004 | aee aae | $BChl_2$ |
| Untreated cells | 100,10 | .0192±.0004 | .0033±.0004 | aee aae | $BChl_2$ |
| Rhodopseudomonas viridis | | | | | |
| Reduced cells | 100,10 | .0154±.0003 | .0036±.0003 | aee aae | $BChl_2$ |
| Untreated cells | 100,10 | .0154±.0004 | .0036±.0004 | aee aae | $BChl_2$ |
| Rhodopseudomonas palustris | | | | | |
| Reduced cells | 100,10 | .0190±.0005 | .0034±.0005 | aee aae | $BChl_2$ |
| Untreated cells | 100 | convoluted | | | LH carotenoid and $BChl_2$ |
| | 10 | .0190±.0005 | .0034±.0005 | aee aae | $BChl_2$ |
| β-carotene | | | | | |
| in micelles | 160 | .0333±.0010 | .0037±.0010 | aea aea | β-carotene |
| in vesicles | 160 | .0331±.0010 | .0037±.0010 | eae aea | β-carotene |

summarized in Table IV-5.

Discussion

The triplet state produced by illumination of reduced cells or reaction centers from the carotenoidless mutant Rps. sphaeroides R-26 is known to be the BChl dimer triplet of the reaction center special pair (3). Its aee aae polarization pattern indicates that a charge separation/recombination process is involved in its formation (32). According to the radical pair recombination mechanism, the system is initially in an excited singlet state. After one electron is transferred from donor ($BChl_2$) to acceptor (BPheo) the electrons are correlated, the system is in a singlet radical pair state. In this state significant quantum mechanical mixing between the singlet and the middle energy high-field triplet spin sublevel, $T_o$, may occur. The effect of this mixing is to produce a spin population in the recombined BChl dimer triplet which is primarily in the $T_o$ level. If the triplet state is then observed by EPR prior to spin lattice relaxation, all $T_o$ to $T_{+1}$ transitions are in abosrption and all $T_o$ to $T_{-1}$ transitions are in emission. For systems where the zero field splitting parameter, D, is positive the observed polarization pattern is aee aae. If D is negative, the polarization pattern eaa eea is observed. These are the polarization patterns observed in reaction center preparations and in some cases whole cells, see below. Normal intersystem crossing from a molecular excited singlet to the triplet state will not

produce this polarization pattern.

Magnetophotoselection

Examination of Figure IV-3 demonstrates the striking dependence of the triplet state EPR spectrum on the direction of polarization of excitation light. Qualitatively, it is apparent that the 870 nm transition moment lies along the x magnetic axis. Quantitative values for the projections of the 870 nm were obtained by computer simulation.

The simulation of the "random" spectrum (broadband excitation) yeilded values of $|D|$ and $|E|$ which agree well with measurements from other laboratories (Table IV-2). The uncertainty of the values from the computer simulations was less than the uncertainty calculated directly from the spectra. (Compare Table IV-2 to Table IV-5).

Exclusive population of the $T_o$ sublevel simplifies calculation of the relative intersystem crossing rates to the ground state (16). The relative values of $k_x$, $k_y$, and $k_z$ extracted by computer simulation are given in Table IV-2. These values lie within the uncertainty of more direct determination by Hoff (33) but disagree with those determined by Clarke's group (34).

Computer simulation of the spectra shown in Figure IV-3 gave a precise value for the projection of the 870 nm transition moment onto the x magnetic axis, $P_x = 0.99 \pm 0.01$. The x axis, as defined here (Figures IV-1 and IV-7) is referred to as the y axis in reference (10). The high degree of precision is a result of the very small ratio $Z^{\pm}/X^{\pm}$ for excitation

polarized parallel to $\underset{\sim}{H}$ and the change in sign of the $Z^{\pm}/ Y^{\pm}$ ratio upon the change of light polarization. These features were reproduced in simulations only when $P_x$ was greater than 0.98. This result argues against significant depolarization of excitation in our experiments.

Simulation of the spectra obtained by 550 nm photoselection (Figures IV-5, IV-6) was found to be less precise. The uncertainty in the determinations of the projections onto the magnetic axes is determined by the computer simulations which produced peak-to-peak ratios which fell within the experimental uncertainty (Table IV-1). The range of values is specified by two of the three possible projections, because the third projection is linearly dependent ($P_x^2 + P_y^2 + P_z^2 = 1$). The 546 nm transition moment lies primarily along the z axis, with a projection, $P_z = 0.82$ in the best fit.

Using the values of $P_x$, $P_y$ and $P_z$ listed in Table IV-3 the angle between the 546 nm and 870 nm transition moments can be calculated. The angle is given by

$$\gamma = \arccos \left| \underset{\sim}{V}_1 \cdot \underset{\sim}{V}_2 \right| \qquad [11]$$

where $V_1 = (\pm .405, \pm .405, \pm .82)$ and $V_2 = (\pm .99, \pm .014, \pm .14)$ are the vectors representing the 546 nm and 870 nm transitions in the principal magnetic axis system. Values for $\gamma$ from equation [11] were found to be $60^{\circ}(120^{\circ})$ and $72^{\circ}(108^{\circ})$. The $60^{\circ}$ value agrees with the value determined by Vermeglio, et. al. (17). To summarize the magnetophotoselection results, the

orientations of the 546 nm and 870 nm transition moments within the principal magnetic axis system of the special pair triplet state are drawn in Figure IV-7.

Boxer and Roelofs (36) have recently published magneto-photoselection studies of the R-26 RC. Their results, where comparable, confirm our own. However, their analysis of the data, based on the assumption that each triplet state spectral peak originates only from those molecular orientations assigned to that conical orientation, is incorrect. Due to the hyperfine width of each contributing orientation and to the EPR field modulation amplitude (16 gauss in our experiments, 20 gauss in (36)) we believe the assumption is only an approximation. Full computer simulation of the observed triplet state spectra is a much better approach for obtaining quantitative information.

Carotenoid Triplet States

The triplet state spectrum observed in RCs of carotenoid containing bacteria (Figure IV-8a) is due to the carotenoid spheroidene, which is known to be associated with the complex (28). This assignment is supported by several arguments:

a) The spectrum of Figure IV-8a is not observed in the carotenoidless mutant of Rps. sphaeroides R-26 under a wide variety of redox, preparative, and temperature conditions (Table IV-5). It is not characteristic of one of the other RC pigments (four BChls and two BPheos). The zero-field splitting parameters of spectrum (a) of Figure IV-8 are well outside the range of parameters expected for BChl or BPheo

monomers or aggregates (32).

(b) The polarization pattern in Figure IV-8 a is eaa eea. Thus the triplet is either directly involved in or closely coupled to the charge separation/recombination process. The latter possibility has been discussed by Monger et. al. (26). They concluded, from optical spectroscopic changes, that the carotenoid triplet was formed by triplet energy transfer from the $BChl_2$ triplet state. If energy transfer from donor to acceptor occurs at a rate comparable to or faster than spin lattice relaxation, then the acceptor may also have a radical pair polarization pattern. Indeed, the $BChl_2$ polarization is aee aae and the new triplet is eaa eea. The difference may be accounted for if the D value of the acceptor (carotenoid) is opposite that of the donor ($BChl_2$) and energy transfer occurs from the $T_o$ level of the $BChl_2$ to the $T_o$ level of the acceptor. Alternatively, if the D values of $BChl_2$ and acceptor are both positive and energy transfer proceeds from the $T_o$ level of the $BChl_2$ to the $T_{+1}$ and $T_{-1}$ levels of the acceptor, the observed polarization pattern would also be observed.

(c) The intensity of the new triplet state relative to the $BChl_2$ triplet state is dependent upon temperature. In reduced cells of Rps. sphaeroides wild type the amplitudes of the signals observed at $100^{o}K$, Figure IV-8a and IV-11a, decrease relative to the $BChl_2$ triplet peaks, Figure IV-8b and IV-11c, as the temperature is lowered to $10^{o}K$. Precisely the same effect was observed by Cogdell, Monger and Parson

(25,26). We have also found that the relative amplitudes of these two signals in isolated RC's are dependent on light intensity. At high light the $BChl_2$ triplet is suppressed. This result may imply triplet-triplet or triplet-singlet annihilation processes within the RC. A discussion of these possibilities is beyond the scope of this discussion and these experiments.

Figure IV-10b shows that untreated cells of Rps. sphaeroides wild type also produce the triplet signals. At $10^{o}K$ the signal is weak; the predominant species is the $BChl_2$ RC triplet. Large free radical signals in the central region indicate that radical formation and decay is occurring at a rate comparable to the chopper frequency. At $100^{o}K$ a triplet state spectrum noticeably different from either the reaction center BChl dimer or carotenoid is observed (Figure IV-10a). Again the zero-field splitting parameters (Table IV-5) are significantly bigger than those observed for BChl or BPheo (32). Because RCs are predominantly in the charge separated state, $BChl_2^{+}BPheo\ Q^{-}$, at these light intensities, we believe this triplet state originates in the antenna pigment array. This hypothesis was confirmed by isolating the major light harvesting complex, the B800+850 protein, and observing its triplet state by EPR. The observed triplet (Figure IV-9) has the same polarization pattern, eae aea, and zero-field splitting parameters as found in untreated cells of Rps. sphaeroides (Table IV-5). The polarization pattern indicates that charge separation/recombination does not play

a role in producing the triplet. The triplet appears to arise from sensitization by BChl. Excitation at wavelengths greater than 545 nm, such that light is abosrbed only by BChl, produce the same triplet spectrum. Furthermore, extraction of the component pigments (3 BChls per carotenoid) into organic solvents and observation of the triplets formed upon light excitation detects a spectrum with typical monomeric BChl parameters(Table IV-5). We believe that in the intact complex the component carotenoid is held close enough to a BChl triplet (formed by intersystem crossing) to participate in triplet-triplet energy transfer. In homogenous solution the average distance between BChls and carotenoids will be much greater and will severely limit such transfer.

Figure IV-12 shows the results of studies of Rsp. rubrum wild type. The same interpretations as given above seem likely. When reaction centers are reduced the triplet spectrum observed is assigned to the RC carotenoid at $100^{o}K$. At $10^{o}K$ the spectrum is a convolution of the carotenoid triplet and the BChl special pair triplet. When reaction centers are unreduced, a carotenoid triplet state is formed in the antenna complex. The polarization patterns under these conditions are identical to those found in Rps. sphaeroides. The zero-field splitting parameters are different. This difference can be attributed to the difference in nature of the carotenoid content in the two species.

Thin layer chormatography (28) of pigments from Rsp. rubrum cells grown in our laboratory revealed only one carotenoid,

spirilloxanthin (35). Reaction centers of Rps. sphaeroides wild type contain only spheroidene (28). The observed differences in |D| values (Table IV-5) may be rationalized in terms of the extent of electron delocalization within the carotenoid molecule. Spirilloxanthin contains a chain of thirteen conjugated carbon-carbon double bonds, whereas spheroidene contains a chain of only ten. The lesser extent of delocalization in spheroidene should lead to greater dipolar interaction between the unpaired electrons in the triplet state, and therefore to a greater |D| value. Because cells of Rsp. rubrum contain only one carotenoid, we might expect the |D| parameter to remain the same in both the reaction center and light harvesting triplets. This is not observed. The reaction center |D| value is significantly smaller (Table IV-5). Rps. sphaeroides triplets show the same trend. This trend suggests that significant environmental or conformational effects are important in determining zero-field splitting parameters of carotenoids.

The final system for discussion is the triplet state of β-carotene. As mentioned previously, formation of the triplet state via intersystem crossing is not highly favored in symmetric polyene hydrocarbons (20,21). Their structures may be such that photochemical or vibrational (radiationless) relaxation competes with intersystem crossing, even at $77^{o}K$. Incorporation of β-carotene into detergent micelles may restrict radiationless decay and allow intersystem crossing

to occur. Similar effects have been observed for aromatic hydrocarbons (37). The similarity of the spectrum observed in Figure IV-13 with spectra IV-10a, IV-9 and IV-12a support its assignment to the triplet state of β-carotene. It is very likely that a triplet state observed in green plants (Signal II of Frank, et. al., reference 23) arose from β-carotene.

## Conclusions

Triplet state EPR spectroscopy has proven to be a valuable technique for probing BChl protein complexes, especially the reaction center. Magnetophotoselection provides a key link between many of the optical and magnetic resonance experiments in photosynthesis research. To translate the magnetic and optical axes depicted in Figure IV-7 into the molecular axes of the BChls of the special pair is the dream of many scientists.

The triplet states detected in the second part of this chapter are significant because they are the first reported EPR spectra assigned to carotenoids. Characterization of carotenoid triplet states by EPR will prove important in molecular spectroscopy and, we hope, in the study of visual processes.

REFERENCES

(1) Frank, H.A., Bolt, J.D., Friesner, R. and Sauer, K., Biochim. Biophys. Acta 547, 502 (1979).

(2) Frank, H.A., Bolt, J.D., Costa, S.M.B. and Sauer, K., submitted to J. Am. Chem. Soc., December 1979.

(3) Blankenship, R. and Parson, W.W., in Topics in Photosynthesis, vol. 3, J. Barber, ed. (Elsevier), New York, N.Y., 1979, p. 71.

(4) McGlynn, S.P., Azumi, T. and Kinoshita, M., in Molecular Spectroscopy of the Triplet State (Prentice-Hall), Englewood Cliffs, N.J., 1969, p. 364.

(5) Kottis, P. and Lefebvre, R., J. Chem. Phys. 41, 3660 (1964).

(6) Lhoste, J.-M., Huag, A. and Ptak, M., J. Chem. Phys. 44, 648 (1966) and 44, 654 (1966).

(7) El-Sayed, M.A. and Siegel, S., J. Chem. Phys 44, 1416 (1966).

(8) Rabold, G.P. and Piette, L.H., Photochem. Photobiol. 5, 733 (1966).

(9) Clements, R.F. and Sharnoff, M., Chem. Phys. Lett. 7, 4 (1970).

(10) Thurnauer, M.C. and Norris, J.R., Chem. Phys Lett. 47, 100 (1977).

(11) Siegel, S. and Goldstein, L., J. Chem. Phys. 43, 4185 (1965).

(12) Siegel, S. and Goldstein, L., J. Chem. Phys. 44, 2780 (1966).

(13) Siegel, S. and Goldstein, L., J. Chem. Phys. 45, 1860 (1966).

(14) Thurnauer, M.C. and Norris, J.R., Biochem. Biophys. Res. Comm. 73, 501 (1976).

(15) Paillotin, G., Vermiglio, A. and Breton, J., Biochim. Biophys. Acta 545, 249 (1979).

(16) Frank, H.A., Friesner, R., Nairn, J., Dismukes, G.C. and Sauer, K., Biochim. Biophys. Acta 547, 484 (1979).

(17) Vermeglio, A., Breton, J., Paillotin, G. and Cogdell, R., Biochim. Biophys. Acta 501, 514 (1978).

(18) Sauer, K., in Bioenergetics of Photosynthesis, Govindjee, ed., (Academic Press, New York, N.Y., 1975, p. 115.

(19) Renger, G. and Wolff, Ch., Biochim Biophys. Acta 460, 47, (1977).

(20) Chessin, M., Livingston, R. and Truscott, T.G., Trans. Faraday Soc. 62, 1519 (1966).

(21) Bensasson, R., Land, E.J. and Maudinas, B., Photochem. Photobiol. 23, 189 (1976).

(22) Truscott, T.G., Land, E.J. and Sykes, A., Photochem. Photobiol. 17, 43 (1973).

(23) Frank, H.A., McLean, M.B. and Sauer, K., Proc. Nat. Acad. Sci., USA 76, 5124 (1979).

(24) Mathis, P., Butler, W.L. and Satoh, K., Photochem. Photobiol. 30, 603 (1979).

(25) Cogdell, R.J., Monger, T.G. and Parson, W.W., Biochim. Biophys. Acta 408, 189 (1975).

(26) Monger, T.G., Cogdell, R.J. and Parson, W.W., Biochim. Biophys. Acta 449, 136 (1976).

(27) Kung, M.C. and DeVault, D., Photochem. Photobiol. 24, 87 (1976).

(28) Cogdell, R.J., Parson, W.W. and Kerr, M.A., Biochim. Biochys. Acta 430, 83 (1976).

(29) Parson, W.W. and Monger, T.G., Brookhaven Symp. Biol. 28, 195 (1977).

(30) Singleton, W.S., Gray, M.S., Brown, M.L. and White, J.L.,J. Amer. Oil Chem. Soc. 42, 53 (1965).

(31) Clayton, R.K. and Yamamoto, T., Photochem. Photobiol. 24, 67 (1976).

(32) Levanon, H. and Norris, J.R., Chem. Rev. 78, 185 (1978).

(33) Hoff, A.J., Biochim. Biophys. Acta 440, 765 (1976).

(34) Clarke, R.H., Connors, R.E. and Frank, H.A., Biochem. Biophys. Res. Comm. 71, 671 (1976).

(35) Cogdell, R.J. and Thornber, J.P., Ciba Foundation Symp. 61, 61 (1979).

(36) Boxer, S.G. and Roelofs, M.G., Proc. Nat. Acad. Sci. USA 76, 5636 (1979).

(37) Kalyanasundaran, K., Grieser, F. and Thomas, J.K., Chem. Phys. Lett. 51, 501 (1977).

# CHAPTER V

## SUMMARY AND PROSPECTS FOR FUTURE WORK

The aim of the experiments described here, especially in Chapters II and III, has been to decipher the pigment arrangement within a small light harvesting BChl protein complex. Because of its simplicity, the LH-R26 protein will be a valuable model for pigment arrangement in other BChl and chlorophyll proteins. A model of the geometrical arrangement of the x and y axes of the BChls is depicted in Figure III-5. This model was deduced in the following way: (a) Linear and circular dichroism were used to resolve the near infrared, $Q_y$, absorption band into the transition moments of the aggregate absorptions, the exciton bands. Exciton theory was used to find the monomeric transition moment directions. LD was unable to resolve the visible, $Q_x$ absorption band into its components. This was due to the low oscillator strength of one of its exciton components as suggested by CD analysis. (b) Fluorescence polarization measurements showed that fluorescence originates from nearly planar degenerate transition moments, probably $Q_y$ monomers. (Alternatively, the fluorescence originates from one or both of the exciton states, and the assumptions concerning band shapes in the CD analysis and limiting dichroic ratios in the LD analysis were incorrect.) The fluorescence polarization of the $Q_x$ absorption band suggested the $Q_x$

transition moments are perpendicular to the fluorescence moments. This result was supported by the previous LD analysis. The three-fold increase in fluorescence yield and the large Stokes shift at low temperatures remain anomalous.

One question which remains unsolved is the exact nature and classification of the coupling of the BChl dimer electronic transitions, whether it is strong, weak, or intermediate (1). One experiment which would help to determine the relation of the fluorescence transitions to the absorption transitions is the measurement of the circular polarization of the fluorescence (2). Emission from an exciton state would be expected to have circular polarization equal and opposite to the corresponding CD. However, the complications in this experiment due to photoselection and the resulting linear polarization of fluorescence are formidable.

Unfortunately the LH-R26 model was not extended beyond the stage shown in Figure III-5. Potentially the CD provides enough data for a complete determination of the geometry. However, current theories were not considered adequate for the analysis. In particular the vibronic character of the exciton transitions need more explicit representation. Several theories attempt to include vibrations by convolution of monomer absorption bands (3). One of the requirements is the knowledge of the monomeric absorption band. This band shape and energy is not known for BChl within the

LH-R26 protein. Experiments which may lead to this determination have been reported (4). The experiment involved selective photobleaching of one of the two BChls of the dimer as it resides in the native membrane. The monomeric $Q_y$ transition energy within the LH-R26 protein is definitely not so high as for BChl in organic solvents. Similar experiments to accurately determine the monomeric BChl absorption in the isolated protein complex, LH-R26, may prove useful. Clearly, improvements in the theory of CD, absorption and fluorescence polarization in molecular aggregates are needed; especially needed is explicit inclusion of vibrational levels of the ground and excited states. Other techniques for orientation may prove useful, particularly those which permit measurement of oreinted fluorescence and CD. Birefringence is a problem in many oriented samples.

The similarity of LD results of the LH-R26 protein and the B800+850 protein, from the mutant and wild types of Rps. sphaeroides, is striking. The overall similarity of the light harvesting complexes from bacteria would require LD analysis of the recently isolated B870 complex (5) and fluorescence polarization experiments on the B870 and B800+850 complexes.

Biochemical analysis will be needed to further reveal the similarities and differences between the two major classes of light harvesting complexes. In particular, amino acid analysis, peptide maps, and especially peptide sequencies may demonstrate the similarities. These data will aid

in interpretation of results from future physical measurements. Nuclear magnetic resonance (NMR) may be useful in determining the similarities and/or differences of the binding sites of the two BChls of LH-R26. NMR may help to determine the fifth and possible sixth ligands of the central Mg of BChls in the protein. The resonance raman technique may also prove useful in probing the BChl site(s). In summary, the LH-R26 protein still provides the simplest native complex for obtaining knowledge of BChl-protein interactions.

The bacterial photosynthetic reaction center presents an even more formidable problem in determining molecular orientations from spectroscopic measurements. It is, of course a more intriguing problem because the RC converts light energy into the chemical energy of stable products. We hope that the methodology used in analysis of the LH-R26 optical properties will be useful in analysis of the RC.

The RC has additional properties which may be used for structure determination. In particular, the absorption changes associated with charge separation have been studied by photoselection (6). The EPR properties described in Chapter IV are another useful probe. Magnetophotoselection was used to locate the transition moments of two relatively pure optical transitions within the principal magnetic axis system of the triplet state (FIgure IV-7). To translate this information into molecular geometry requires several approaches. First, the optical transition moments should be

accurately located in the monomeric magnetic axis system of BChl. The only published experiments of this type were interpreted qualitatively (7). Quantitative analysis is needed. Second, the relation between aggregate (dimer) geometry and aggregate triplet magnetic axes must be defined. Clarke has proposed a model for these relations and has tested several model systems (8). However, the model is not yet accepted by many investigators (9). Third, the optical properties must be related to the aggregate geometry, a problem discussed above. Fourth, the magneto-photoselection experiments must be performed at all accessible wavelengths, as is now being pursued by Boxer and Roelofs (10).

It is clear that use of only one type of experimental result is insufficient to define molecular geometries. We feel that any proposed geometry for the RC pigments, particularly the BChl special pair, must be consistent with all of the available experimental results. For example the presence of large exciton induced CD of the special pair (11) is inconsistent with a plane parallel geometry of the dimer. Nevertheless, this geometry is often quoted as a fact.

Returning to the problem of the LH-R26 protein, it is apparent that its triplet state properties would help to determine the BChl arrangement. The triplet state is useful because it provides three molecular axes which are

orthogonal by definition. In contrast, optical experiments define one, or in the best cases such as BChl, two axes, which are not guaranteed to be orthogonal. To date our attempts to observe the triplet of LH-R26 by EPR have failed. Detection of the triplet of LH-R26 may still be possible by optical detection of magnetic resonance (8).

In the last half of Chapter IV, the first reported detection of carotenoid triplet states by EPR was described. Our knowledge of BChl protein complexes proved very useful in interpreting these results. The triplet states of polyenes may prove useful in understanding their other photochemical and spectroscopic properties. Naturally, the next experiments which we are planning will include magnetophotoselection.

The study of BChl proteins has been an intriguing one. More importantly, we feel that knowledge on a molecular level of the organization of components in photosynthetic membranes is essential in describing their function. A molecular description of each component is one of the basic steps in obtaining a picture of this organization. Because photosynthetic organisms are able to use visible and near infrared light energy efficiently, a detailed description of their functions will prove invaluable in schemes for utilizing solar energy. It is hoped that the advances described in this work will further the understanding of the photosynthetic apparatus.

# REFERENCES


(1) Forster, Th., in Modern Quantum Chemistry Part III, Sinanoglu, O., ed., (Academic Press) New York, N.Y., 1965, p. 93.

(2) Steinberg, I.Z., Meth. Enqymol. 49, 179 (1978), Tinoco, I., Ehrenberg, B. and Steinberg, I.Z., J. Chem. Phys. 66, 916 (1977).

(3) Hemenger, R.P., J. Chem. Phys. 69, 2279 (1978).

(4) Rafferty, C.N., Bolt, J., Sauer, K. and Clayton, R.K., Proc. Nat. Acad. Sci. USA 76, 4429 (1979).

(5) Broglie, R.M., Hunter, C.N., Delepelaire, P., Neiderman, R.A., Chua, N.-H. and Clayton, R.K., Proc. Nat. Acad. Sci. USA, in press for January 1980.

(6) Vermeglio, A., Breton, J., Paillotin, G. and Cogdell, R., Biochim. Biophys. Acta 501, 514 (1978).

(7) Thurnauer, M.C and Norris, J.R., Chem. Phys. Lett. 47, 100 (1977).

(8) Clarke, R.H., Hobart, D.R., and Leenstra, W.R., J. Am. Chem. Soc. 101, 2416 (1979).

(9) Levanon, H. and Norris, J.R., Chem. Rev. 78, 185 (1978).

(10) Boxer, S.G. and Roelofs, M.G., Proc. Nat. Acad. Sci. USA 76, 5636 (1979), and personal communications.

(11) Philipson, K.D. and Sauer, K., Biochemistry 12, 535 (1973).

# APPENDIX

## PREPARATION OF BACTERIOCHLOROPHYLL PROTEINS

### Chromatophore Membranes

Cells were grown on either a yeast extract or a modified Hutners' nutrient medium (1). The yeast extract medium (5 g/l yeast extract, 3 g/l casein amino acids, 0.87 g/l $K_2HPO_4.7H_20$) was preferred due to its simplicity. The Hutners' medium was used for R-26 cultures to discourage growth of contaminating microorganisms. Growth conditions were essentially identical to Austin's. Cells were stored as frozen pastes. Chromatophore membranes were isolated from cells as described by Austin (1). For best results the chromatophores were purified on step sucrose gradients.

### Purification of LH-R26

Two methods have been described previously for isolation of the light harvesting protein of Rps. sphaeroides carotenoidless mutant R-26. Austin used Triton X-100, sucrose density gradients, and gel permeation chromatography in SDS solution (1). This method was found to be not reproducible. Also, yields were low. A second method described by Bolt and Sauer (2), used dodecyldimethylamine oxide (DDAO), sucrose gradients and Sephadex G200 chromatography in SDS solution. Although the method was reproducible its yield was low.

A third method, using hydroxyapatite was developed and

is described here. All procedures were performed at 10°C. Hydroxylapatite was prepared as described by Siegelman et. al. (3) on a five mole scale. Membranes with an absorbance at 862 nm of 50/cm were solubilized by one tenth volume of 10% SDS and diluted to five times the original volume with 10 mM TrisHCl, pH 7.5. The solubilized membranes were loaded onto a hydroxylapatite column equilibrated with 0.05 M $Na_2HPO_4/NaH_2PO_4$, 0.1 M NaCl, 0.1% SDS, pH 7.0. A column of 50 ml packed volume was suitable for 10 to 12 ml original volume of membrane suspension. A flow rate of about 2 ml per minute was maintained with a peristaltic pump. The column was eluted successively with 75 ml volumes of 0.05 M, 0.10 M, and 0.15 M phosphate buffers containing NaCl and SDS in the concentrations stated above. A sharp blue band containing the LH-R26 protein eluted with the 0.15 M phosphate. Fractions were monitored by the ratio A848/A275 using a Cary 14 recording spectrophotometer, and fractions with ratios greater than 2.9 were pooled.

SDS polyacrylamide gel electrophoresis in gels containing 6.5 M urea was performed as described by Swank and Munkres (4). The gels resolved peptides of molecular weight 2,000 to 20,000 daltons. Myoglobin and its cyanogen bromide fragments were used as standard molecular weight markers. The LH-R26 protein contained two peptides resolved in the gel. Molecular weights of 10,200 and 10,500 were calculated from a plot of molecular weight versus relative mobility.

The extinction coefficient of the LH-R26 protein was determined after extraction of BChl into acetone: methanol (5): $E_{848} = 1.2 \pm 0.1 \times 10^5\ M^{-1}\ cm^{-1}$ per BChl.

Amino acid analysis after acid hydrolysis was performed on a Beckman Model 120C amino acid analyzer by the Chemistry Department analytical laboratory. Table A-1 compares the amino acid composition of the present preparation with the Triton X-100 preparation of Austin (1). The analyses are similar but not identical.

The isolation procedure outlined here is quicker than the two previous methods. From purified membranes it takes one day to prepare the LH-R26 protein, whereas the previous methods required three days. Furthermore, the protein is in a more concentrated form facilitating further studies. Based on the longest wavelength absorption maximum near 850 nm 50% to 60% of the BChl can be recovered from original membranes as the light harvesting complex. This is a vast improvement over previous methods.

One possible disadvantage is a slight alteration of the wavelength maximum of the near infrared absorption. With previous preparations the maximum shifted from 862 nm to 854 nm upon isolation. After isolation on hydroxylapatite, the maximum shifts to 848 nm. This may indicate differences between the conformation of the isolated proteins and their conformation in the membrane. Nevertheless, the linear dichroism and fluorescence polarization (6) are the same for both the previous preparation and the preparation

TABLE A-1

AMINO ACID ANALYSIS OF LH-R26 PROTEIN

| Amino Acid | Mole Percent | |
|---|---|---|
| | Current Preparation | Previous Preparation[a] |
| Lys | 3.63 | 3.58 |
| His | 3.48 | 2.05 |
| Arg | 1.82 | 2.08 |
| Asx | 4.70 | 5.89 |
| Thr | 7.15 | 7.26 |
| Ser | 3.05 | 5.97 |
| Glx | 8.58 | 8.14 |
| Pro | 6.05 | 4.94 |
| Gly | 8.09 | 9.77 |
| Ala | 21.00 | 17.99 |
| Cys | 0.00 | 0.00 |
| Val | 11.13 | 7.31 |
| Met | .06 | 2.36 |
| Ile | 4.23 | 3.39 |
| Leu | 10.77 | 10.73 |
| Tyr | 1.76 | 2.45 |
| Peh | 4.03 | 3.94 |
| (Trp)[b] | (1.55) | 2.15 |

[a] Reference (1).

[b] Based on Trp to Tyr ratio determined by Austin (1).

using hydroxylapatite.

Preparation of B800+850

The method described here was used on membranes from wild type Rps. sphaeroides [2.4.1]. Cogdell reports that the method is applicable to any carotenoid containing strain of Rps. sphaeroides (7).

Chromatophores (A850 = 50/cm) in 0.1 M $KH_2PO_4$ pH 7.0 were made 0.3% in DDAO (Ammonyx LO, Onyx Chemical Co.) by addition of an appropriate volume of 30% DDAO at 27°C. After ten minutes the solution was centrifuged at 100,000g for 1 hour. Supernate was saved. The pellet was resuspended to A850 = 50/cm in 0.3% DDAO, phosphate buffer at 27°C as described above. After centrifugation the supernate was saved. The pellet contained a pure B800+850 spectrum in the visible and near IR absorption bands. Nonpigmented proteins were removed by treatment with Triton X-100 and DDAO as described by Clayton and co-workers (8): The pellet was at 10,000g ten minutes. After a second wash with Triton the pellet was suspended in 0.2% DDAO, 10mM EDTA and layered over a 0.6 M/1.2M sucrose step gradient. Centrifugation at 150,000g (SW41) for 2 hours gave a band at the interface of the two sucrose layers. It was removed and dialized against 10 mM Tris HCl pH 7.5.

SDS gel electrophoresis in 6 M urea as described above resolved two peptides of 10,000 and 9,500 daltons.

Reaction Centers, wild type Rps. sphaeroides

The supernates from 0.3% DDAO washing of chromatophores see above, were pooled. Purification by ammonium sulfate precipitation using the procedure of Clayton and Wang (9) gave a pure RC absorption spectrum.

Reaction Centers, R-26

The procedure of Clayton and Wang (9) was followed. For use in reconstituted membranes, the RCs were purified on Sephadex G200.

# REFERENCES

(1) Austin, L.A., Ph.D. Thesis, University of California, Berkeley, 1976.

(2) Bolt, J. and Sauer, K., Biochim. Biophys. Acta 546, 54 (1979).

(3) Siegelman, H.W., Wieczorek, G.A., and Turner, B.C., Anal. Biochem. 13, 402 (1965).

(4) Swand, R.T., And Munkres, K.D., Anal. Biochem. 39, 462 (1971).

(5) Straley, S.C. Parson, W.W., Mauzerall, D.C., Clayton, R.K., Biochim. Biophys. Acta 305, 597 (1973).

(6) See Chapters II and III.

(7) Cogdell, R.J., personal communication.

(8) Clayton, R.K. and Clayton, B.J., Biochim. Biophys. Acta 283, 492 (1972), and Heathcote, P.H. and Clayton, R.K., Biochim. Biophys. Acta 459, 506 (1977).

(9) Clayton, R.K. and Wang, R.T., Methods Enzymol. 23, 696 (1971).